AN ABSTRACT OF THE THESIS OF

Steven G. Mayer for the degree of Doctor of Philosophy in Chemistry presented on August 18, 1997. Title: **Size Estimates of Molecular Clusters Using Elastic Light Scattering and CARS Spectroscopy.**

Redacted for Privacy

Abstract approved: _____ Joseph W. Nibler

The coherent anti-Stokes Raman scattering (CARS) intensity of a vibrational transition is approximately independent of the extent of molecular aggregation, whereas Rayleigh scattering intensity increases quadratically with the number of monomer units contained in a cluster. This study exploited this difference and combined Rayleigh-CARS measurements to determine a mean diameter of 12.4 ± 0.7 nm for CO_2 clusters formed in a neat free jet expansion. This result agrees well with size estimates of 11.3 ± 1.3 nm from empirical scaling laws and ~ 20 nm from a cluster cooling curve model. In addition, the Rayleigh-CARS data yield density variation and cluster growth profiles in the expansions.

When colder clusters are produced in dilute CO_2/He expansions, the CARS spectra exhibit two peaks red-shifted from the monomer that we propose are due to molecules on the surface and in the core of the cluster. The relative intensities of these peaks measured for a 12% CO_2/He expansion gave a mean diameter of 13.7 ± 3.2 nm compared with a value of 13.2 ± 1.1 nm, by the Rayleigh-CARS method. Similarly, a 5%

CO_2/He expansion produced clusters of mean diameter 8.5 ± 2.6 nm compared with 7.6 ± 1.2 nm by the Rayleigh-CARS method.

The differential cross section for scattering of a plane monochromatic wave from a small particle also contains an angular dependence, which is a strong indicator of the size of the scatterer. We present angular scattering measurements for "calibration" microspheres of known size and from clusters formed in a neat CO_2 supersonic jet expansion. Under very extreme expansion conditions, clusters with a mean diameter of 400 nm to 500 nm were produced as deduced from fits of the angular scattering curves using Mie's formulae. Measurements and calculations were also made for the milder neat CO_2 expansion conditions which gave 14.4 ± 2.0 nm mean diameters from the Rayleigh-CARS method. The absence of angular intensity variations and the Mie calculations confirm that these clusters were indeed much smaller than 500 nm—the condition necessary to justify using a simple quadratic size dependence of the Rayleigh scattering intensity.

Size Estimates of Molecular Clusters Using Elastic Light Scattering and CARS Spectroscopy

by

Steven G. Mayer

A THESIS

submitted to

Oregon State University

in partial fulfillment of
the requirements for the
degree of

Doctor of Philosophy

Presented August 18, 1997
Commencement June 1998

Doctor of Philosophy thesis of Steven G. Mayer presented on August 18, 1997

APPROVED:

Redacted for Privacy

Major Professor, representing Chemistry

Redacted for Privacy

Chair of Department of Chemistry

Redacted for Privacy

Dean of Graduate School

I understand that my thesis will become part of the permanent collection of Oregon State University libraries. My signature below authorizes release of my thesis to any reader upon request.

Redacted for Privacy

Steven G. Mayer, Author

ACKNOWLEDGMENTS

I would like to thank my advisor Professor Joseph W. Nibler for mentoring me as a scientist and scholar. His patience, integrity, attention to detail and fascination with the physical world have convicted me to strive for excellence in my chosen field of study. Joe is a gifted teacher and the lessons I have learned from him will remain with me as I develop my own teaching style. I am grateful to have had the opportunity to learn from him.

I would also like to acknowledge the assistance of many people who contributed to the work in the laboratory during my time at OSU. Thanks to Phil Minarik for assisting in the development of the Rayleigh-CARS method and for singing show tunes with me while waiting for spectra; Marshall Crew for many helpful discussions regarding scattering theory; and Engelene Chrysostom for assisting with collection of the Mie scattering results for very large clusters. I benefited a great deal from our time working together on this project. I thank Ted Hinke for teaching me many valuable machining skills and for his timely and skillful production of several intricate pieces of equipment.

Thanks to my community of friends whose prayer and support have sustained me through this stage of my journey. I thank Mike and Jennifer Jacobson, Bob and Beth Mumford, Scott and Jackie Eberhart, Bill Greenwood, Ken Jones, Darren Williams and the community at Logos House. I thank Gary, Pam and Daniel (a.k.a. Skippy) Hough for providing the "gravity" of home during these last trying months of my time in Corvallis. May our Lord's light burn bright at your table all the days of your life!

Finally, I'd like to thank my family for their support through the years. My wife Shannon has been faithful and true, walking beside me through the joy and the pain of these past four years. My brother John has helped me to consider carefully "which hill to die on."

In the end, all glory and honor be to the only wise God, our Lord, Jesus Christ; for in Him all things hold together, Amen!

TABLE OF CONTENTS

TABLE OF CONTENTS (Continued)

TABLE OF CONTENTS (Continued)

TABLE OF CONTENTS (Continued)

LIST OF FIGURES

LIST OF FIGURES (Continued)

LIST OF FIGURES (Continued)

LIST OF TABLES

DEDICATION

All who are led by the spirit of God are sons of God. You did not receive a spirit of slavery leading you back into fear, but a spirit of adoption through which we cry out, "Father!" Romans 8:14,15.

We all have a story to tell. Mine begins with a father who abandoned my mother and me before I was yet one year old. God, in His infinite wisdom and tender mercy, provided me with a father—a man of integrity, who gave me his name through adoption. My early life is a parable unveiled for it reflects the truth of our adoption as sons of God through the sacrifice of Christ. My Dad committed his life to raise me and provided me with the means to earn an education, an opportunity he never received. I proudly bear his name for it is a testimony of love, worked out through sacrifice and commitment. I dedicate this thesis to my father

Patrick Joseph Mayer.

SIZE ESTIMATES OF MOLECULAR CLUSTERS USING ELASTIC LIGHT SCATTERING AND CARS SPECTROSCOPY

1. INTRODUCTION

1.1 MOLECULAR CLUSTERS

1.1.1 Interest in Clusters

Molecular clusters in the nanometer size regime have been the focal point of the research interests of many scientists, including our group at Oregon State University. Over the past decade our laboratory has used coherent Raman spectroscopy in several different configurations to probe the spectral and physical properties of these clusters. Most recently, we began using ionization detected stimulated Raman spectroscopy (IDSRS) [Crew, 1997] and elastic light scattering [this work] as new techniques to examine various aspects of these clusters. Nanoclusters of 1 to 100 nm radius are particularly interesting because they span the range between isolated gas molecules and bulk material. By studying clusters in this range, we gain further understanding of the mechanisms and rates of phase changes, interfacial energies between phases, and structure of the solid phase.

1.1.2 Cluster Formation in a Supersonic Jet Expansion

Van der Waals interactions in the gas phase are very weak due to the large separation between individual molecules whereas the liquid and solid phases are held

together by these forces. A supersonic jet expansion is a means of cooling molecules so that these forces can serve to condense molecules into clusters. Depending upon the expansion conditions, clusters may range from 2 to 10^8 molecules in size. Clusters are formed during the early, first cooling that occurs on expanding a high pressure gas out of a nozzle into a vacuum. Abraham, et al. [1981] studied nozzle types and other parameters to determine the conditions which produce the most efficient clustering; in general, large nozzle diameters, low nozzle temperatures and high driving pressure tend to produce the largest clusters. For studies using infrared absorption spectroscopy, the nozzle openings are typically slits of 2 cm to 10 cm in length, which are needed to give a long sample path length [Sharpe, 1990]; large clusters are difficult to form with such nozzles so most IR work has focused on dimers and trimers. However, due to the high sensitivity of IR spectroscopy one can study molecules deposited on the surface of small clusters. For example, Goyal, et al. [1993] devised a method where an effusive jet of SF_6 molecules was used to coat cold Ar clusters formed in a supersonic jet. In the present work, we observe the surface "coat" of CO_2 on a CO_2 "core" using coherent anti-Stokes Raman scattering (CARS) spectroscopy. Thus, jet expansions provide a novel approach to the study of surfaces of small molecular aggregates.

1.1.3 Size Dependent Characteristics of Clusters

Clusters in the 2 to 100 molecules size range are interesting because information about the molecular interactions and arrangements of molecules in the solid can be determined. Such information can be used, for example, when modeling atmospheric

processes such as droplet formation or ozone production (i.e., from studies of the oxygen dimer complex). Small clusters are also interesting because they can display novel molecular dynamics such as internal rotation and tunneling motions. The spectral splittings resulting from such effects are important for gaining a more detailed understanding of the intermolecular potential surfaces.

Clusters in the 100 to 10,000 molecules size range are interesting because they more closely approximate the macroscopic condensed phases of molecules. For example, our group at OSU has used CARS spectroscopy to study the internal vibrations of carbon dioxide clusters in this size range [Pubanz, et al., 1986]. Barth and Huisken [1990] observed the low frequency external librational modes in crystalline CO_2 clusters. In this size range, a significant fraction of the molecules are on the surface of the cluster and we expect to spectroscopically distinguish these molecules from those in the core. Previously, we stated that CO_2 clusters give rise to a unique peak in the CARS spectrum shifted to the blue of the core cluster peak [Richardson, 1993].

Clusters in the size range greater than 10,000 molecules are essentially macroscale and can be used to study the bulk phase properties and phase transitions of liquids and solids. This is an effective way of studying homogeneous phase transitions because clusters have very few impurities per sample and they do not have containing walls to initiate heterogeneous phase transitions. Previous OSU work showed that large nitrogen [Beck, et al., 1990] and acetylene [Lee, et al., 1994] clusters exhibit phase transitions upon cooling in supersonic jets. Bartell, et al. [1989] have done extensive work in this area using electron diffraction.

1.2 MODELS FOR ESTIMATING CLUSTER SIZE

1.2.1 Scaling "Law" Model

Experimentally, cluster size is difficult to determine. Electron diffraction is an excellent technique for well-ordered samples but the diffraction lines become blurred with disorder in the crystal or liquid; mass spectral analysis works well for small clusters but is problematic for large clusters due to fragmentation upon ionization. One method for deriving cluster size is the application of an empirical scaling "law" based upon mass spectral and electron diffraction data for small clusters [Torchet, et al., 1984]. Hagena and Obert [1972] derived a relationship between cluster size and pressure and temperature in a condensing supersonic expansion. Also, the scaling is dependent upon nozzle diameter. The scaling "laws" are useful for predicting mean cluster size in a condensing supersonic jet expansion. However, we are reticent about extrapolating this method to larger clusters ($N_c > 1000$ molecules) and the method does not map cluster growth as a function of distance from the nozzle.

1.2.2 Cooling Curve Model

A more recent empirical model for determining cluster size is the application of cooling curves from supersonic jet experiments [Richardson, 1993]. The method models heat transfer into and out of a cluster to account for condensation and evaporation, respectively. The heat flux scales linearly with cluster surface area and the cooling depends upon the cluster heat capacity which is related to the volume of the cluster. The

temperature, as deduced from the Raman line position and the change with jet position, is modeled to deduce a mean cluster size.

1.2.3 Rayleigh Scattering and CARS Spectroscopy

Rayleigh scattering intensity is a non-linear function of cluster size. It has been used to monitor cluster growth [Stein and Moses, 1972] and estimate mean size of clusters [Bell, et al., 1993]. However, it is only a qualitative measure since large clusters dominate the detected scattering signal. The present thesis work combines the quadratic size dependence of Rayleigh scattering with information about extent of clustering from CARS spectroscopy to deduce mean cluster size of medium to large clusters.

1.2.4 Sizes from Surface/Core CARS Intensities

When a cluster is small enough, an appreciable fraction of the molecules reside on the surface of the cluster and are distinct from molecules in the interior. CARS spectra can exhibit distinct features for each molecular type and from the relative intensities of surface and interior features we deduce a mean cluster size. The aim of this work is to develop these methods for determining cluster size and to compare results obtained with them.

1.2.5 Sizes from the Angular Dependence of Mie Scattering for Large Clusters

When a plane monochromatic wave scatters from a large particle, the differential scattering cross section of the particle contains an angular dependence. This angular

dependence is a strong indicator of the size of the scatterer. If the cluster diameter is of the order of the wavelength of the incident light, interference effects become significant; the scattering intensity varies with the angle of detection. We can measure the angular dependence of such scattering, termed Mie scattering, from clusters formed in a supersonic jet expansion and fit the angular scattering curves using a solution of Mie's formulae. In Chapter 3, we examine the use of such angular measurements for very large clusters formed under extreme expansion conditions. We tested our measurement apparatus by applying Mie's formulae to angular scattering profiles of latex spheres of known size. Studies of CO_2 clusters using the same apparatus establish some bounds on the sizes of clusters that can be formed in jet expansions.

2. SIZE ESTIMATES OF CO_2 CLUSTERS USING RAYLEIGH SCATTERING AND CARS SPECTROSCOPY

2.1 ABSTRACT

The coherent anti-Stokes Raman scattering (CARS) intensity of a vibrational transition is approximately independent of the extent of molecular aggregation, whereas Rayleigh scattering intensity increases quadratically with the number of monomer units contained in a cluster. This study exploited this difference and combined Rayleigh-CARS measurements to determine a mean diameter of 12.4 ± 0.7 nm for CO_2 clusters formed in a neat free jet expansion. This result agrees well with size estimates of 11.4 ± 1.3 nm from empirical scaling laws and ~ 20 nm from a cluster cooling curve model. In addition, the Rayleigh-CARS data yield density variation and cluster growth profiles in the expansions.

When colder clusters are produced in dilute CO_2/He expansions, the CARS spectra exhibit two peaks red-shifted from the monomer that we propose are due to molecules on the surface and in the core of the cluster. The relative intensities of these peaks measured for a 12% CO_2/He expansion gave a mean diameter of 13.7 ± 3.2 nm compared with a value of 13.2 ± 1.1 nm, by the Rayleigh-CARS method. Similarly, a 5% CO_2/He expansion produced clusters of mean diameter 8.5 ± 2.6 nm compared with 7.4 ± 0.2 nm by the Rayleigh-CARS method.

2.2 INTRODUCTION

Molecular interactions in the gas phase are very weak due to the large separations between nearest neighbor molecules. In contrast, molecular interactions in the liquid and solid phases are much stronger and the molecular arrangements more ordered. A supersonic jet expansion provides a means of condensing small numbers of molecules into clusters. Small aggregates (dimers and trimers) formed in this way have been the subject of many studies, since they give information about intermolecular potentials. Medium-sized clusters (N = 10-1000 units) are also interesting because they can display properties intermediate between those of isolated molecules and bulk phase solid. In the case of large clusters (N >1000 units) studies have focused on the mechanism and rates of phase transitions, from which we can deduce the interfacial energies (surface tensions) between phases. Interest in these size dependent characteristics is part of the impetus for our investigation of molecular clusters; in this paper, we focus on the specific problem of determining the mean cluster size as characterized by the diameter or, equivalently, by the number of monomeric units N_c.

2.3 EMPIRICAL SIZE ESTIMATES

2.3.1 Scaling "Laws"

Experimentally, an average size for clusters formed in jet expansions can be difficult to measure. Direct mass spectral analysis works well for small clusters but is problematic for large clusters due to fragmentation upon ionization. Electron diffraction

is a feasible technique for the latter well-ordered solid samples but the width of the diffraction rings, which gives the size information, become blurred with disorder in the crystal and in liquids. One approach to estimating sizes of larger clusters from the more reliable mass spectral data for small clusters (N_c < 500 molecules) is the application of empirical scaling "laws" [Torchet, et al., 1984]. For example, Hagena and Obert [1972] deduced from measurements that, for a given mean value of N_c = 500, there was a constant relationship between initial pressure P_0 and temperature T_0 in a condensing supersonic expansion, i.e.,

$$P_0 T_0^{(1.25\gamma - 0.5)/(1-\gamma)} = \left(C_1\right)_{D,N_c} \tag{2.1}$$

Here $\gamma = C_p/C_v$ is the heat capacity ratio which, for linear molecules, is 7/5. These workers also deduced a second empirical "law" which showed that the same N_c value resulted when the pressure and nozzle diameter D satisfied the constant relationship.

$$P_0 D_{nozzle}^{q} = \left(C_2\right)_{T,N_c} \tag{2.2}$$

Here the scaling parameter q was found to be 0.6 for CO_2 by measurement of N_c for various values of P_0 and D at fixed T_0. By combining these scaling "laws" using reference values at mild expansion conditions (T_0 = 295 K, D = 0.4 mm), we obtain the relation

$$\log N_c = a \log\left[P\left(\frac{T}{295}\right)^{-25/8}\left(\frac{D}{0.15}\right)^{0.6}\right] + b \tag{2.3}$$

From the mass spectral measurements of N_c versus P by Falter, et al. [1970] Torchet, et al. [1984] deduced a value for the parameter a and applied this scaling relation to estimate N_c values for strongly condensing expansions where larger clusters ($N_c \leq 1000$ molecules) were formed. They found reasonable agreement with the scaling relations and others have similarly used these relations for $N_c > 1000$ but experimental verification of the validity of this extrapolation by an independent method is desirable. The present study using Rayleigh scattering permits such a comparison and, moreover, gives information about cluster growth as a function of distance from the nozzle (the scaling "laws" apply only to the final mean cluster size at large X/D values in the expansion).

2.3.2 Cooling Curves

A more recent approach for determining larger cluster sizes involves the modeling of cooling of clusters as functions of X/D in the supersonic jet experiment [Richardson, 1993]. The method models heat transfer into and out of a cluster to account for condensation and evaporation, respectively. The heat flux scales linearly with cluster surface area and the cooling depends upon the cluster heat capacity which is related to the volume of the cluster. The temperature, as deduced from the Raman line position, and its change with jet position is modeled to deduce a mean cluster size.

2.3.3 Rayleigh/Mie Scattering

Rayleigh scattering intensity has also been used to monitor cluster growth [Stein and Moses, 1972] and to estimate mean size of clusters [Bell et al., 1993]. However, it is

only a qualitative measure since it is a non-linear function of cluster size (i.e., large clusters dominate the detected scattering signal) and they had no means by which to measure extent of clustering. The present work combines the quadratic size dependence of Rayleigh scattering with information about extent of clustering from CARS spectroscopy to deduce the mean size of medium to large clusters. In Chapter 3, we consider the possible use of Mie scattering for size deduction of very large clusters.

2.3.4 Surface to Core Measurements

Finally, when a cluster is small enough, an appreciable fraction of the molecules reside on the surface of the cluster and these are distinct from molecules in the interior. CARS spectra can distinguish features for each molecular type and, from the relative intensities of surface and interior features, one can deduce a mean cluster size. The overall aim of this work has been to develop these various methods for determining cluster size and to compare results obtained with them.

2.4 RAYLEIGH SCATTERING

2.4.1 Historical Notes

In the late nineteenth century, the Honorable John W. Strutt (a.k.a. Lord Rayleigh) [1871] proposed a theory of light scattering that explained several observations made by Leonardo Da Vinci (c. 1500) [Richter, 1970]: large particles scatter light more effectively than small particles; particles with diameter less than the wavelength of light scatter

shorter wavelengths more efficiently than longer wavelengths; light scattered at 90° to the incident beam is polarized. Rayleigh showed that light scattering is a function of particle size, distance from the particle to the observer, wavelength of incident radiation, and refractive indices of the particle and the environment. From classical electromagnetic theory, he demonstrated that the scattered light intensity decreases as the distance squared and is proportional to the particle volume squared.

2.4.2 Theoretical Description of Rayleigh Scattering

We begin with a plane monochromatic wave incident on a scatterer. The incident electric field is given by

$$\mathbf{E}_0 = \varepsilon_0 E_0 e^{i\mathbf{k}_0 \cdot \mathbf{r}} \tag{2.4}$$

with amplitude E_0 and direction of polarization ε_0. The incident wavevector $\mathbf{k}_0$ is given by

$$\mathbf{k}_0 = k\,\mathbf{n}_0 \tag{2.5}$$

where $k = 2\pi/\lambda$ is the magnitude of the wavevector and $\mathbf{n}_0$ is the direction of propagation. When the plane wave interacts with a particle, the incident fields induce electric and magnetic multipoles that oscillate in definite phase relationship with the incident wave and radiate energy in all directions. The angular distribution of radiated energy depends upon the coherent superposition of multipoles induced by the incident field and the polarization of the incident wave. If the wavelength of the radiation is long compared to

the size of a cluster of monomers, the scattering by the lowest multipoles, the electric and magnetic dipoles induced in the monomers, will be coherent. For an elastic scattering process, the incident and scattered photons have the same wavelength. Thus, the wavevector of the scattered wave can be expressed as

$$\mathbf{k}_s = k\,\mathbf{n}_s \tag{2.6}$$

where $\mathbf{n}_s$ is the direction of propagation of the scattered wave. At large distance r from the scatterer, the electric field of the scattered wave is given by [Jackson, 1975]

$$\mathbf{E}_s = k^2 \frac{e^{ikr}}{r}[(\mathbf{n}_s \times \mathbf{p}) \times \mathbf{n}_s - \mathbf{n}_s \times \mathbf{m}] \tag{2.7}$$

In this equation $\mathbf{p}$ and $\mathbf{m}$ are the electric and magnetic dipole moments, respectively, induced by the incident field. We will neglect the magnetic dipole contribution since it is small. The momentum transfer $\hbar k$ in the scattering process is

$$\mathbf{k} = \mathbf{k}_0 - \mathbf{k}_s = k(\mathbf{n}_0 - \mathbf{n}_s) \tag{2.8}$$

where the magnitude of $\mathbf{k}$ is

$$|\mathbf{k}| = 2k \sin\left(\frac{\theta}{2}\right) \tag{2.9}$$

and θ is the angle between $\mathbf{n}_0$ and $\mathbf{n}_s$. Figure 2-1 shows the relationship between the incident and scattered wavevectors [Hobbie and Sung, 1996]. The angular dependence of the scattered intensity comes from the interference of the amplitudes of the scattered waves for an ensemble of particles.

The detector at a distance r from the sample measures an intensity which is proportional to the differential scattering cross section, i.e., the relative power radiated in a direction **n** with polarization ε, per unit solid angle, per unit incident flux in the direction $\mathbf{n}_0$ with polarization ε_0 [Jackson, 1975]. This cross section is given by

$$\frac{d\sigma}{d\Omega}(\mathbf{n}_s,\varepsilon_s;\mathbf{n}_0,\varepsilon_0)=\frac{r^2\frac{c}{8\pi}\left|\varepsilon_s^*\cdot\mathbf{E}_s\right|^2}{\frac{c}{8\pi}\left|\varepsilon_0^*\cdot\mathbf{E}_0\right|^2}=r^2\frac{I_s}{I_0} \tag{2.10}$$

where the electric field of the incident wave is given by (2.4). Substituting Equations (2.4) and (2.7) into Equation (2.10) we can write the differential scattering cross section as

$$\frac{d\sigma}{d\Omega}(\mathbf{n}_s,\varepsilon_s;\mathbf{n}_0,\varepsilon_0)=\frac{k^4}{E_0^2}\left|\varepsilon_s^*\cdot\mathbf{p}\right|^2 \tag{2.11}$$

where k^4 is proportional to λ^{-4}, which is the familiar wavelength dependence associated with Rayleigh scattering.

The development of (2.11) assumes scattering of an incident plane wave from a single, spherical scatterer. If we consider an ensemble of spherical scatterers of fixed separation at the time of scattering, each scatterer generates an amplitude like (2.7). The total scattering intensity comes from the superposition of the individual amplitudes. The scattered electric fields of (2.7) differ by a *phase factor* given by $e^{i\mathbf{k}\cdot\mathbf{r}_j}$ which accounts for the distribution of the scatterers [Jackson, 1975]. The resulting differential cross section (total scattering intensity) of the ensemble can be written

$$\frac{d\sigma}{d\Omega} = \frac{k^4}{E_0^2}\left|\sum_j \left[\varepsilon_s^* \cdot \mathbf{p}_j\right] e^{ik\cdot r_j}\right|^2 \tag{2.12}$$

For scattering from identical scatterers $\varepsilon_s^* \cdot \mathbf{p}_j$ factors out of the sum and the cross section can be written as the product of the cross section for one scatterer times a structure factor F(**k**).

$$F(\mathbf{k}) = \left|\sum_j e^{ik\cdot r_j}\right|^2 = \sum_j \sum_{j'} e^{ik\cdot r_j} e^{-ik\cdot r_{j'}} = \sum_j \sum_{j'} e^{ik\cdot(r_j - r_{j'})} = \sum_j \sum_{j'} e^{ik\cdot r_{jj'}} \tag{2.13}$$

If we consider an "ensemble" consisting of only two identical scatterers (N = 2) then F(**k**) becomes

$$\begin{aligned} F(\mathbf{k}) &= e^{ik\cdot(r_1 - r_1)} + e^{ik\cdot(r_1 - r_2)} + e^{ik\cdot(r_2 - r_1)} + e^{ik\cdot(r_2 - r_2)} \\ &= 2 + e^{ik\cdot r_{12}} + e^{-ik\cdot r_{12}} = 2\left(1 + \cos \mathbf{k}\cdot\mathbf{r}_{12}\right) \end{aligned} \tag{2.14}$$

The j = j' terms reduce to 2 and the j ≠ j' terms reduce to 2 cos θ where θ is given by $\mathbf{k}\cdot\mathbf{r}_{12}$. When $\mathbf{k}\cdot\mathbf{r}_{12} \approx 0$ so that the two particles are "clustered", then θ ≈ 0 and F(**k**) = 4 (or N^2). When the particles are not held together, $\mathbf{r}_{12}$ covers all distances and then averaging over all $\mathbf{r}_{jj'}$ gives $\langle \cos\theta \rangle = 0$ so that F(**k**) = 2 (or N). Therefore, F(**k**) = N when the scatterers are randomly distributed over the sampled volume (i.e., the j ≠ j' terms contribute nothing to the total scattering intensity) and F(**k**) = N^2 when the scatterers are localized or "clustered" (i.e., the j ≠ j' terms contribute to the total scattering intensity). This case is illustrated in Figure 2-2.

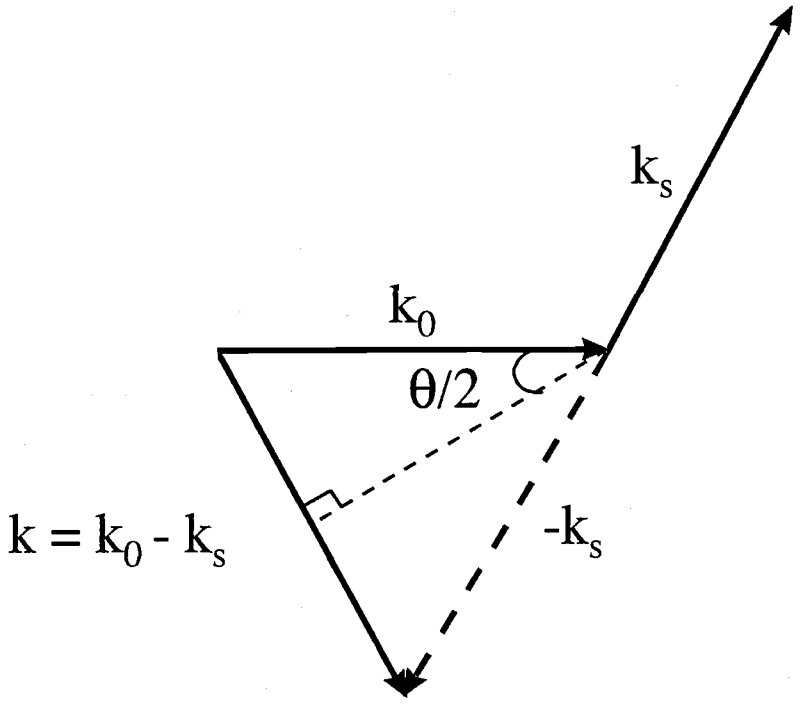

Figure 2-1 A plane wave propagating in a direction $\mathbf{n_0}$ with polarization ε_0, expressed as the wavevector $\mathbf{k_0}$, incident upon a particle scatterers in a direction $\mathbf{n_s}$ with polarization ε_s, expressed as wavevector $\mathbf{k_s}$.

This same number density dependence results if one takes into account the tensor properties of the polarizability in the ensemble averaging, i.e., if one considers non-spherical molecules. (The author is indebted to Professor Glenn Evans for an illuminating clarification of this point [1996]). If we assume that the induced dipole in one scatterer does not, in turn, induce a dipole in a neighboring particle, then we can write the polarizability as a sum over all scatterers j in the ensemble.

$$\alpha(\mathbf{k}) = \sum_{j}^{N} e^{i\mathbf{k}\cdot\mathbf{r}_j}\,\alpha_j \tag{2.15}$$

Here we include the phase factor of the scattered wave as part of the polarizability definition. For linear and other symmetric top molecules we can write the polarizability tensor for one scatterer j in terms of molecule fixed basis vectors **u**, **v**, and **w** where the unique axis points along **u**.

$$\alpha = \mathbf{uu}\alpha_{\parallel} + (\mathbf{vv} + \mathbf{ww})\alpha_{\perp} \tag{2.16}$$

where $\alpha_{\parallel}$ and $\alpha_{\perp}$ are the principal components of the molecular polarizability. The molecular polarizability can be rearranged as

$$\alpha = \overline{\alpha}\mathbf{I} + \Delta\alpha\mathbf{P}_2(\mathbf{u}) \tag{2.17}$$

where **I** is the unit tensor and

$$\overline{\alpha} = \left(\frac{1}{3}\right)(\alpha_{\parallel} + 2\alpha_{\perp}) \tag{2.18}$$

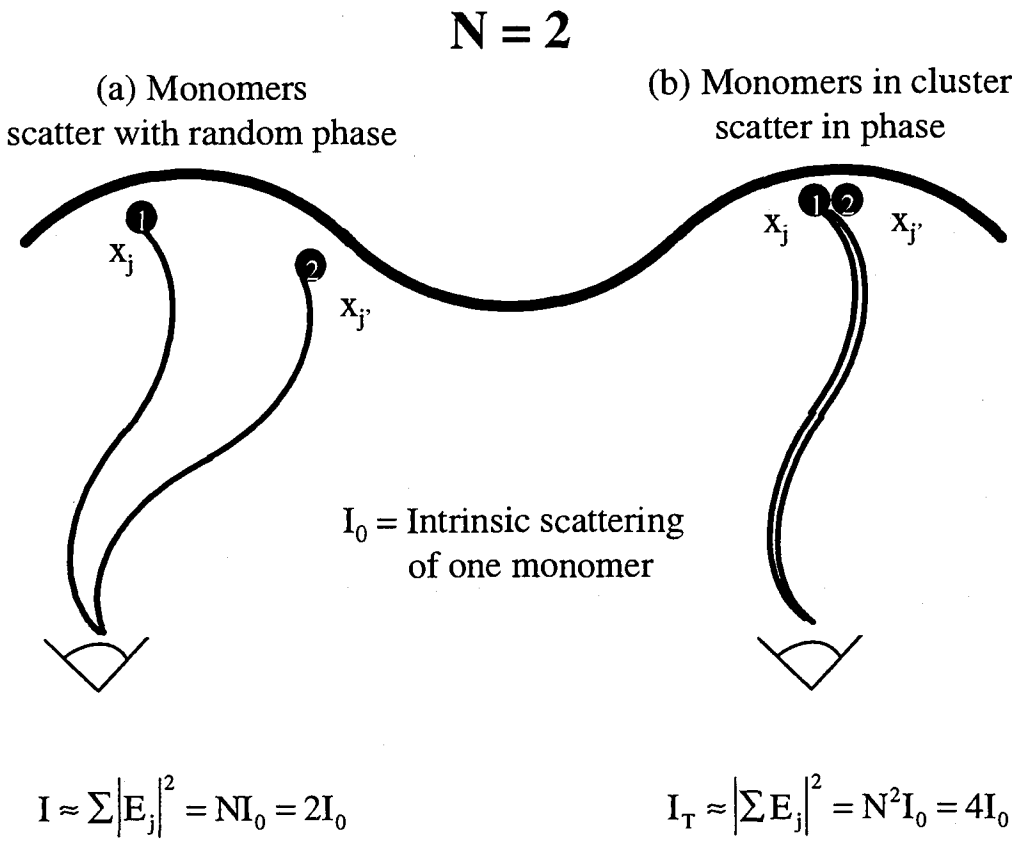

Figure 2-2 Rayleigh scattering intensity depends upon the particle size. This figure shows two possibilities when N = 2. (a) incoherent scattering by monomers 1 and 2. (b) coherent scattering by monomers 1 and 2 bound in a cluster.

$$\Delta\alpha = \left(\frac{2}{3}\right)(\alpha_{\parallel} - \alpha_{\perp}) \tag{2.19}$$

$$\mathbf{P}_2(\mathbf{u}) = \left(\frac{1}{2}\right)(3\mathbf{uu} - \mathbf{I}) \tag{2.20}$$

In this decomposition of α we have separated the isotropic part of polarizability $\overline{\alpha}$ from the fully anisotropic part represented by the vector generalization of the second Legendre polynomial, $\mathbf{P}_2$. $\mathbf{P}_2$ makes no contribution to the purely isotropic scattering and the isotropic part, measured by $\overline{\alpha}$, makes no contribution to the anisotropic (depolarized) scattering.

If incident radiation along the x-axis is polarized along the laboratory V = z axis then we define one scattering geometry as VV where the incident and scattered polarizations are parallel to each other and the other geometry as VH where the incident and scattered polarizations are perpendicular to each other. Within a proportionality constant, the scattered intensities measured along the y-axis are [Evans, 1996]

$$I_{VV} \approx \overline{\alpha}^2 \sum_{jj'} \left\langle e^{i\mathbf{k}\cdot\mathbf{r}_{jj'}} \right\rangle + \Delta\alpha^2 \sum_{jj'} \left\langle e^{i\mathbf{k}\cdot\mathbf{r}_{jj'}} P_2(\mathbf{u}_j \cdot \mathbf{z}) P_2(\mathbf{u}_{j'} \cdot \mathbf{z}) \right\rangle \tag{2.21}$$

$$I_{VH} \approx \left(\frac{3}{2}\right)^2 \Delta\alpha^2 \sum_{jj'} \left\langle e^{i\mathbf{k}\cdot\mathbf{r}_{jj'}} \mathbf{u}_j \cdot \mathbf{z}\mathbf{u}_{j'} \cdot \mathbf{z}\mathbf{u}_j \cdot \mathbf{x}\mathbf{u}_{j'} \cdot \mathbf{x} \right\rangle \tag{2.22}$$

The $\Delta\alpha^2$ coefficients involve the direction cosine between the unit vectors in the lab and molecule frames and, since the system is rotationally invariant, we can simplify these expressions by averaging over the orientations in the laboratory frame of reference, giving [Wilson, Decius and Cross, 1955]

$$I_{VV} \approx \bar{\alpha}^2 \sum_{jj'} \left\langle e^{ik\cdot r_{jj'}} \right\rangle + \left(\frac{1}{5}\right)\Delta\alpha^2 \sum_{jj'} \left\langle e^{ik\cdot r_{jj'}} P_2(\mathbf{u}_j \cdot \mathbf{u}_{j'}) \right\rangle \tag{2.23}$$

$$I_{VH} = \left(\frac{3}{20}\right)\Delta\alpha^2 \sum_{jj'} \left\langle e^{ik\cdot r_{jj'}} P_2(\mathbf{u}_j \cdot \mathbf{u}_{j'}) \right\rangle \tag{2.24}$$

The intensity of polarized scattered light due to the isotropic term $\bar{\alpha}^2$ is

$$I_{pol} = I_{VV} - \left(\frac{4}{3}\right) I_{VH} = \bar{\alpha}^2 \sum_{jj'} \left\langle e^{ik\cdot r_{jj'}} \right\rangle \tag{2.25}$$

As illustrated earlier for two particles, if $\mathbf{k} \cdot \mathbf{r}_{jj'} \approx 0$, the sum reduces to

$$I_{pol} = \bar{\alpha}^2 \sum_{jj'}^{N} 1 = N^2 \bar{\alpha}^2 \tag{2.26}$$

whereas if $\mathbf{k} \cdot \mathbf{r}_{jj'} >> 0$, the averaging process gives zero for cross terms.

$$I_{pol} = \bar{\alpha}^2 \sum_{j=j'}^{N} 1 + \bar{\alpha}^2 \sum_{j\neq j'}^{N} \left\langle e^{ik\cdot r_{jj'}} \right\rangle = N\bar{\alpha}^2 \tag{2.27}$$

The depolarized scattering is given by [Evans, 1996]

$$\begin{aligned} I_{dep} = I_{VH} &= \frac{3}{20}\Delta\bar{\alpha}^2 \sum_{jj'} \left\langle e^{ik\cdot r_{jj'}} P_2\left(\mathbf{u}_j \cdot \mathbf{u}_{j'}\right) \right\rangle \\ &= \frac{3}{20} N\Delta\alpha^2 \sum_{j'} \left\langle e^{ik\cdot r_{j'}} P_2\left(\mathbf{u}_j \cdot \mathbf{u}_{j'}\right) \right\rangle \equiv \frac{3}{20} N\Delta\bar{\alpha}^2 g_2(k) \end{aligned} \tag{2.28}$$

where g_2 is the light scattering g-factor, a measure of correlation of molecular orientations. For an ideal gas or for randomly ordered liquid clusters, $g_2 = 1$ so that the depolarized scattering will not show the strong N^2 dependence expected for the polarized

case. If however, the cluster is solid, with the relative orientation of all monomeric units fixed, the $P_2(\mathbf{u}_j \cdot \mathbf{u}_{j'})$ term of (2.28) will be constant and the averaging for $\mathbf{k} \cdot \mathbf{r}_{jj'}$ gives the same result as for the polarized case. The latter is the case expected for the solid CO_2 clusters examined in this study and, since we measure I_{VV}, we obtain the result that

$$I_{VV} = N^2\left(\overline{\alpha}^2 + \frac{3}{20}\Delta\overline{\alpha}^2\left\langle P_2\left(\mathbf{u}_j \cdot \mathbf{u}_{j'}\right)\right\rangle\right) \tag{2.29}$$

Note that if the clusters were liquid or amorphous, the second term would no longer give an N^2 dependence and would be negligible compared to the first. Thus, comparing the N dependence of the I_{VH} and I_{VV} experiments might be used to determine the extent of ordering in the clusters. This effect was not examined in our study of solid CO_2 clusters but this feature might warrant further investigation in future work on CO_2 and, especially, on other clusters where both liquid and solid forms are possible.

It is interesting to consider the limit when the density of the collection of clusters increases to the extent that one forms a macroscopic sample of liquid. Here the distance between individual particles is the same as that in a van der Waals cluster, yet the total scattering intensity becomes linear with respect to number density, as in a bulk liquid. This restoration of the gas-like N dependence results from the fact that the dimension of the collection of particles is now much larger than the wavelength of incident light, so that the averaging process for $\left\langle e^{i\mathbf{k}\cdot\mathbf{r}_{jj'}}\right\rangle$ necessarily gives zero. The sum of all constructively and destructively interfering waves, thus, gives rise to a total scattering intensity that is, effectively, just the sum of the scattering for each individual particle.

Of course, liquid or bulk solid samples exhibit density fluctuations that increase the scattering. The density fluctuations cause local groups of molecules or "cells" to have different polarizabilities because the dielectric constant for each cell changes. Assume a collection of scatterers in the liquid phase such that the total volume is much larger than the wavelength of incident radiation. If we imagine the collection divided into cells of equal volume such that the cell volume is large enough for fluctuations in neighboring cells to be independent, yet, small enough such that all parts of the cell scatter in phase then this high density collection will behave more like a dilute collection of van der Waals clusters.

Similarly, as one approaches the critical point from either the vapor or liquid side, the isothermal compressibility approaches infinity, density fluctuation became large, and the scattering intensity becomes very large—the condition known as critical opalescence. The Rayleigh result fails there because the effective length for the density fluctuations becomes greater than a wavelength [Jackson, 1975]. The conditions for seeing these latter effects are not met in our experiments so we ignore them in this work.

2.5 COHERENT ANTI-STOKES RAMAN SCATTERING

2.5.1 Historical Notes

In 1928, driven by a fascination with the opalescent blue color of the Mediterranean Sea, Chandrasekhara Venkata Raman discovered an inelastic scattering effect for which he received the Nobel Prize in physics in 1930 [Raman, 1928]. Raman

scattering is interesting because the wavenumber shift of the scattered light gives information about molecular transitions. Raman spectroscopy became extremely popular following the advent of the laser in 1960, since the high brightness of such sources made the weak scattering easier to observe. Since that time, many useful applications of Raman scattering have emerged.

Nonlinear Raman spectroscopy began with the discovery of stimulated Raman scattering by Woodbury and Ng [1962] and the observation of coherent anti-Stokes Raman scattering (CARS) by Maker and Terhune [1965]. Since that time, several excellent reviews have been written that explore the details of the technique and the interested reader will find descriptions of the fundamental theory and experimental methods in the literature [Bloembergen, 1977; Harvey, 1981; Hieftje, 1978; Levenson, 1988; Nibler, 1979; Nibler, 1988; Shen, 1984]. The following section provides a brief review of CARS since this method is part of our technique of combined Rayleigh scattering and CARS spectroscopy for the estimation of cluster size.

2.5.3 Stimulated Raman Scattering

While Rayleigh scattering results from an elastic collision of a photon with a particle, Raman scattering is the consequence of an inelastic collision. The process is inelastic because, for example, if the particle absorbs part of the energy of the incident photon, the scattered photon has less energy. When observed spectroscopically, this red-shifted photon corresponds to a Stokes transition. The anti-Stokes transition occurs when

the incident photon absorbs energy from the particle, producing a scattered photon of higher energy.

The Hamiltonian describing the interaction of an incident electric field with one scatterer is

$$H_{int} = -\mu_{ind} \cdot \mathbf{E}_{inc} \tag{2.30}$$

where μ_{ind} is the induced dipole moment operator, defined as

$$\mu_{ind} = \alpha \mathbf{E}_{inc} \tag{2.31}$$

We can expand this expression to include non-linear effects such that

$$\mu_{ind} = \alpha \mathbf{E} + \beta \mathbf{E}^2 + \gamma \mathbf{E}^3 + \ldots \tag{2.32}$$

where the coefficient α is the polarizability tensor of rank 2 and β and γ are the hyperpolarizability tensors of rank 3, and 4 respectively. Equivalently, the induced polarization, P, in the scatterer can be written as

$$\mathbf{P} = \chi^{(1)} \mathbf{E} + \chi^{(2)} \mathbf{E}^2 + \chi^{(3)} \mathbf{E}^3 + \ldots \tag{2.33}$$

where the $\chi^{(i)}$ are the dielectric susceptibility tensors of rank i +1 [Tolles and Harvey, 1981]. $\chi^{(1)} = \alpha$ is the dominant term for all normal optical interactions with matter. However, when the electric field is intense, terms involving $\chi^{(2)}$ and $\chi^{(3)}$ are no longer negligible and thus, can contribute to the polarization of the scatterer [Goyot-Sionnest and Shen, 1988]. $\chi^{(2)}$ is zero for isotropic samples such as liquids and gases. $\chi^{(3)}$ is the definitive term for all nonlinear Raman spectroscopy and has the form

$$\chi^{(3)} = \chi^{NR} + \sum_{i,f} \frac{c^4}{4\hbar\omega_2^4} \frac{N_i - N_f}{(\omega_3 - \omega_1 + \omega_2 - i\Gamma)} \left(\frac{d\sigma}{d\Omega}\right) \tag{2.34}$$

where χ^{NR} is the nonresonant electronic susceptibility, ω_1 is the fixed pump frequency, ω_2 is the Stokes frequency, ω_3 is the anti-Stokes frequency, N is the number density, Γ is the Raman transition linewidth, and $(d\sigma/d\Omega)$ is the differential Raman scattering cross section of the material [Tolles, et al., 1977]. The nonlinear mixing of the light waves with the sample yields the signal intensity relation

$$I(\omega_3) = k\left|\chi^{(3)}_{CARS}\right|^2 I(\omega_1)^2 I(\omega_2) \tag{2.35}$$

where $I(\omega_1)$ and $I(\omega_2)$ are the intensities of the incident beams and k is a collection of constants [Tolles and Harvey, 1981]. Since the CARS signal is the product of the intensities of the incident beams, using lasers of high peak power brought to a tight focus yields an intense signal from very dilute systems. In general, we gain the same information from stimulated Raman scattering as from spontaneous Raman scattering. However, the stimulated Raman signal is typically 10^5 times higher than the spontaneous Raman signal because, for CARS, the electric field amplitudes of the scattered photons are in phase and add coherently. There is, thus, an N^2 dependence for CARS but in this case, it is the same whether the sample is monomeric or in cluster form. Accordingly, the total CARS signal is nearly independent of the extent of clustering, whereas Rayleigh scattering is not.

2.6 MEAN CLUSTER SIZE FROM RAYLEIGH SCATTERING AND CARS SPECTROSCOPY

2.6.1 Combining Rayleigh Scattering and CARS Data

In Section 2.4.2, we showed that Rayleigh scattering scales quadratically with respect to number of units within a van der Waals cluster. Assuming a narrow size distribution, a mean cluster size can be deduced from the Rayleigh scattering intensity if a calibration can be made and if the fraction, f, of clusters in the scattering volume can be measured. The calibration can be done by measuring the scattering of a static sample of monomers at known density in the jet apparatus. If the CARS spectrum exhibits a significant frequency shift from the monomer to the cluster, f can be deduced from the relative intensities of the cluster and monomer peaks. The following equations develop an operational expression, using these assumptions.

We begin with the intrinsic scattering of a single monomer, I_0, which is related to the signal, I_s, measured at 90° by the relation

$$I_0 = \frac{I_s}{\rho_s V} \tag{2.36}$$

Here $\rho_s = n_s kT$ is the number density of monomeric scatterers in the sampled volume V, which is taken to be the laser focal volume viewed by the detector (a cylinder of about 0.1 mm diameter and 1 mm length; the precise volume is not important since it cancels out in the final expression). We assume that the same volume is viewed in the jet experiment and that the density is constant throughout the volume, an approximation that is very

good at large X/D (>3) and is reasonable even at smaller X/D values. For a jet expansion in which no clustering occurs, the Rayleigh signal will be $\rho_J V I_0$ where ρ_J is the number density of monomers at the X/D sampling point. ρ_J can be estimated from the usual isentropic expansion relation [Miller, 1988].

$$\rho_J = \frac{P_0}{RT_0}\left(\frac{T}{T_0}\right)^{\frac{1}{\gamma-1}} \tag{2.37}$$

where

$$\frac{T}{T_0} = \frac{1}{\frac{\gamma}{2}M^2} \tag{2.38}$$

The Mach number, M, is the velocity divided by the local speed of sound as a function of X/D, and is given by empirical expressions based on measurements for large scale jet expansions [Miller, 1985].

If clustering occurs, one extreme view is that the gas consists of mainly monomers plus some clusters all of a single size with each containing N_C monomer units. We term this the bimodal delta model. The total scattering intensity from the particles in such a jet is

$$I_J = \rho_m V I_0 + \rho_c V N_c^2 I_0 = n_m I_0 + n_c N_c^2 I_0 \tag{2.39}$$

Here, the total number of molecules in the volume V is assumed to be constant and to satisfy the relation

$$n_J = n_m + n_c N_c = \rho_J V = (\rho_m + \rho_c N_c)V \tag{2.40}$$

The cluster/monomer ratio is

$$f = \frac{n_c N_c}{n_m} = \frac{\rho_c N_c}{\rho_m} \tag{2.41}$$

and can be determined from the CARS spectra, thus,

$$\rho_J = \rho_m (1+f) \tag{2.42}$$

Combining (2.39), (2.40), (2.41), and (2.42) we obtain for the total Rayleigh scattering signal for the clustering jet

$$I_J = \rho_m V I_0 (1+fN_c) = \frac{\rho_J}{\rho_s} I_s \left(\frac{1+fN_c}{1+f} \right) \tag{2.43}$$

Rearranging, we get for the number of monomer units in the cluster

$$N_c = \left[\left(\frac{I_J \rho_s}{\rho_J I_s} \right) \left(\frac{1+f}{f} \right) \right] - \frac{1}{f} \tag{2.44}$$

N_c characterizes the mean cluster size. Note that the term "size" is used loosely here and can refer to N_c, volume, or diameter for the cluster. The diameter can be deduced from N_c since the average volume per molecule in solid CO_2 over a temperature range of 213 K to 140 K (density 1.58 g/cm^3) is 0.0462 nm^3, thus,

$$r_c \text{ (nm)} = \left[\frac{3 \times 0.0462 N_c}{4\pi} \right]^{1/3} = \left(\frac{N_c}{90.7} \right)^{1/3} \tag{2.45}$$

2.6.2 Effect of a Distribution of Sizes

Equation (2.44) provides a basis for combining Rayleigh scattering and CARS data to deduce a mean cluster size. However, the method assumes a bimodal delta size distribution for the clusters, which is clearly a gross simplification. As an improvement, we consider two simple models, a Gaussian and a log-normal distribution of clusters about a mean N_c. In the first case, the distribution is assumed to be random about the mean N_c value;

$$n_N = n_c e^{-\left(\frac{N-N_c}{a}\right)^2} \tag{2.46}$$

Here n_c is the number of clusters containing N_c units and the width of the distribution, a, in terms of half-width at half-maximum (HWHM) is

$$a = \frac{HWHM}{\sqrt{\ln 2}} \tag{2.47}$$

As before, we assume that an appreciable fraction of the jet will remain monomeric, i.e., a bimodal distribution, so that the total number of molecules in the sampled volume will be

$$n_J = n_m + \int n_N N\, dN = n_m + \int_2^\infty n_c N e^{-\left(\frac{N-N_c}{a}\right)^2} dN \tag{2.48}$$

We substitute the following variables into (2.48).

$$x = \frac{N-N_c}{a} \qquad N = ax + N_c \qquad dN = a\,dx$$

to obtain

$$n_J = n_m + n_c a\left[N_c \int_{-\infty}^{\infty} e^{-x^2}\,dx + a\int_{-\infty}^{\infty} x e^{-x^2}\,dx\right] \tag{2.49}$$

In this expression, little error results from the extension of the lower limit of integration from $x = \frac{2-N_c}{a}$ to $-\infty$ (assuming $N_c >> 2$) so that integration gives

$$n_J = n_m + n_c \sqrt{\pi}\, aN_c = n_m(1+f) \tag{2.50}$$

where the cluster/monomer ratio deduced from a CARS measurement is now

$$f = \frac{n_c \sqrt{\pi}\, aN_c}{n_m} \tag{2.51}$$

The Rayleigh intensity for such a distribution will be

$$I_J = n_m I_0 + \int n_N \left(N^2 I_0\right) dN \tag{2.52}$$

$$I_J = n_m I_0 + n_c I_0 a \int_{-\infty}^{\infty} \left(ax + N_c\right)^2 e^{-x^2} dx \tag{2.53}$$

$$I_J = n_m I_0 + n_c I_0 a \int_{-\infty}^{\infty} \left(a^2 x^2 + 2axN_c + N_c^2\right) e^{-x^2} dx \tag{2.54}$$

$$I_J = n_m I_0 + n_c I_0 a^3 \frac{\sqrt{\pi}}{2} + n_c a N_c^2 \sqrt{\pi} \tag{2.55}$$

Now let the width of the distribution a equal some fraction p of N_c ($a = pN_c$) giving

$$f = \frac{n_c \sqrt{\pi}\, p N_c^2}{n_m} \tag{2.56}$$

$$n_J = n_m + n_c \sqrt{\pi}\, p N_c^2 = n_m (1+f) \tag{2.57}$$

$$\frac{I_J}{I_0} = n_m + n_c p^3 N_c^3 \frac{\sqrt{\pi}}{2} + n_c p N_c^3 \sqrt{\pi} \tag{2.58}$$

$$\frac{I_J}{I_0} = n_m \left[1 + f \frac{p^2}{2} N_c + f N_c \right] = \frac{n_J}{1+f} \left[1 + f \frac{p^2}{2} N_c + f N_c \right] \tag{2.59}$$

$$\frac{I_J}{I_0 n_J} = \frac{I_J}{I_0 (\rho_J V)} = \frac{I_J}{\left(\frac{I_s}{\rho_s V} \right) (\rho_J V)} = \left(\frac{I_J \rho_s}{I_s \rho_J} \right) = \left[\frac{1 + f \left(\frac{p^2}{2} + 1 \right) N_c}{1+f} \right] \tag{2.60}$$

We see that (2.60) takes the same form as (2.43) but with the factor $1 + p^2/2$ to modify the N_c value deduced from (2.44).

A second model, the log-normal distribution, is commonly applied to particle sizes observed in droplet formation and also fits reasonably well the small cluster distributions reported by Gspann and Körting [1973]. This function assumes a normal distribution in ln N instead of N;

$$n_N = n_c \exp\left(-\left(\frac{\ln N - \ln N_c}{a} \right)^2 \right) \tag{2.61}$$

Here $a = \frac{HWHM}{\sqrt{\ln 2}}$ where HWHM is in terms of ln N. As before we assume a bimodal distribution with

$$n_J = n_m + n_c \int_2^\infty N \exp\left(-\left(\frac{\ln N - \ln N_c}{a}\right)^2\right) dN \tag{2.62}$$

Substitution of $z = \frac{1}{a}\ln\left(\frac{N}{N_c}\right)$ gives

$$\begin{aligned} n_J &= n_m + n_c N_c^2 a \int_{-\infty}^{\infty} \left(e^{az}\right)^2 e^{-z^2} dz \\ &= n_m + n_c N_c^2 a e^{a^2} \sqrt{\pi} = n_m(1+f) \end{aligned} \tag{2.63}$$

where the cluster/monomer ratio from CARS is

$$f = \frac{n_c N_c^2 a e^{a^2} \sqrt{\pi}}{n_m} \tag{2.64}$$

The Rayleigh intensity for such a distribution is

$$
\begin{aligned}
I_J &= n_m I_0 + \int_2^\infty n_N \left(N^2 I_0\right) dN \\
&= n_m I_0 + n_c I_0 N_c^3 a \int_{-\infty}^{\infty} \left(e^{az}\right)^3 e^{-z^2}\, dz \\
&= n_m I_0 + n_c I_0 N_c^3 a e^{\frac{9a^2}{4}} \sqrt{\pi} \\
&= n_m I_0 \left(1 + f N_c e^{\frac{5a^2}{4}}\right)
\end{aligned}
\tag{2.65}
$$

thus,

$$
\frac{I_J}{I_0 n_J} = \frac{I_J \rho_s}{I_s \rho_J} = \left[\frac{1 + f e^{\frac{5a^2}{4}} N_c}{1+f}\right] \tag{2.66}
$$

and, by comparison with equations (2.43) and (2.60), we see that

$$
N_c(\text{delta}) = N_c(\text{Gaussian})\left(1 + \frac{p^2}{2}\right) = N_c(\text{Log} - \text{Normal})\, e^{\frac{5a^2}{4}} \tag{2.67}
$$

From Gspann and Körting's data [1973] for small clusters, values of p ~ 1 or a ~ 0.75 give reasonable fits to the distributions. Thus, the correction factors are $1 + p^2/2 \approx 1.5$ and $e^{\frac{5a^2}{4}} \approx 2.0$ respectively. Within about a factor of two, the mean N_c value deduced is independent of the distribution model. Correspondingly, the cluster diameters are similar to within a factor of $2^{1/3} = 1.26$. For simplicity, in the remainder of this thesis, N_c and diameter values will be those calculated for the bimodal delta model.

2.6.3 Cluster Diameter from CARS Surface/Core Spectral Data

As a second method of deducing cluster size, we note that when clusters are small enough to have a measurable fraction of molecules on the surface, the CARS spectra can exhibit separate features for molecules in the interior and molecules on the surface. The intensities of these features give the relative number of molecules in the surface layer compared to the core and hence permit a calculation of cluster size. If we take the diameter of a single CO_2 molecule (0.44 nm) as a measure of the thickness of the surface layer, then the fraction of molecules on the surface of a cluster of radius r is

$$X_s = \frac{N_{Surface}}{N_{Total}} = \frac{r^3 - (r-0.44)^3}{r^3} = 1 - \left(1 - \frac{0.44}{r}\right)^3 \tag{2.62}$$

From this, we obtain the cluster size as

$$r(nm) = \frac{0.44}{1-(1-X_s)^{1/3}} \tag{2.63}$$

A comparison of sizes deduced from this relation with those from Rayleigh intensities was part of the objective of this work.

2.7 THE EXPERIMENT

2.7.1 Apparatus

Figure 2-3 shows the Rayleigh-CARS spectroscopy apparatus used for this experiment. The primary light source is a Quanta Ray DCR-1A Nd:YAG laser that produces an 8 ns, frequency-doubled output pulse at 532 nm. Single mode operation is induced by injection seeding with a Lightwave Electronics S-100 monolithic isolated end pumped ring (MISER) laser which gives a linewidth of 0.003 cm^{-1}. The Stokes pump source is a Lumonics Hyperdye 500 dye laser. The resolution is determined by the grating in the laser cavity which has 2400 grooves/mm and is used in 5^{th} order. This configuration produces a linewidth of 0.04 cm^{-1}, as confirmed by a linewidth measurement of an I_2 transition. The injection seeding scheme and multimode shot rejector have been described elsewhere [Yang, 1990].

The 532 nm output beam is split by a dichroic mirror with 1/3 of the power used for the CARS ω_1 beam and the remaining power is used to pump the dye laser which provides the ω_2 or Stokes pump beam. As shown in Figure 2-3, a spatial delay of the ω_1 beam of ~8 ns was needed in order to overlap the two ω_1 beams and the ω_2 beam in time. All beams are combined in a folded BOXCARS arrangement [Eckbreth, 1978] and the ω_1 signal beam was spatially filtered prior to further discrimination by a 532 nm holographic filter (not shown) and a McPherson 218 0.3 m dispersive monochromator. The CARS signal is detected with an RCA 31034A photomultiplier tube and averaged with an SRS

Model SR250 gated integrator. The signal is averaged over 10 shots, stored and displayed using a Microsoft Visual Basic program written by Mr. Mikhail Orlov.

The Rayleigh scattering detector was mounted 90° to the laser crossing axis outside of the vacuum chamber (not shown). It consisted of a Nikon 50 mm, 1:1.2 camera lens with an aperture adjustable from f/1.2 to f/22, a filter holder (for neutral density filters), a polarizer, a spatial filter, and an RCA 1340 photomultiplier tube. The small laser crossing section was the source of the intense Rayleigh scattering imaged onto the detector. The I_{VV} signal was taken simultaneous with the CARS signal, with all Rayleigh measurements during the CARS scan averaged and recorded as a single number.

2.7.2 Method

Clusters were formed in a supersonic jet apparatus (shown in Figure 2-4) that has been described elsewhere [Pubanz, 1986]. The nozzle used for this experiment had an orifice diameter of 0.3 mm and a thickness of 0.3 mm. It was mounted in a dewar assembly, cooled by a cold air stream, and pulsed at 10 Hz with a pulse width of ~300 μs which, after about 10 μs, approximates a continuous flow.

The combined Rayleigh-CARS data were taken as a function of distance X from the nozzle and measured in units of X/D. Many experiments were done but the results presented here are for three sets of data taken for neat CO_2, 12% CO_2/He, and 5%

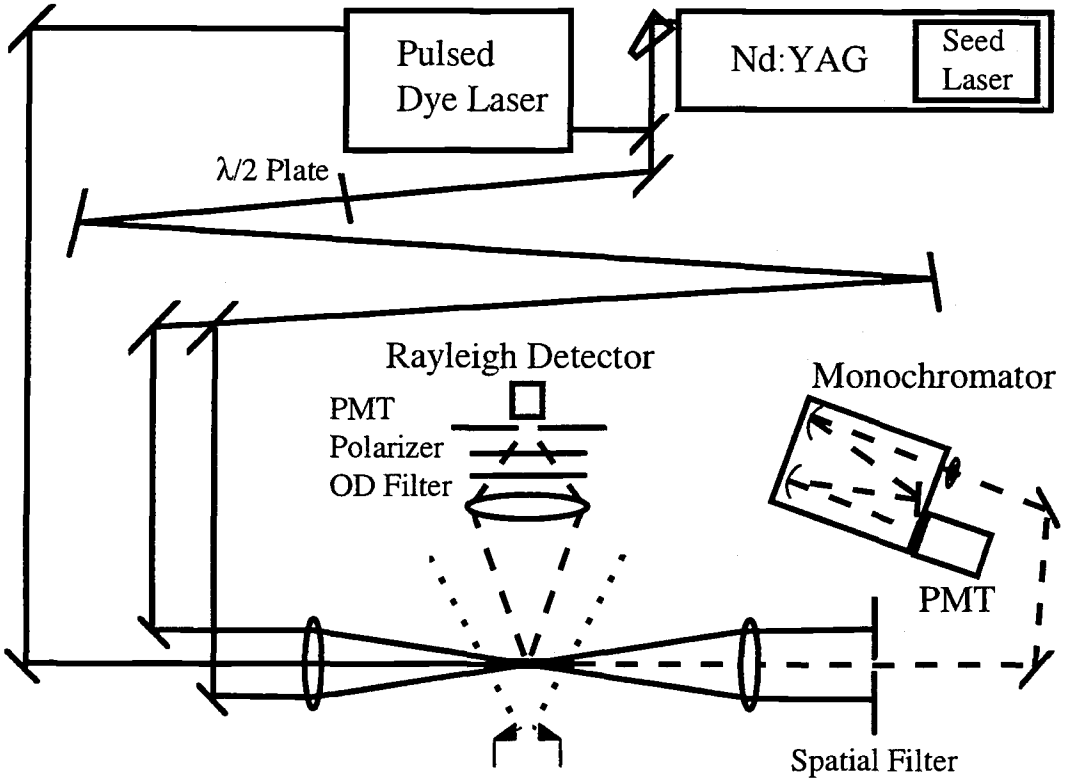

Figure 2-3 The Rayleigh-CARS spectroscopy apparatus.

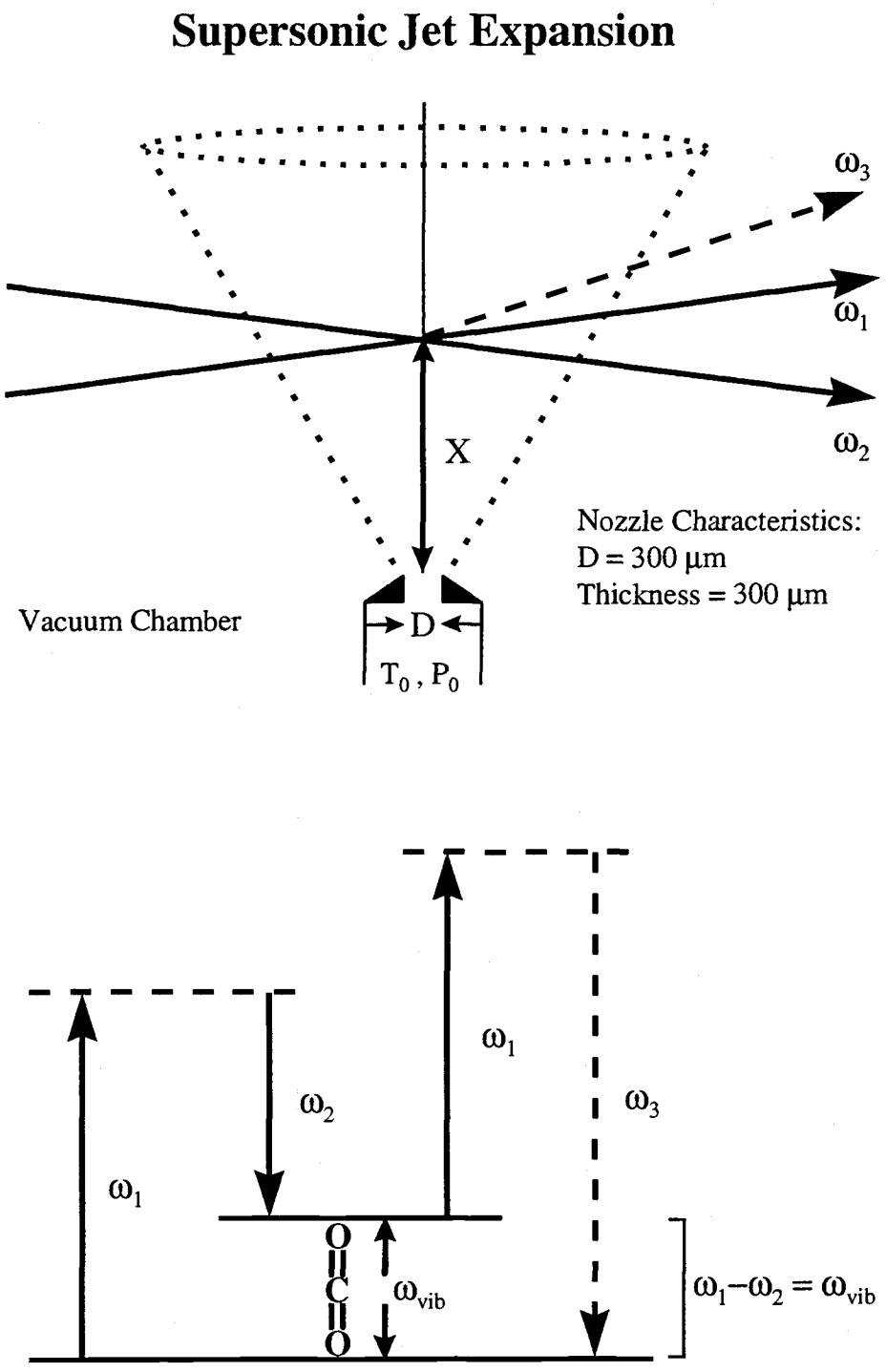

Figure 2-4 Supersonic jet expansion showing the CARS beams crossing and the levels involved in the CARS process.

CO_2/He expansions. The nozzle driving pressure, P_0, was held constant for all three experiments and the nozzle temperature, T_0, was varied slightly to achieve optimum cluster formation. In addition, one experiment was done using only Rayleigh scattering to characterize the jet profile of an expansion of neat CO_2 as a function of Z/D, where Z is perpendicular to both X and the laser beam propagation axis Y. This experiment served to locate the centerline of the jet expansion for optimal positioning of the nozzle relative to the laser and detector.

2.8 RESULTS AND DISCUSSION

2.8.1 Radial Density Distribution

In addition to giving an estimate of cluster sizes, Rayleigh intensities can provide information about the spatial characteristics of a jet expansion. For example, Figure 2-5 shows Rayleigh intensities at constant X/D as a function of Z/D, thus, giving a measure of the radial density distribution of a condensing jet expansion. The experimental conditions were P_0 = 2400 kPa, T_0 = 260 K, and nozzle diameter = 0.3 mm. The dashed lines show the predicted density distribution if the expansion is not condensing. This distribution is given by

$$\rho(\theta) = \rho_0 \cos^2\theta \cos^2\left(\frac{\pi\theta}{2\phi}\right) \tag{2.64}$$

where

$$\theta = \arctan\left(\frac{Z/D}{X/D}\right) \tag{2.65}$$

ϕ is an empirical parameter which increases as the heat capacity of the molecule increases and ρ_0 is the density at the nozzle opening [Miller, 1988]. For the case of an isentropic expansion of CO_2 without condensation, ϕ = 1.662, and the predicted distributions are shown in the Figure 2-5. The full cone angle at which the monomer density drops 50% is 68°.

We observe that the experimental intensity for a clustering jet shows localization more near the center line of the jet expansion. The full cone angle in this case is reduced to 34°—a factor of two. This effect is due to cancellation of the transverse velocity components of the condensing molecules, thus, concentrating the clusters on axis. The parameter ϕ was empirically adjusted to fit (2.64) to the cluster data of Figure 2-5, yielding values of ϕ = 0.7, 0.55 and 0.49 for clusters at X/D = 8.6, 21 and 32, respectively. These smaller values of ϕ are consistent with the reduced heat capacity per molecule when condensation occurs.

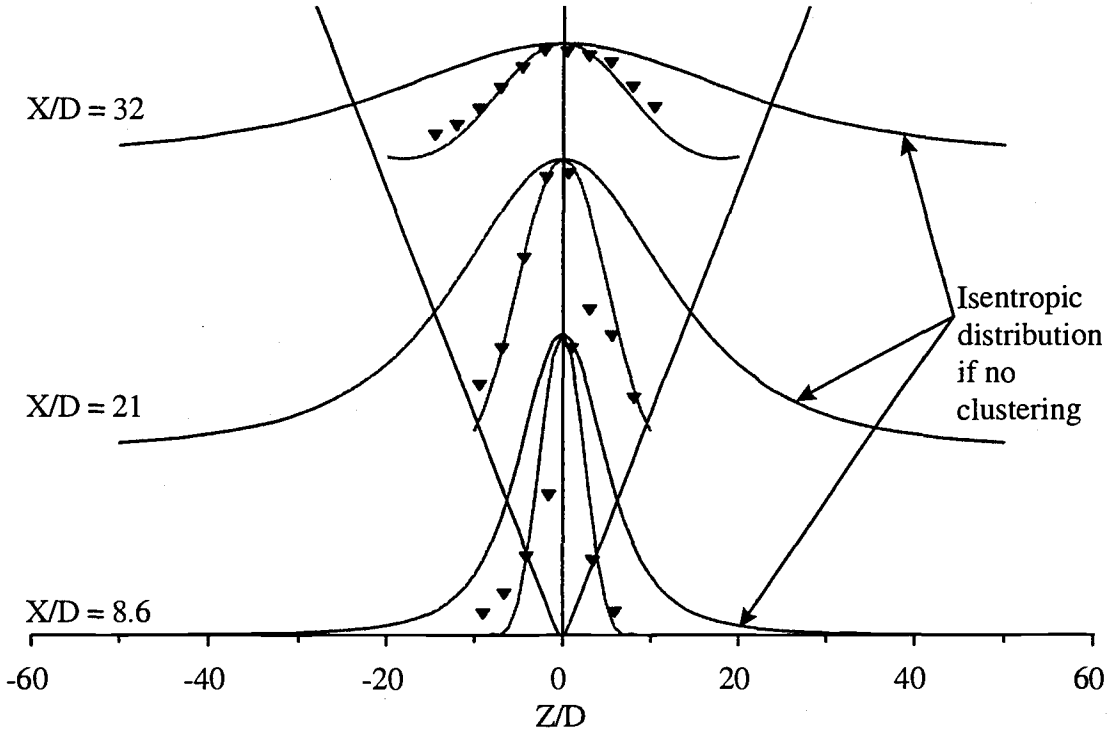

Figure 2-5 Radial density distribution in a supersonic jet expansion of neat CO_2 compared with the predicted curves for isentropic expansions with initial conditions P_0 = 2400 kPa, T_0 = 260 K, and nozzle diameter = 0.3 mm. The vertical axis is not to scale; the full cone angle is ~ 34° and 68° for the clustering and non-clustering curves, respectively.

2.8.2 Onset of Cluster Formation

The CO_2 clusters studied in this work were formed in a supersonic jet expansion, which has the effect of cooling a gas below its saturation point—the condition necessary to stimulate nucleation. Figure 2-6 shows the isentropes of a non-condensing gas in a jet on a logP-logT plot [Farges, 1975; Hagena, 1981]; such a display provides a useful visual representation of the expansions studied in this work. The jet begins expanding at point $A(P_0, T_0)$ which, in the case for the three CO_2 expansions described later, begins in the gas phase region. Upon the nozzle opening, the expansion continues along the isentrope to some point B, where the nucleation rate is large. At this point, condensation occurs and the pressure and temperature of the monomeric gas will deviate from those in an isentropic expansion. The newly-formed cluster will be warmer than the background gas (due to heat of condensation) and will be at a temperature corresponding to some point on the solid-gas coexistence curve $P_v(T)$ (or to an extrapolation of the liquid curve into the non-equilibrium super cooled regime).

Also shown in Figure 2-6 is a dashed vertical line describing initial expansion points for a Rayleigh scattering experiment which yielded information about the clustering onset point. Figure 2-7 shows the result on the Rayleigh intensity of gradually increasing P_0 at X/D = 5.4 and T_0 = 298 K. The interesting characteristic of this data set is the dramatic increase in scattering intensity at approximately 2200 kPa, where the intensity

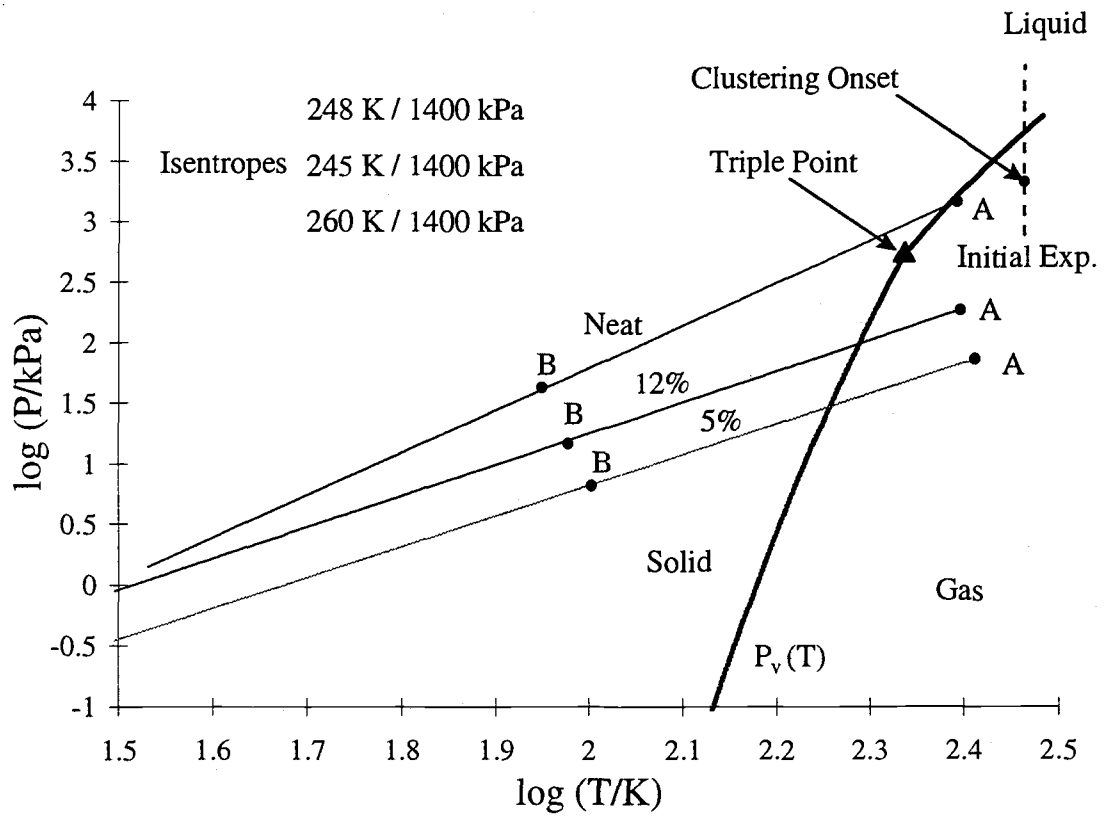

Figure 2-6 The isentropes of three expansion conditions compared with the solid-gas and liquid-gas coexistence curves on a logP-logT plot. In addition, the vertical dashed line shows the locus of initial P_0 choices for the T_0 expansion of Figure 2-7.

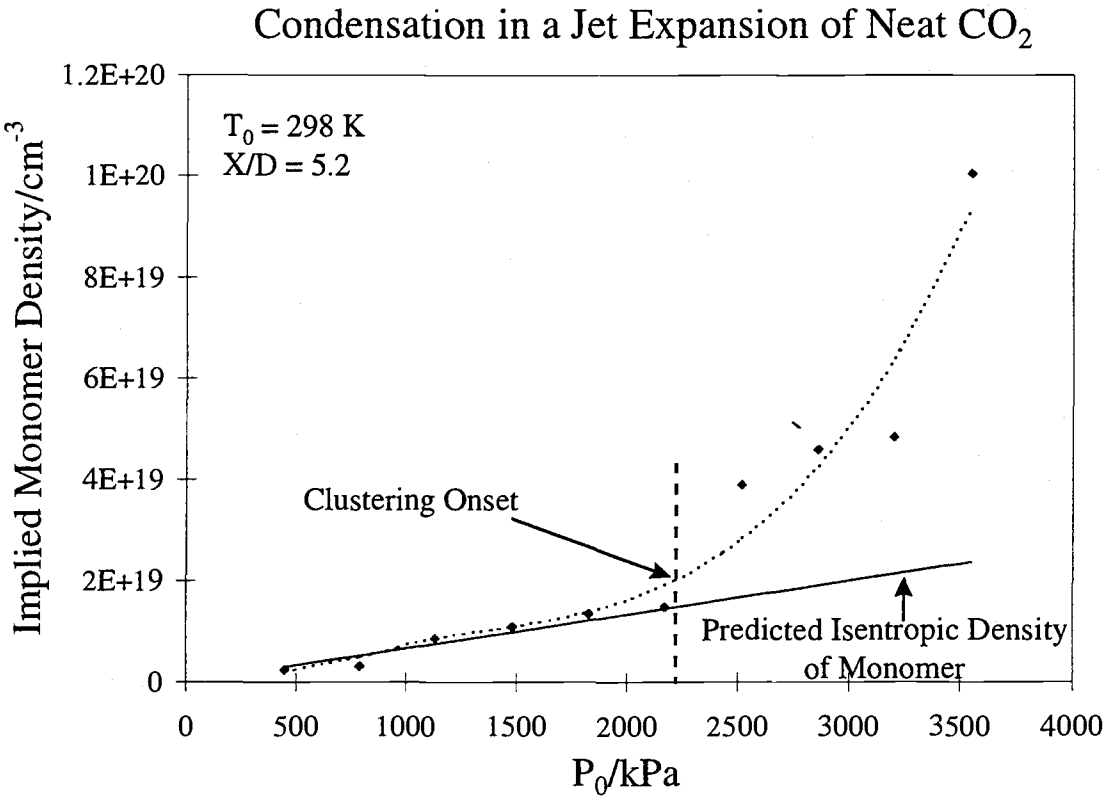

Figure 2-7 The effect of increasing the initial pressure behind the nozzle. The solid line shows the linear density relation predicted for an isentropic expansion. The vertical axis shows the density implied by the I_{VV} Rayleigh intensity if no clustering is assumed.

deviates from the linearity expected for a non-condensing jet. This point corresponds to the onset of clustering in the jet. As the pressure increases, the jet produces larger clusters which gives a greater positive slope; a direct result of the quadratic dependence of Rayleigh scattering on cluster size.

The y-axis displays a quantity, the *Implied Monomer Density*, which is a conversion of the measured Rayleigh scattering intensity I_s into a gas density value corresponding to that expected if only monomers were present in the jet. This is done by dividing I_J by the intrinsic scattering, I_0, of a single monomer, a quantity measured for the apparatus by filling the cell to a known static pressure of CO_2. For jet expansions with low P_0 values, the densities deduced from the Rayleigh intensities are in good accord with those calculated from the usual density expression (2.37) for an isentropic expansion of monomers. However, the values calculated from the intensities for P_0 greater than 2200 kPa reveal that the CO_2 has condensed into clusters and that the cluster size or concentration of clusters, or both, increase with pressure.

Rayleigh scattering gives a clear indication of the onset of clustering in jet expansions. At P_0 values greater than the onset value or at lower T_0 values, dramatic increases in scattering occur. For example, Figure 2-8 compares the expansion shown in Figure 2-7 with a more strongly condensing expansion over the same P_0 range, but at a reduced T_0 = 263 K. Note that the density is plotted on a log axis in this figure. It is remarkable that, under the more severe expansion conditions, the jet yields a strongly condensing expansion in which the implied monomer density differs from the isentropic density prediction by seven orders of magnitude! This pronounced nonlinearity for

Rayleigh scattering by clusters was exploited in the analysis shown in the figures below for the three main experiments.

Finally, we note that a check on the actual monomer density predicted by (2.38) for a non-condensing jet is possible using the CARS intensities measured as a function of X/D. Conversion of these to densities is done by measuring CARS signals for static samples of known density. Figure 2-9 shows the calculated monomer density for a non-condensing jet as a function of X/D, assuming an isentropic flow, ideal gas behavior, constant C_p, and continuum flow and the empirical expressions of Miller [1988] for the Mach number M. The generally good agreement between the calculated and measured monomer densities is worth stressing since it validates the use of the isentropic relations in our analysis of cluster sizes. Furthermore, we can accurately establish the 0 X/D position by matching the data with the theoretical curve in the X/D dimension.

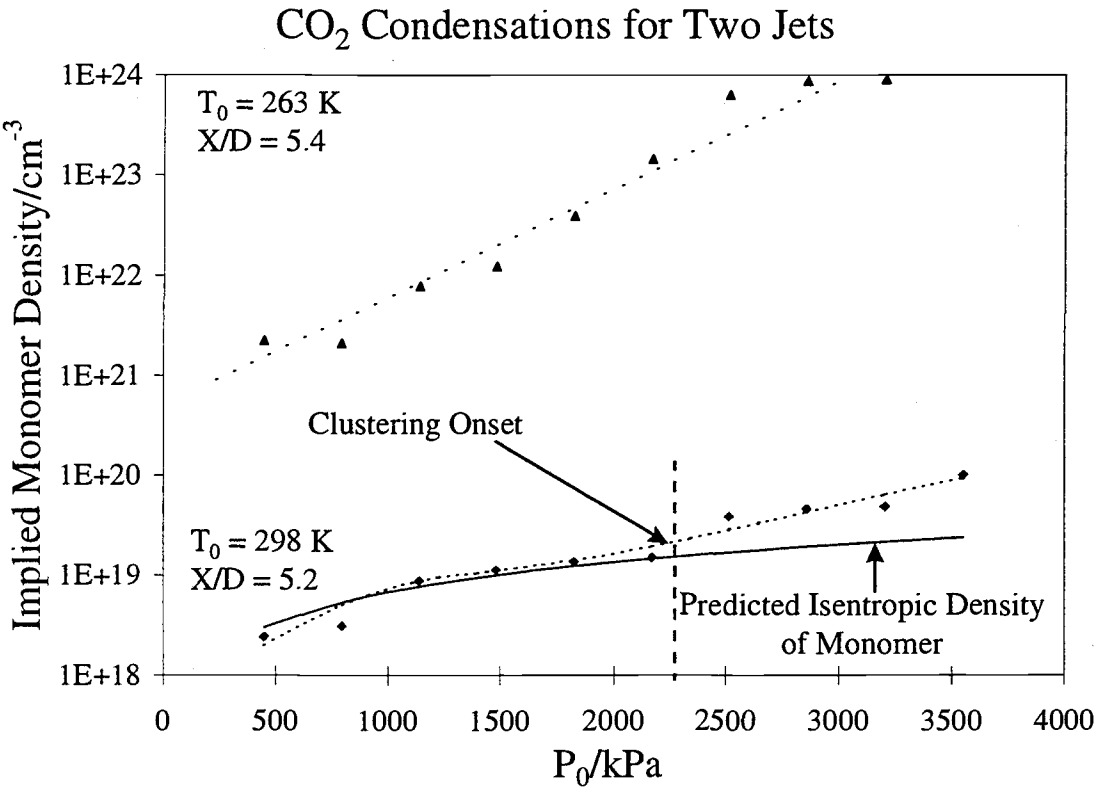

Figure 2-8 Strongly condensing expansion compared with weakly condensing expansion from Figure 2-7. The solid line shows the density predicted for a non-condensing jet for T_0 = 298 K. The corresponding curve for T_0 = 263 K is almost indistinguishable.

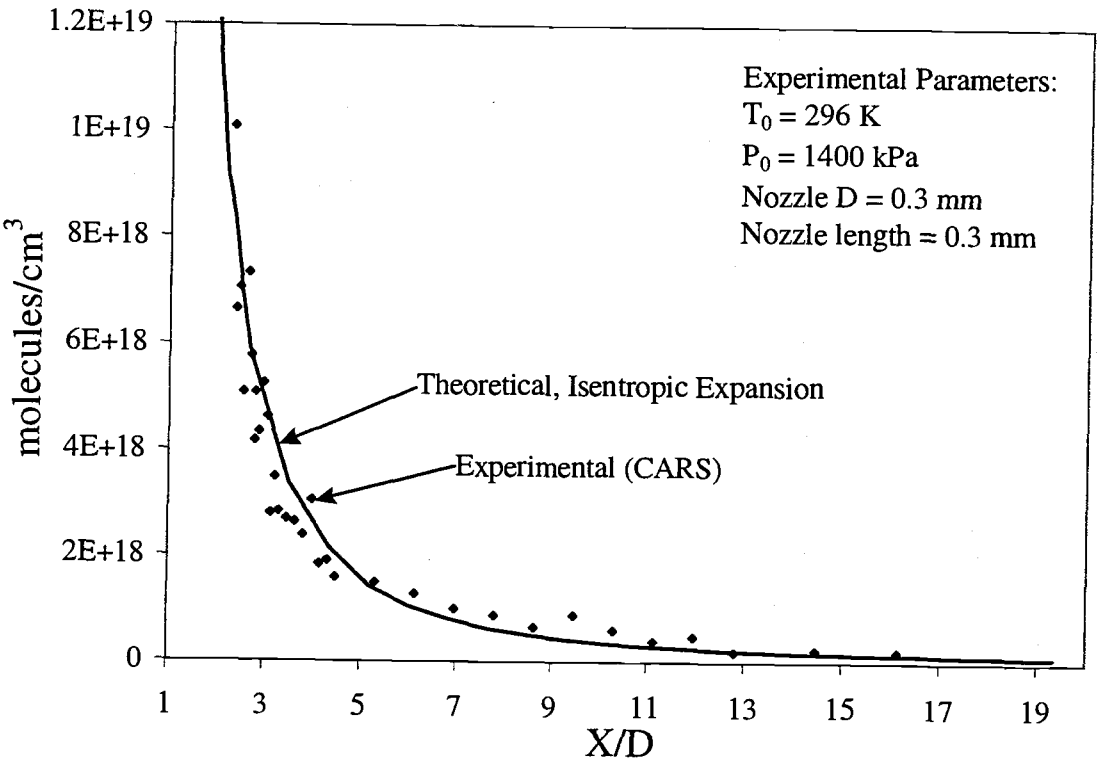

Figure 2-9 The relative monomer density in a non-condensing jet as a function of X/D exactly follows an isentropic expansion. Since the exact X/D = 0 reference point is poorly defined, an increment, Δ was added to the measurement X/D values and varied to best match the experimental data to the isentropic curve, yielding $\Delta = 1.8$.

2.8.3 Rayleigh-CARS Data: Neat CO_2 Study

Figure 2-10 shows CARS spectra of the lower wavenumber member of the $\nu_1/2\nu_2$ Fermi resonance diad of CO_2. The data are displayed for several X/D positions in a neat jet expansion for which $T_0 = 248$ K and $P_0 = 1400$ kPa. The monomer Q branch appears at about 1285.46 cm^{-1} and the cluster peak at about 1276 cm^{-1}. From the relative intensities, the extent of clustering is about 25%. Several spectra were taken over a range of X/D positions and Table 2-1 summarizes the peak positions, Rayleigh intensities, CARS peak areas, cluster fraction, and size results. Note that CARS peaks areas were not measured for some X/D positions. Because the cluster/monomer ratio was reasonably constant with X/D, the average ratio of $f = 0.41$ was used in all N_c calculations.

By combining the Rayleigh data and CARS data according to (2.44), we deduce the mean cluster size from (2.45). Figure 2-11 gives the mean cluster diameter in nm as a function of X/D and we see that the clusters appear to grow and fluctuate in the $X/D \leq 8$ region and level off at about a diameter of 12.4 ± 0.7 nm. Such a cluster contains about 23,000 monomer units.

It is interesting to compare this N_c value with that predicted from the empirical scaling "laws" of Hagena and Obert [1972]. In section 2.3.1 we combined these scaling "laws" with the electron diffraction data of Torchet, et al. [1984] to give an expression (2.3) for the number of molecules per cluster, i.e.,

Jet Position	ρ_J		Peak Area $(Area)^{1/2}$	$(Area)^{1/2}$	Peak Position				Cluster Diameter
X/D	molecules/cm^3	Rayleigh I	Monomer	Cluster	Monomer	Cluster	T_c/K	N_c	nm
2.0	1.39E+19	8301	1.01	0.34	1285.453	1276.95	213	1522	5.1
2.1	1.28E+19	70757	1.04	0.52	1285.452	1277.04	218	14192	10.8
2.2	1.08E+19	124171	0.88	0.40	1285.448	1276.85	206	29438	13.7
2.4	9.23E+18	142408	0.80	0.22	1285.443	1276.84	205	39464	15.2
2.6	7.98E+18	147574	0.86	0.38	1285.439	1276.80	202	47332	16.1
2.7	6.96E+18	122723	0.86	0.43	1285.435	1276.79	202	45154	15.9
2.9	6.11E+18	110844			1285.432	1276.33	162	46416	16.0
3.1	5.41E+18	100925			1285.43	1276.33	162	47755	16.2
3.4	4.32E+18	67940	0.97	0.34	1285.426	1276.32	161	40284	15.3
4.2	2.68E+18	34322	0.79	0.34	1285.421	1276.25	154	32818	14.3
5.9	1.31E+18	11380			1285.416	1276.22	151	22274	12.5
7.6	7.70E+17	8160			1285.414	1276.12	140	27129	13.4
9.2	5.06E+17	5481			1285.413	1276.11	139	27720	13.5
10.9	3.58E+17	2875			1285.413	1276.11	139	20573	12.2
12.6	2.66E+17	2427			1285.412	1276.11	139	23344	12.7
14.2	2.06E+17	1841			1285.412	1276.00	127	22905	12.6
15.9	1.64E+17	1356			1285.411	1276.02	129	21200	12.3
17.6	1.33E+17	1088			1285.411	1275.92	117	20867	12.3

The intrinsic scattering for a monomer, I_0, measured for a static sample at 1 atm was 1.34E-18 cm^3 molecules^{-1}

These data are from spreadsheets: CO2 Size and CO2 neat 296. The X/D position has been corrected by addition of $\Delta = 1.8$ based on the density calibration discussed in the text.

Table 2-1 Summary of Rayleigh-CARS Neat CO_2 Experimental Results.

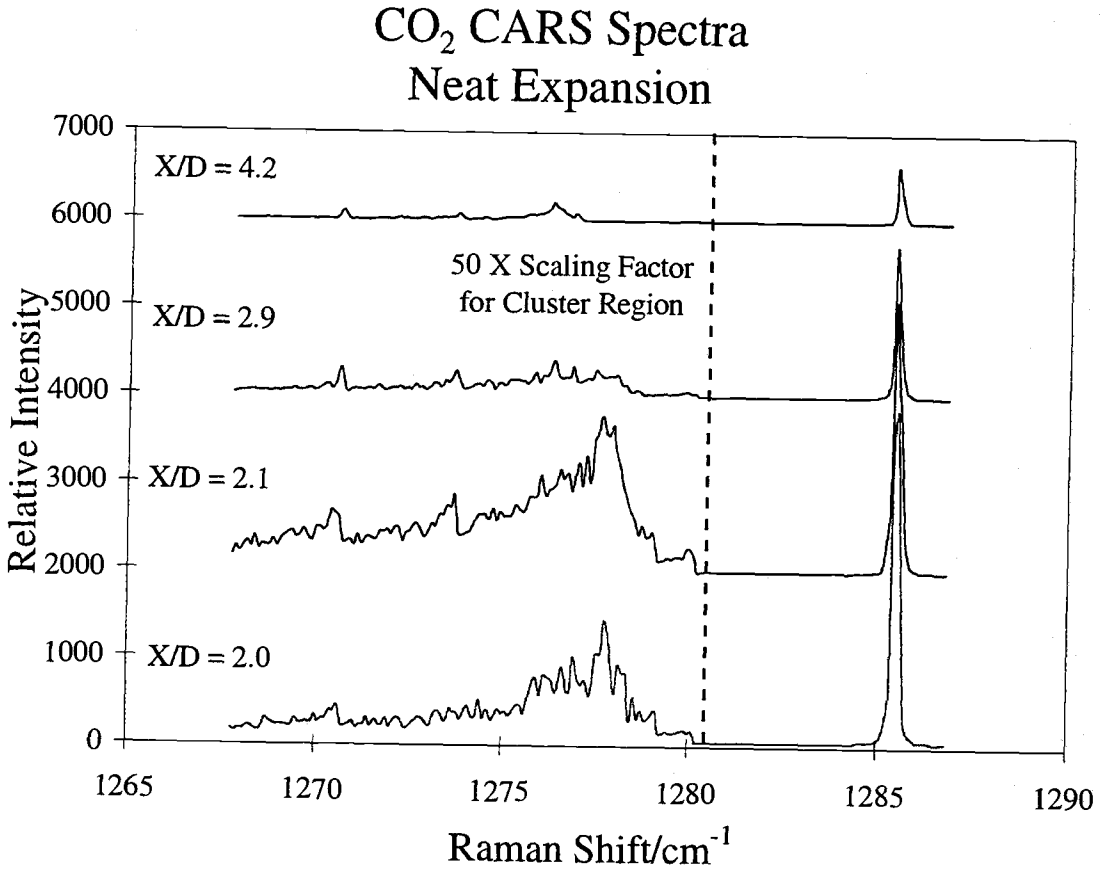

Figure 2-10 CARS spectra of the lower wavenumber member of the $\nu_1/2\nu_2$ Fermi resonance diad of CO_2. The data were taken for a neat free jet expansion at T_0 = 248 K and P_0 = 1400 kPa. The monomer Q branch appears at 1285.46 cm^{-1} and the cluster peak at about 1276 cm^{-1}. Small, regular features due to O_4, O_6, and O_8 lines of the monomer are also seen.

$$\log N_c = a \log\left[P_0 \left(\frac{T_0}{295}\right)^{-25/8} \left(\frac{D}{0.15}\right)^{0.6} \right] + b$$

To deduce the value of a for neat expansions, we use the mass spectral results given in Figure 5 of Falter, et al. [1970], obtaining a = 2.67. We note that this is in reasonable accord with values of a = 2.2 to 2.4 cited by Torchet, et al. [1984, 1996]. In application, the relation involves scaling by T_0 and nozzle diameter to account for deviations from the conditions used in the initial experiment, namely, T_0 = 295 K and nozzle diameter D = 0.15. Our experimental conditions were T_0 = 248 K and D = 0.3 mm. Equation (2.3) then predicts that our conditions should give a mean cluster diameter of 11.3 ± 1.3 nm in remarkable agreement with our Rayleigh-CARS result of 12.4 ± 0.7 nm for large X/D. Alternatively, our results can be scaled to the P_0 value appropriate to the conditions of Falter, et al. [1970] (T_0 = 295 K, D = 0.15 mm). Figure 2-12 displays a line predicted using this data along with two sets of electron diffraction results by Torchet, et al. [1984, 1996], and our Rayleigh-CARS result for the neat CO_2 expansion. A second point from a similar expansion using the separate apparatus described in Chapter 3 is also shown. The slopes of the two sets of electron diffraction data are the same as predicted by the scaling law but there seems to be some systematic offset. Overall, all the results shown in Table 2-2 agree well with the predictions of the scaling "laws" and offer reassurance that they can be used for cluster sizes varying over four orders of magnitude.

Another independent size estimate can be obtained from the cooling curve calculated for the neat expansion of CO_2 using the method described in detail elsewhere [Richardson, 1993]. The cooling curve method has several limitations,

	Mass Spectral Data		Electron Diffraction Data				This Work			
T_0	295 K		295 K		295 K		248 K		265 K	
D	0.15 mm		0.40 mm		0.10 mm		0.30 mm		0.30 mm	
	P_0/kPa	N	P_0/kPa	N	P_0/kPa	N	P_0/kPa	N	P_0/kPa	N
	1000	449	357	87	1364	604	3850	22000	3129	35311
	1093	569	539	197	1801	1106				
	1193	721	1077	1070	2873	2584				
	1291	900	2702	8000	3413	4196				
	1389	1147								
	1487	1300								
	1585	1505								
	1680	1800								

Table 2-2 Comparison of mean size data from mass spectrometry, electron diffraction and our Rayleigh-CARS method for CO_2 clusters formed in a neat supersonic jet expansion.

however; three body collisions and cluster coalescence are not accounted for in the method, therefore, it is unreliable at X/D positions less than about 5. It is also extremely sensitive to the absolute temperature of the clusters, the determination of which is difficult since it is dependent upon an accurate frequency measurement of the cluster peak position. The cluster peak is broad and noisy which makes this measurement difficult. The method is also sensitive to the sticking fraction which is the percentage of molecules that collide with the cluster and actually stick. For an estimate of 5%, several curves were calculated, as shown in Figure 2.13. A rough cluster diameter determined by this method was ~20 nm, which is in reasonable agreement with the values of 13 nm deduced from both the Rayleigh-CARS and scaling "laws".

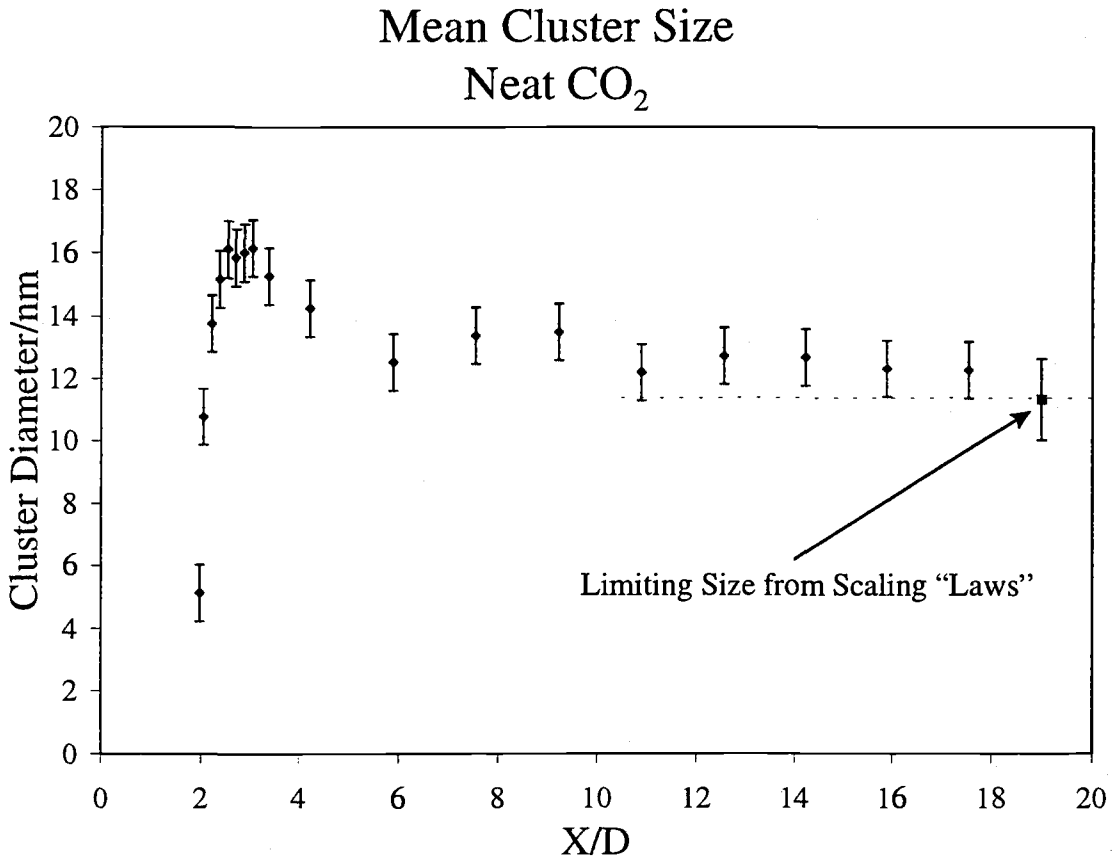

Figure 2-11 The mean cluster diameter as a function of X/D for an expansion of neat CO_2. The error bars derive from estimates of the uncertainties in the CARS peak areas. The limiting size predicted by scaling "laws" is indicated to the right; the error bar here is an estimate based on uncertainties in measurement of P_0 and T_0.

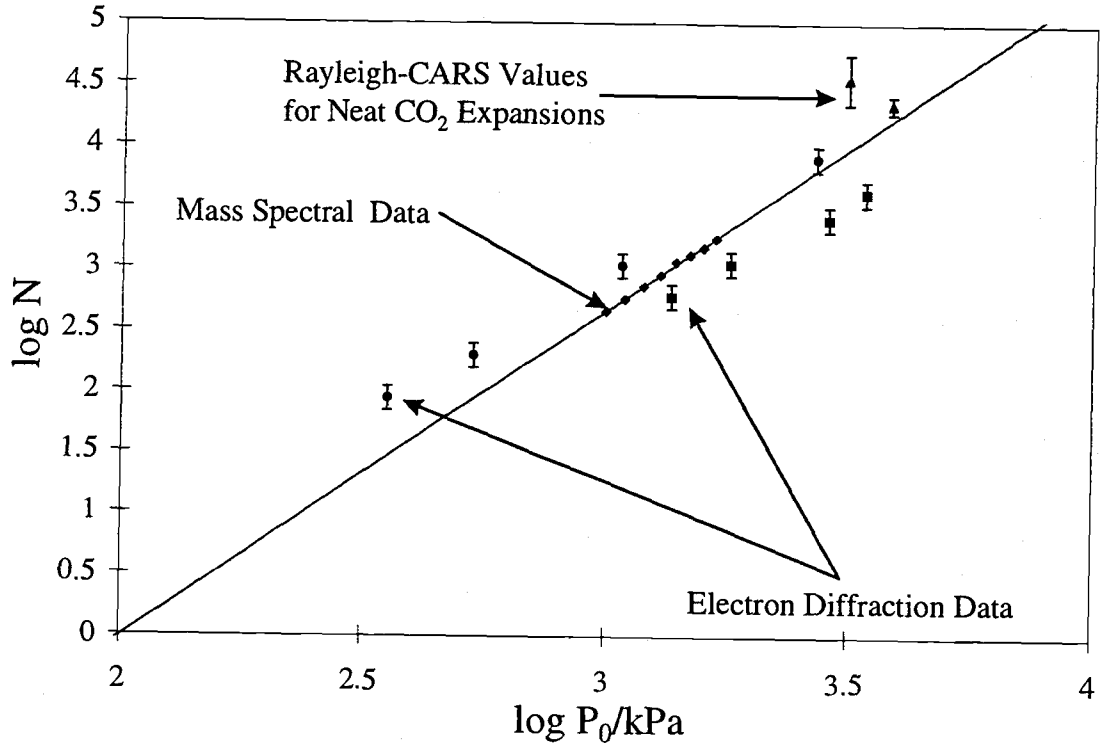

Figure 2-12 The scaled curves are fits of (2.3) using the data of Falter [1970]. The electron diffraction measurements are from Torchet, et al. [1984 and 1996]. Our Rayleigh-CARS results for two neat CO_2 expansions are superimposed on the fit of (2.3). All data points are scaled to T_0 = 295 K and D = 0.15 mm used by Hagena and Obert [1972] for the original mass spectral data. Note that our new results extend the useful size range of the scaling "laws" by an order of magnitude!

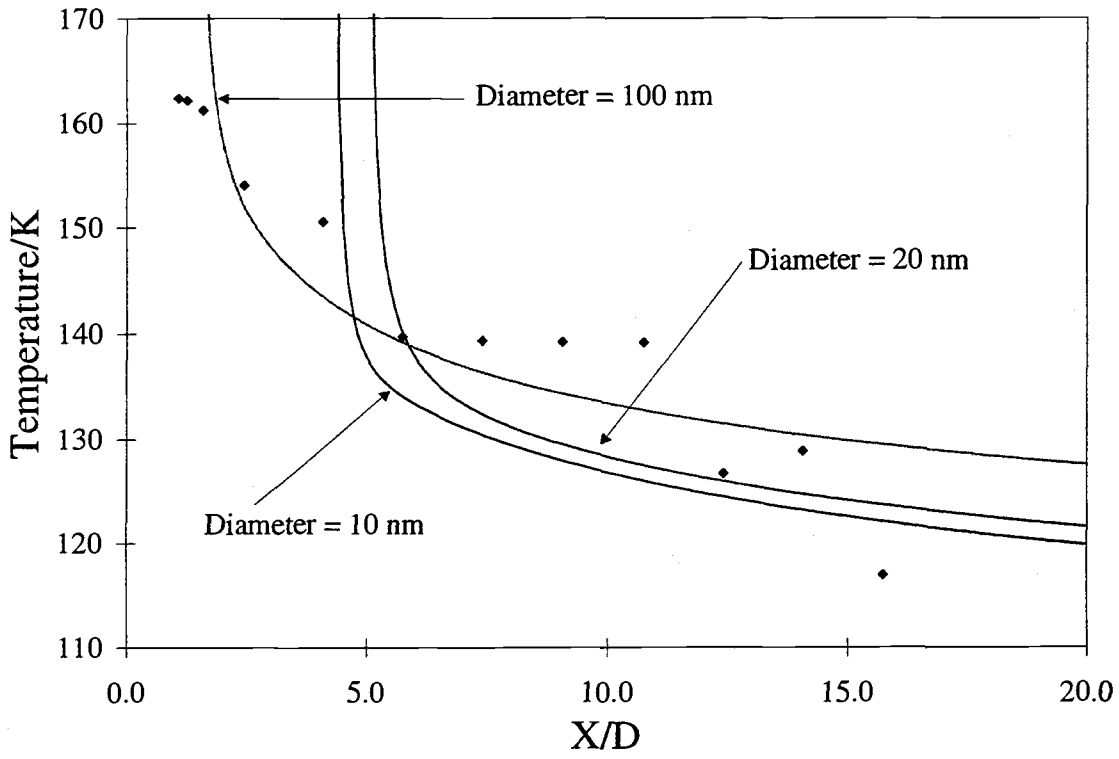

Figure 2-13 The cooling curves for a neat CO_2 expansion.

2.8.4 Rayleigh-CARS Data: 12% CO_2 in He Study

Dilute expansions are often used to produce colder and, usually, smaller, clusters. Figure 2-14 shows CARS spectra for several X/D positions in a 12% CO_2/He jet expansion for which $T_0 = 245$ K and $P_0 = 1400$ kPa. As for neat samples, the monomer Q branch appears at 1285.46 cm^{-1} and the cluster peak at about 1276 cm^{-1}; a new feature is also seen as a small peak at 1279 cm^{-1}. Several spectra were taken over a range of X/D positions and Table 2-2 summarizes the peak positions, Rayleigh intensities, CARS peak areas, cluster fraction, and size results. Though the density of CO_2 in the jet is less than that of the neat expansion, the extent of clustering is greater because the cooling is more rapid and extensive. The Rayleigh scattering and CARS data were combined using (2.45) to give mean cluster size. Figure 2-15 reveals that the mixture produced clusters approximately the same size as the neat expansion but the growth region is smaller and the signal dies out sooner due to the lower CO_2 density in the jet.

The clusters of this study were colder (see Table 2-2) thus, giving rise to a narrower cluster peak. This results in separate features which we attribute to CO_2 molecules in the interior and on the surface of the cluster. We assign the small peak at 1279 cm^{-1} to the higher frequency vibration of molecules on the surface of the cluster. From the area of a plot of the square root of the CARS intensity of each peak relative to the other and equations (2.62) and (2.63) we calculate mean cluster diameter as a function of X/D. This is shown in Figure 2-16. The average value is about 14 nm, which is

Jet Position	ρ_J		Peak Area $(Area)^{1/2}$	$(Area)^{1/2}$	$(Area)^{1/2}$	Peak Position					Cluster Diameter R.S.-CARS	Surface/Core
X/D	molecules/cm^3	Rayleigh I	Monomer	Surface	Core	Monomer	Surface	Cluster	T_c/K	N_c	nm	nm
2.1	1.55E+18	5262	1.11	0.08	0.42	1285.45	1279.35	1276.26	155	14363	10.8	16.6
2.2	1.31E+18	8051	1.01	0.13	0.72	1285.45	1279.35	1276.19	148	17228	11.5	16.0
2.4	1.14E+18	10129	0.89	0.08	0.67	1285.44	1279.30	1276.15	143	24209	12.9	23.6
2.6	9.69E+17	11717	0.84	0.07	0.60	1285.43	1279.32	1276.12	140	34054	14.4	24.0
2.7	8.45E+17	11411	0.63	0.31	0.68	1285.43	1279.30	1276.08	135	30286	13.9	7.5
2.9	7.42E+17	11449	1.08	0.18	0.99	1285.43	1279.33	1276.06	134	37710	14.9	16.4
3.1	6.57E+17	10831	0.68	0.78	0.92	1285.42	1279.24	1276.01	128	33449	14.3	4.8
3.2	5.85E+17	10103	1.21	0.31	1.54	1285.42	1279.37	1276.05	132	36023	14.7	14.8
3.4	5.24E+17	9480	1.30	0.42	1.72	1285.42	1279.28	1275.99	125	37055	14.8	12.5
3.6	4.72E+17	9178	1.04	0.29	1.38	1285.42	1279.12	1275.92	116	39667	15.2	14.1
3.7	4.27E+17	8631	1.25	0.36	1.34	1285.42	1279.17	1275.81	104	45508	15.9	11.7
3.9	3.89E+17	7762	1.07	0.38	1.68	1285.42	1279.19	1275.84	107	38148	15.0	13.5
4.1	3.55E+17	7406	1.22	0.34	1.93	1285.42	1279.08	1275.87	111	39742	15.2	16.8
4.2	3.25E+17	6947	1.36	0.51	2.11	1285.41	1279.15	1275.83	106	40918	15.3	12.6
5.1	2.20E+17	4779	1.32	0.53	2.40	1285.41	1278.99	1275.76	97	39157	15.1	13.7
5.9	1.59E+17	3031	0.47		1.62	1285.41		1275.70	88	32007	14.1	
6.7	1.20E+17	1971	0.60		1.99	1285.41		1275.68	86	24707	13.0	
7.6	9.35E+16	1691	1.12		2.60	1285.41				27462	13.4	

The intrinsic scattering for a monomer, I_0, measured for a static sample at 1 atm was 8.58E-19 cm^3 molecules^{-1}.

These data are from spreadsheets: CO2 Size and CO2 12% 296. The X/D position has been corrected by addition of $\Delta = 1.8$ based on the density calibration discussed in the text.

Table 2-3 Summary of Rayleigh-CARS 12% CO_2/He Experimental Results.

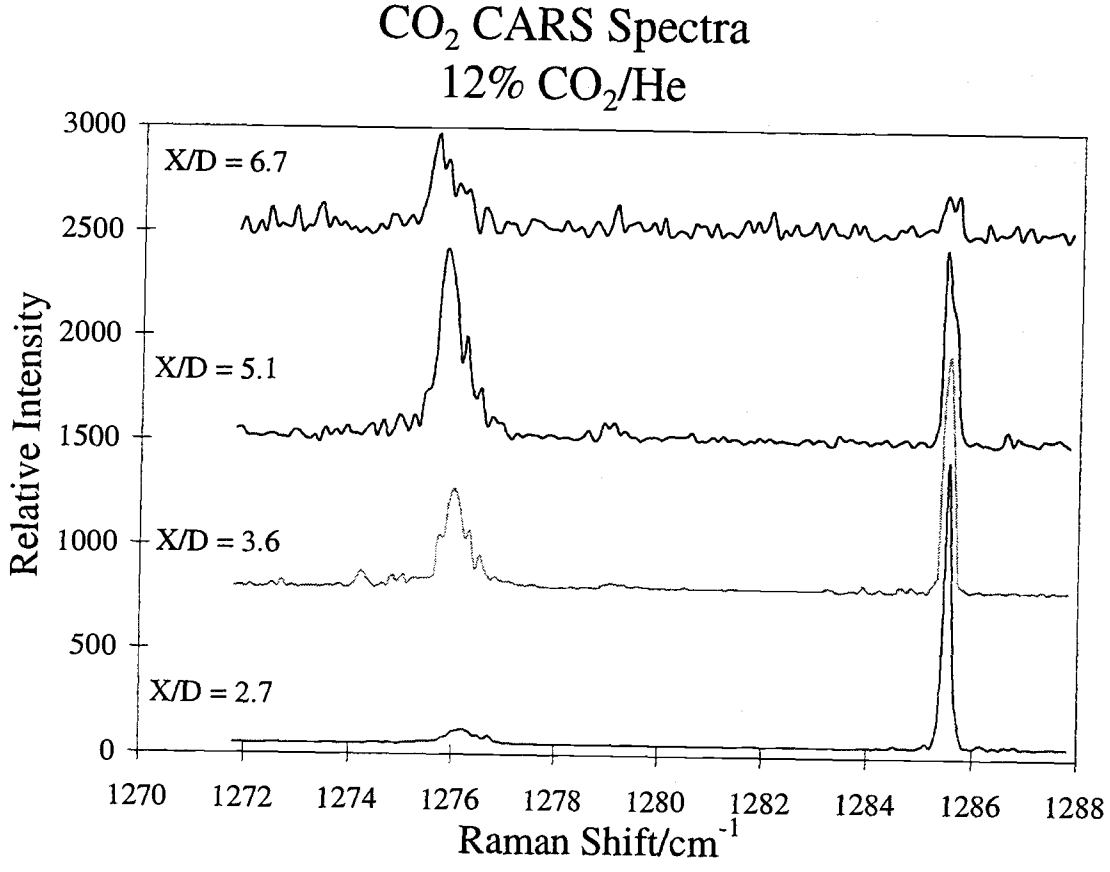

Figure 2-14 CARS spectra of the lower wavenumber member of the $\nu_1/2\nu_2$ Fermi resonance diad of CO_2. The data were taken for a 12% CO_2/He jet expansion at T_0 = 245 K and P_0 = 1400 kPa.

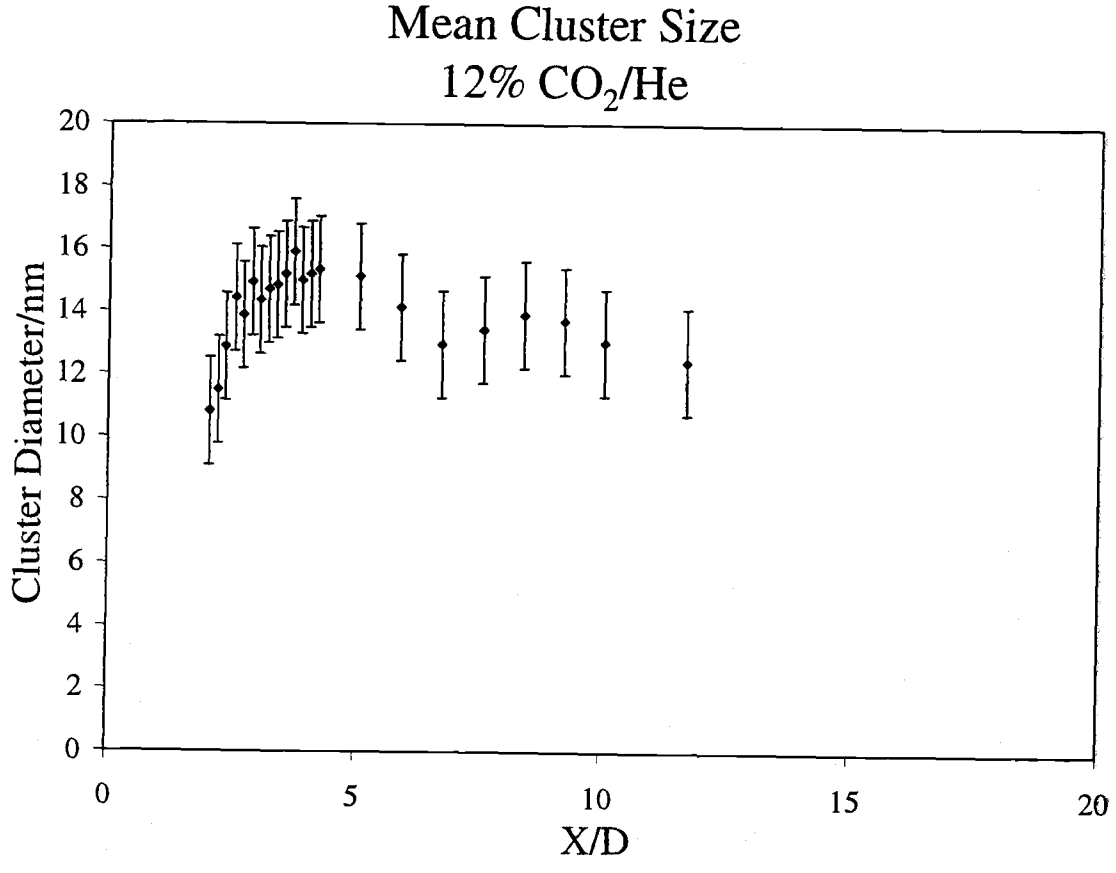

Figure 2-15 The 12% CO_2/He mixture gave much smaller clusters due to the lower CO_2 density in the jet. The growth region is much closer to the nozzle (X/D < 4) and the size appears to level off close to the size at the growth maximum.

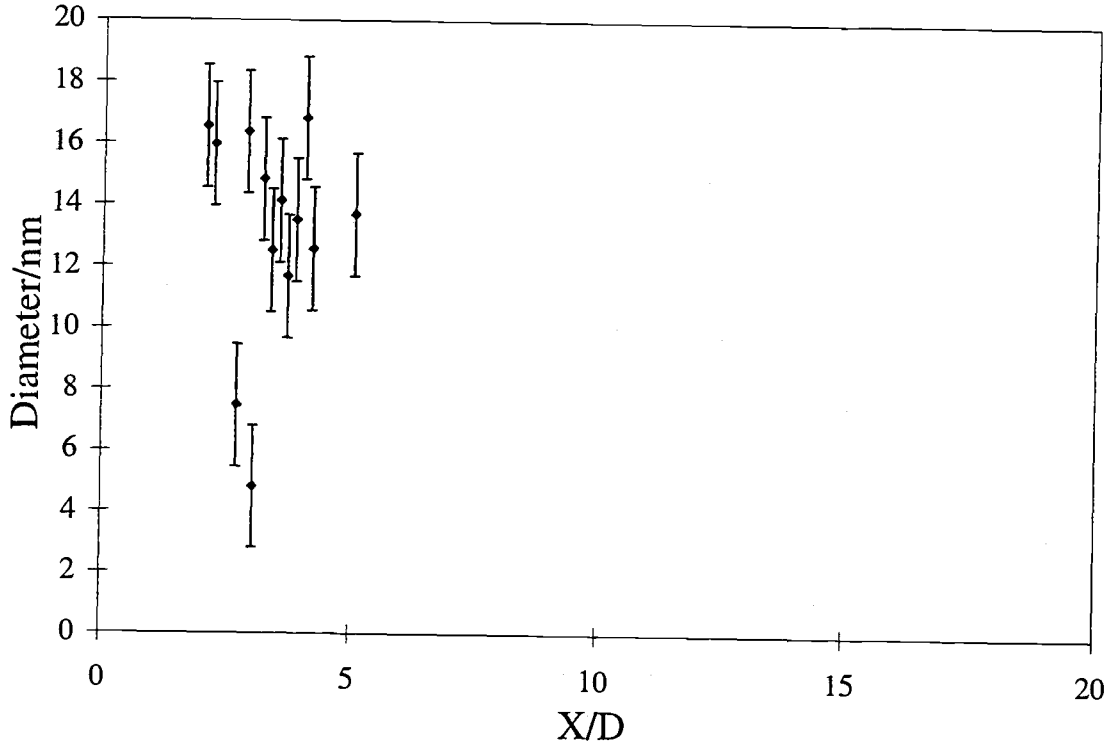

Figure 2-16 Mean cluster size deduced from surface/core ratios from CARS spectra as a function of X/D for a 12% CO_2/He expansion.

remarkably close to the Rayleigh-CARS value of about 13 nm. The comparison of these values may lead to a reasonable width for either a Gaussian or log-normal distribution of the cluster sizes.

2.8.5 Rayleigh-CARS Data: 5% CO_2 in He Study

Figure 2-17 shows CARS spectra taken for a 5% CO_2/He jet expansion at T_0 = 260 K and P_0 = 1400 kPa. The monomer Q branch appears at 1285.46 cm^{-1} and the cluster interior peak at about 1276 cm^{-1} and the cluster surface peak at 1279 cm^{-1}. Several spectra were taken over a range of X/D positions and Table 2-3 summarizes the peak positions, Rayleigh intensities, CARS areas, cluster fraction and size results. As in the previous studies, the Rayleigh scattering and CARS data were combined using (2.44) to give mean cluster size. Figure 2-18 reveals that the mixture gave smaller clusters than the 12% mixture due to higher T_0. The last data point was taken at ~5 X/D units from the jet orifice since the jet density dropped below the CARS detection limit.

The clusters of this study were colder (see Table 2-3) thus, giving rise to a narrower cluster peak. This resulted in the appearance of separate features, shown in Figure 2-19, which we attribute to CO_2 molecules in the interior and on the surface of the cluster. We assign the small peak at 1279 cm^{-1} to the higher frequency vibration of molecules on the surface of the cluster. From the square root of the area of each peak relative to the other and (2.62) and (2.63) we calculate mean cluster diameter as a

Jet Position	ρ_j		Peak Area					Peak Position							Cluster Diameter	
			$(Area)^{1/2}$	$(Area)^{1/2}$	$(Area)^{1/2}$	$(Area)^{1/2}$	$(Area)^{1/2}$								R.S.-CARS	Surface/Bulk
X/D	molecules/cm^3	Rayleigh I	Pk(m)	A	B	Surface	Bulk	Monomer	A	B	Surface	Bulk	T_r/K	N_c	nm	nm
2.2	5.41E+17	1207	0.89	0.24		0.50	0.92	1285.45	1281.22		1279.21	1276.31	160	4187	7.1	6.6
2.3	4.99E+17	2274	0.78	0.23		0.55	1.22	1285.45	1281.19		1279.17	1276.27	157	8053	8.8	7.5
2.3	4.61E+17	2663	0.81	0.20		0.45	1.15	1285.44	1281.30		1279.13	1276.31	160	9643	9.4	8.3
2.4	4.27E+17	2345	0.97	0.33		0.97	1.56	1285.44	1281.05		1279.15	1276.24	153	8683	9.1	5.9
2.5	3.97E+17	1420	1.23	0.37		0.88	1.72	1285.44	1281.25		1279.11	1276.18	147	6030	8.0	6.8
2.6	3.70E+17	1344	0.77	0.35		0.76	1.83	1285.43	1281.20		1279.09	1276.14	142	5556	7.8	8.1
2.7	3.45E+17	1138	0.91	0.39		0.65	1.82	1285.43	1280.96		1279.18	1276.04	132	5231	7.7	9.1
2.8	3.23E+17	947	1.12	0.69		0.88	1.68	1285.43	1281.20		1279.08	1276.06	133	4854	7.5	6.7
2.8	3.03E+17	840	1.13	0.55		0.84	2.22	1285.42	1281.06		1279.14	1276.03	130	4451	7.2	8.6
3.0	2.67E+17	854	1.06	0.42		0.65	1.61	1285.42	1281.24		1279.01	1275.98	124	5431	7.7	8.2
3.1	2.52E+17	672	1.23	0.49		0.98	2.05	1285.42	1281.19		1279.04	1275.95	121	4392	7.2	7.2
3.2	2.38E+17	673	0.80	0.38	0.21	0.57	1.49	1285.42	1281.20	1279.98	1278.87	1275.94	119	4494	7.3	8.6
3.3	2.13E+17	572	1.36	0.63	0.18	0.83	2.11	1285.42	1281.05	1280.13	1279.04	1275.94	119	4473	7.3	8.4
3.5	1.91E+17	556	1.40	0.43	0.34	0.81	2.53	1285.42	1281.21	1280.11	1278.94	1275.86	109	4750	7.4	9.9
3.7	1.73E+17	541	1.08	0.55	0.14	0.78	3.05	1285.42	1280.96	1279.96	1278.98	1275.86	110	4735	7.4	12.0
3.8	1.57E+17	454	0.90	0.53	0.11	0.90	2.34	1285.42	1281.10	1279.97	1278.86	1275.72	91	4343	7.2	8.5
4.0	1.43E+17	448	1.18	0.58	0.12	1.09	3.40	1285.41	1281.06	1279.94	1278.85	1275.81	103	4682	7.4	9.9
4.2	1.31E+17	429	0.93	1.42		0.90	3.48	1285.41	1280.94		1278.86	1275.71	90	4636	7.3	11.9
4.3	1.20E+17	389	0.72	0.75	0.39	1.41	3.57	1285.41	1280.94	1279.91	1278.66	1275.71	90	4409	7.2	8.4
4.5	1.11E+17	348	1.05	0.44	0.66	1.39	3.78	1285.41	1280.47		1278.88	1275.65	82	4473	7.3	8.9
4.7	1.03E+17	348	0.80	0.51	0.49	1.36	4.06	1285.41	1280.58		1278.92	1275.72	91	4663	7.4	9.6
4.8	9.51E+16	335	0.58	0.82	0.24	1.33	3.19	1285.41	1281.02	1279.84	1278.85	1275.66	83	4751	7.4	8.0
5.0	8.84E+16	321	0.69			1.46	3.26	1285.41			1278.89	1275.69	87	5080	7.6	7.6
5.2	8.24E+16	293	0.74	0.35		1.21	3.15	1285.41	1281.22		1278.85	1275.60	74	5020	7.5	8.6
5.3	7.69E+16	267	0.70			1.42	3.50	1285.41			1278.85	1275.63	79	4841	7.5	8.2
5.5	7.20E+16	253	0.51			1.09	3.04	1285.41			1278.69	1275.59	73	4824	7.4	9.1
5.7	6.76E+16	204	0.87			1.35	3.51	1285.41			1278.65	1275.49	60	4331	7.2	8.6

The intrinsic scattering for a monomer, I_o, measured for a static sample at 1 atm was 8.20E-19 volts cm^3 molecules^{-1}

These data are from spreadsheets: CO2 Size and CO2 12% 296. The X/D position has been corrected by addition of $\Delta = 1.8$ based on the density calibration discussed in the text.

Table 2-4 Summary of Rayleigh-CARS 5% CO_2/He Experimental Results.

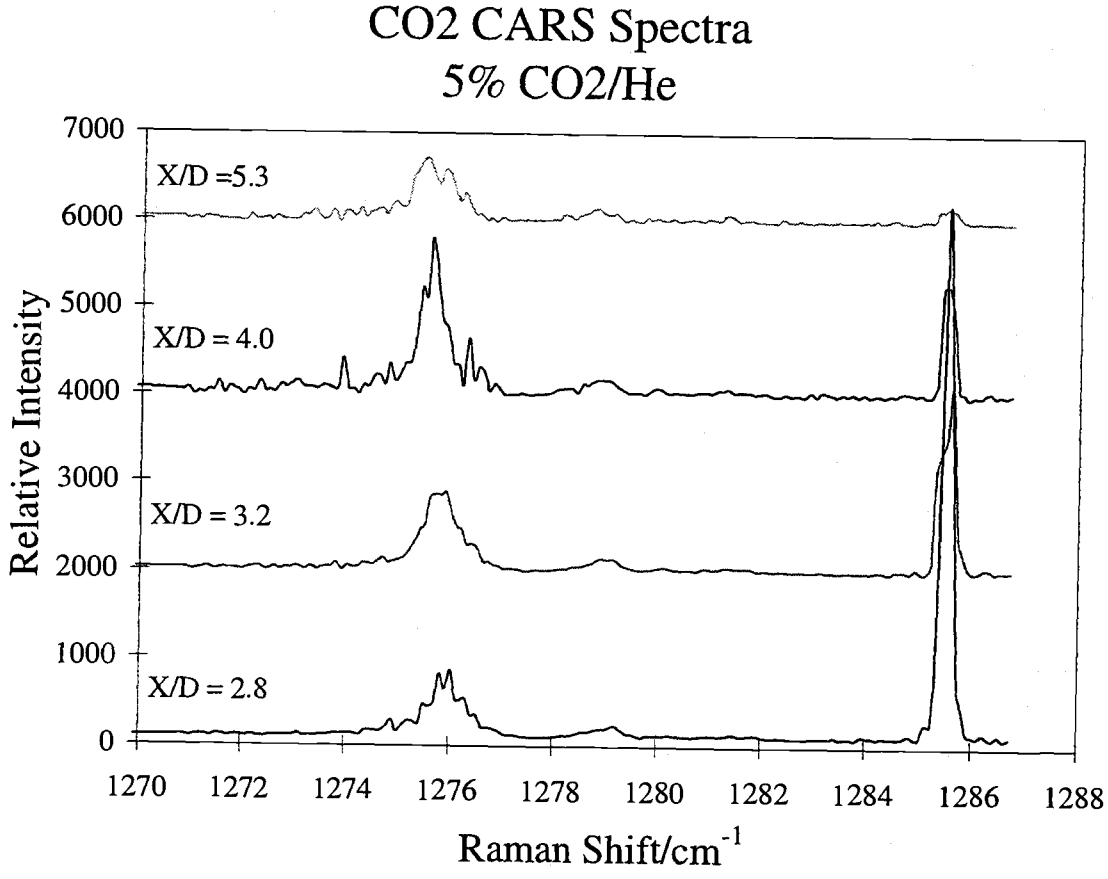

Figure 2-17 CARS spectra of the lower wavenumber member of the $\nu_1/2\nu_2$ Fermi resonance diad of CO_2. The data were taken for a 5% CO_2/He jet expansion at T_0 = 260 K and P_0 = 1400 kPa.

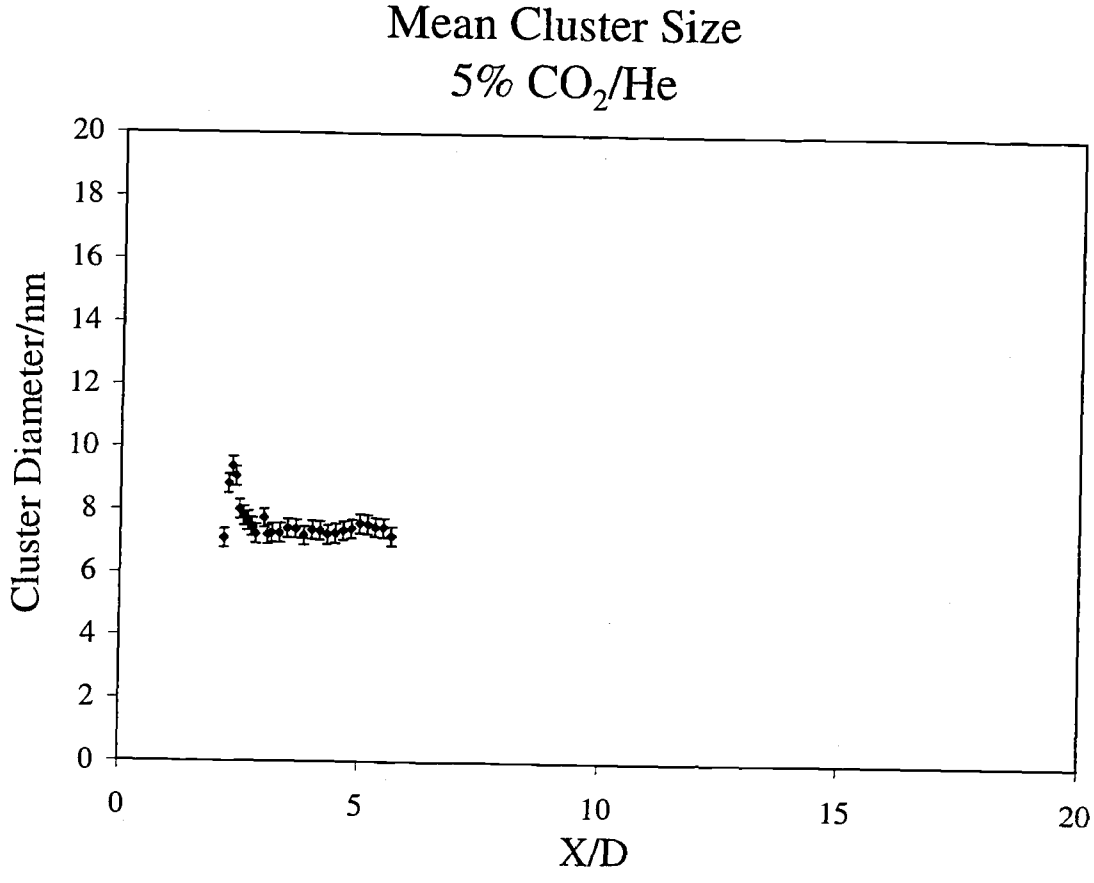

Figure 2-18 The 5% CO_2/He mixture gave smaller clusters than the 12% mixture due to greater collisional cooling and lower CO_2 density in the jet.

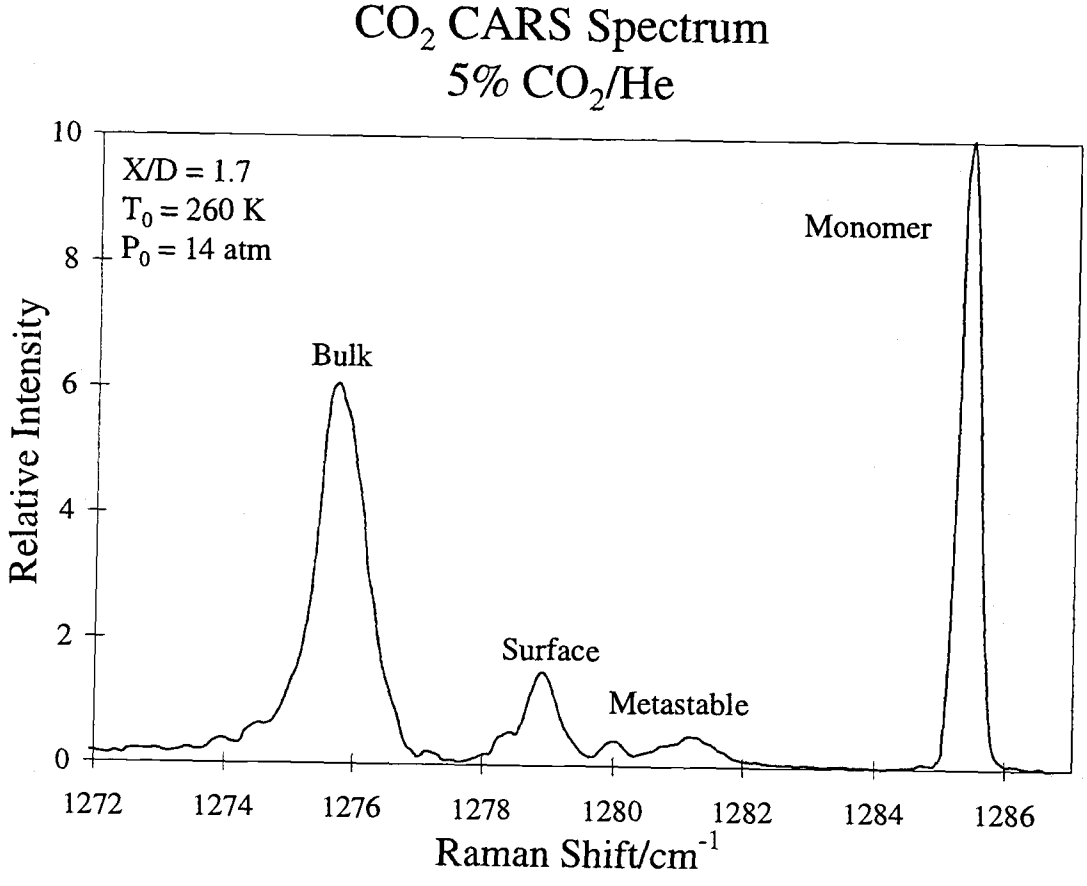

Figure 2-19 An expanded view of the CARS spectrum at 1.7 X/D showing two new features: a peak at 1280 cm^{-1} and one at 1281.5 cm^{-1}.

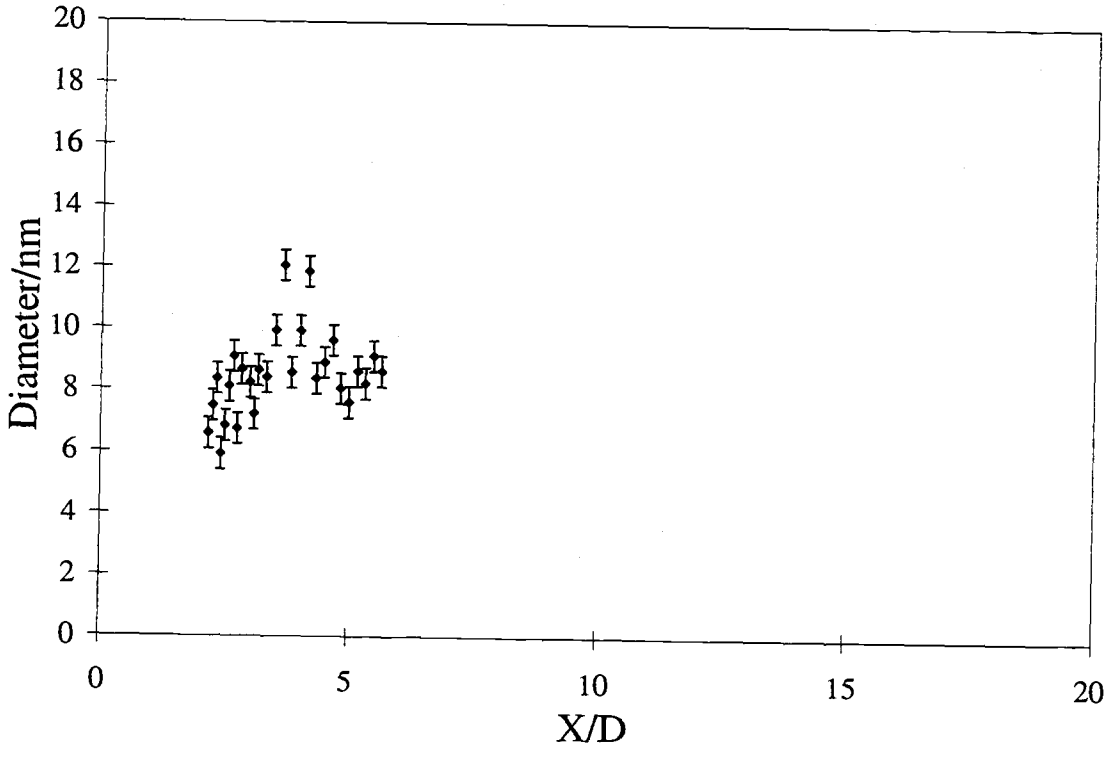

Figure 2-20 Mean cluster size deduced from surface/core ratios from CARS spectra as a function of X/D for a 5% CO_2/He expansion.

function of X/D shown in Figure 2-20. The average is about 8 nm, again consistent with the Rayleigh-CARS value.

2.8.6 Evidence for Metastable Structures

Unlike the two previous data sets, this set exhibits two new peaks: one at 1280 cm^{-1} and one at 1281.5 cm^{-1}. These peaks, shown in Figure 2-19, are present in all spectra taken over the full range of X/D positions and do not vary in area relative to the cluster interior peak as does the peak at 1279 cm^{-1}. Therefore, we reject the possible attribution of these to layers of a CO_2 cluster, in which the outer layers would presumably give peaks less shifted from the monomer. Also, we do not believe that these features can be assigned to dimer and trimer forms since these are expected to be present in only those concentrations and, moreover, Brown [1991] has attributed features due to these species to such structure seen much closer to the monomer position. That such small species would show small shifts is also supported by the calculations of Montero [1992].

An alternative explanation that seems more plausible is that the small peaks at 1280 cm^{-1} and 1281 cm^{-1} are due to structures unlike the bulk phase arrangement. Based on potential energy minimization calculations, van de Waal [1983] proposed three structures for smaller CO_2 clusters—pentagonal bipyramid, cuboctahedral, and regular icosahedral for the, so called, magic numbers, seven and thirteen. These structures are shown in Figure 2-22. A special stability for heptamers was also noted by Kaelberer, et al. [1976] who found a high probability and stability of pentagonal bipyramidal

arrangements of rare-gas atoms even at elevated temperatures. Furthermore, van de Waal's [1983] study showed that the bulklike 13-molecule cuboctahedral arrangement of CO_2 will spontaneously collapse into a regular icosahedral cluster with a gain in binding energy of 4.1 kJ/mol.

The idea that there may be a progression through several structural forms as clusters grow was examined more recently by Torchet, et al. [1996], who combined electron diffraction results with molecular dynamics simulations of $(CO_2)_N$ clusters. They predicted the same arrangements as van de Waal but with additional evidence that suggests a transformation from the icosahedral structure to a crystalline structure is a general process that occurs during the growth of van der Waals clusters of small molecules. Bulk solid CO_2 forms crystals of cubic symmetry (Pa3 space group) which has been observed using electron diffraction [Stein and Armstrong, 1973]. The transformation occurs when the number of molecules per cluster, $N_c \approx 30$. They found that the $N_c = 25$ model gave entirely polyicosahedral structure and the $N_c = 32$ model gave entirely cubic crystal structure.

Our results seem to be in accord with the above calculations. The 1281.5 cm^{-1} peak we attribute to small clusters formed around a pentagonal bipyramidal core. We then assigned the slightly redshifted peak at 1280 cm^{-1} to clusters formed around an icosahedral core. Finally, as clusters grow to sizes ≥ 30, conversion to a bulklike cuboctahedral core occurs, leading to the surface and core features at 1279 cm^{-1} and 1276 cm^{-1}, respectively.

2.9 CONCLUSIONS

Rayleigh scattering is a good qualitative method for determining sample densities and cluster growth in molecular jets. Combined with CARS results, Rayleigh scattering data yield quantitative mean cluster sizes in agreement with those predicted by empirical scaling "laws" and cluster cooling curves. Also, when the extent of clustering is sufficiently high, and the clusters are very cold, the CARS spectra exhibit a peak red-shifted from the monomer that we propose is due to molecules on the surface of the cluster. The size deduced from a comparison of the surface peak to the core peak gives sizes in excellent agreement with the Rayleigh-CARS method. This may lead to deducing a reasonable width of either a Gaussian or log-normal cluster size distribution. Finally, for very cold, dilute, 5% CO_2 in the expansions, two new features are seen at 1280 cm^{-1} and 1281 cm^{-1}, and these are attributed to metastable structures.

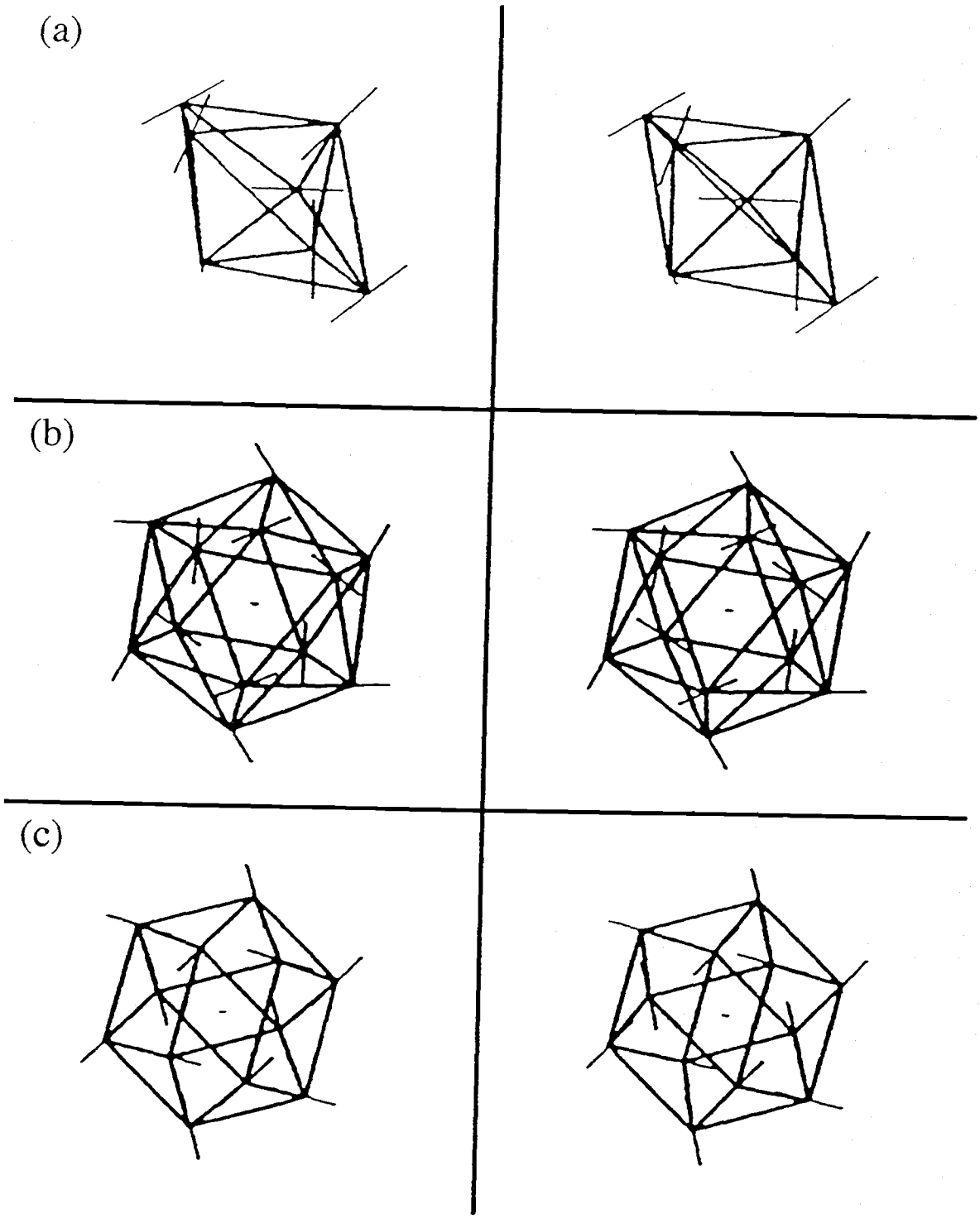

Figure 2-21 Metastable structures corresponding to (a) N =7, pentagonal bipyramid, (b) 13<N<25, icosahedron, and (c) N>30 cuboctahedron. The three possibilities given here are stereo projections. (To see the 3D image, stare at the solid line in the middle of the page and relax your eyes).

3. SIZE ESTIMATES OF MOLECULAR CLUSTERS USING THE ANGULAR DEPENDENCE OF MIE SCATTERING

3.1 ABSTRACT

The differential cross section for scattering of a plane monochromatic wave from a small particle also contains an angular dependence, which is a strong indicator of the size of the scatterer. We present angular scattering measurements for "calibration" microspheres of known size and from clusters formed in a neat CO_2 supersonic jet expansion. Under very extreme expansion conditions, clusters with a mean diameter of 400 nm to 500 nm were produced as deduced from fits of the angular scattering curves using Mie's formulae. Measurements and calculations were also made for the milder neat CO_2 expansion conditions which gave 14.4 ± 2.0 nm mean diameters from the Rayleigh-CARS method. The absence of angular intensity variations and the Mie calculations confirm that these clusters were indeed much smaller than 500 nm—the condition necessary to justify using a simple quadratic size dependence of the Rayleigh scattering intensity.

3.2 INTRODUCTION

For the study of molecular clusters we desire a dependable experimental method to determine the size of the clusters. Several empirical methods exist for use over the small to large range of cluster sizes ($N = 2$ to $N \approx 10^8$) [Hagena, 1972; Torchet, 1984; Richardson, 1993]. In Chapter 2, we considered the combination of Rayleigh scattering

and coherent anti-Stokes Raman scattering for size determinations and showed that this gives reasonable results for CO_2 clusters of a few nanometers diameter. However, this Rayleigh-CARS method of determining mean cluster size is only valid when the clusters are much smaller than the wavelength of incident light. If the clusters are of the order of the wavelength of the incident light, interference effects become significant; the scattering intensity varies appreciably with the angle of detection. In this chapter, we examine the use of such angular measurements for very large clusters formed under extreme expansion conditions. We tested our measurement apparatus by measuring angular scattering profiles of latex spheres of known size and by modeling these profiles using Mie's formulae. Studies of CO_2 clusters using the same apparatus establish some bounds on the sizes of clusters that can be formed in jet expansions.

3.3 MIE SCATTERING THEORY

3.3.1 Historical Notes

Light scattering by small particles is the phenomenon responsible for brilliant red sunsets, beautiful blue skies, and fluffy white clouds—visual phenomena that have delighted countless individuals throughout the ages. Not only artists and poets find inspiration in this most beautiful facet of creation but physicists as well. In 1908, Gustav Mie published a paper describing his theory regarding a plane monochromatic wave diffracting from a homogeneous sphere of any size and composition in a homogeneous medium. The theory is applicable, as well, to a collection of monodisperse spheres when

the distance between them is much larger than the wavelength of light—a feature that renders the theory useful for a variety of scattering problems. Of course, Mie was not solely responsible for developing this scattering theory; the interested reader will find a history of the development of the theory and the people involved in an account by Kerker [1969].

3.3.2 Mie's Formulae

In Chapter 2 we described the interaction of a plane electromagnetic wave with a particle. The incident field induces electric and magnetic multipoles that oscillate in definite phase relationship with the incident wave and radiate energy in all directions. The angular distribution of radiated energy depends upon the coherent superposition of multipoles induced in different particles by the incident field and on the interference of the scattered waves from these particles. It also depends upon the polarization of the incident wave. In Chapter 2, we treated the case wherein the size of the ensemble of particles—the cluster—is much less than the wavelength of incident radiation. Here we are interested in the case when the cluster is of the order of the wavelength of incident radiation, producing a phenomenon called Mie scattering named after Gustav Mie [1908].

In discussing Mie scattering, it is conventional to define a term $q = 2m\pi a/\lambda = ka$ where $m = n_s/n_m$ is the index of refraction of the scatterer relative to the medium, a is the radius of the scatterer, and λ is the wavelength of incident light. Figure 3-1 is a cartoon

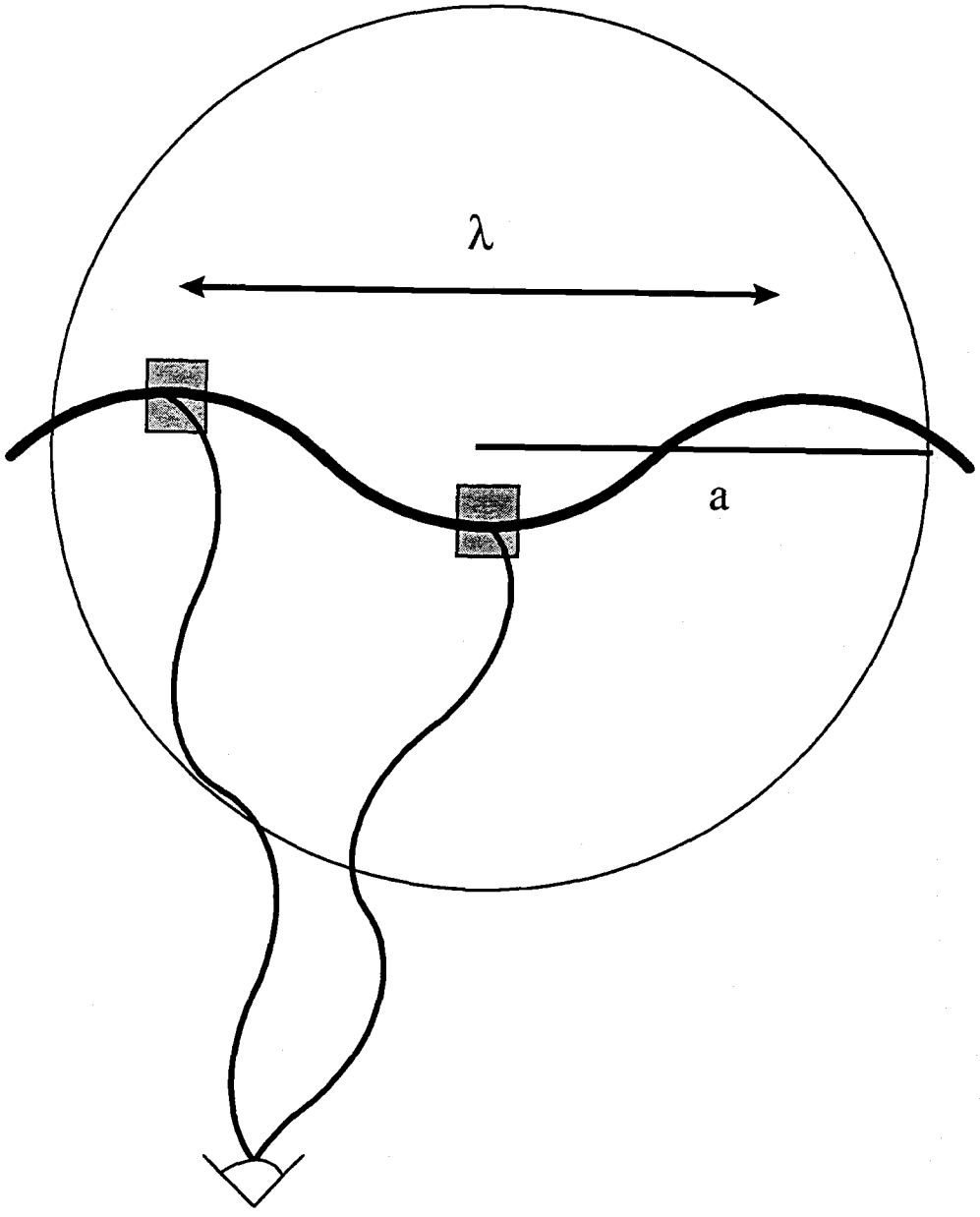

Figure 3-1 The phenomenon called Mie scattering occurs when the cluster radius is of the order of the wavelength of incident radiation. Scattered waves from regions within the particle interfere at the detector, which is normally much further away from the particle than is shown.

representation of a plane wave scattering from a particle of $q > 1$. The shaded regions indicate local areas of dimension much less than the wavelength of incident light. The scattered waves interfere as they strike the detector. As the detector is moved in an arc about the point of observation, the scattered intensity varies with angle. Figures 3-2 and 3-3 show this intensity variation as a function of angle for the cases when $q = 0.8$ and $q = 8$, respectively. The case for $q = 0.8$ corresponds to the scattering expected for a particle of about 100 nm diameter for $\lambda = 500$ nm and shows the nearly circular dependence expected for I_{VV} for Rayleigh scattering. Some enhancement of scattering in the 0° forward direction is apparent however. The I_{VH} case in which the polarization of the scattered light is orthogonal to that of the incident polarization is also distorted somewhat from the "p orbital" shape of Rayleigh scattering. Note that the I_{VH} intensity is very low at 90°.

The angular scattering pattern for $q = 8$ corresponds to that of a particle of 1000 nm diameter and is much more peaked in the forward direction than for the case with $q = 0.8$. It also shows pronounced angular variations for both I_{VV} and I_{VH}. This angular variation will be "washed out" somewhat for a polydisperse sample with different sizes but the I(0°)/I(180°) ratio will remain very large compared to Rayleigh scattering where it is unity. In practice, it is very difficult to measure scattering at these extremes and the scattering over more feasible experimental angles is shown in Figure 3-14 for several particle sizes and for $\lambda = 500$ nm.

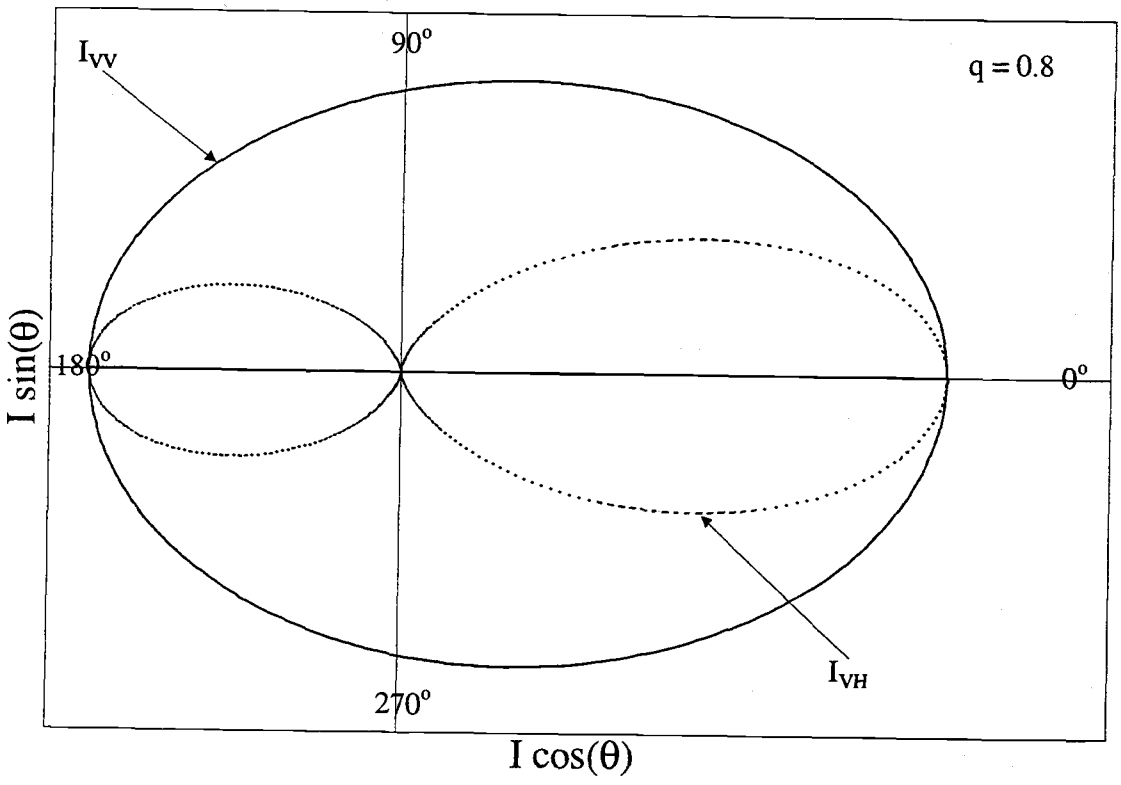

Figure 3-2 The angular variation of scattering intensity of a spherical particle as a function of angle for the case when q = 0.8.

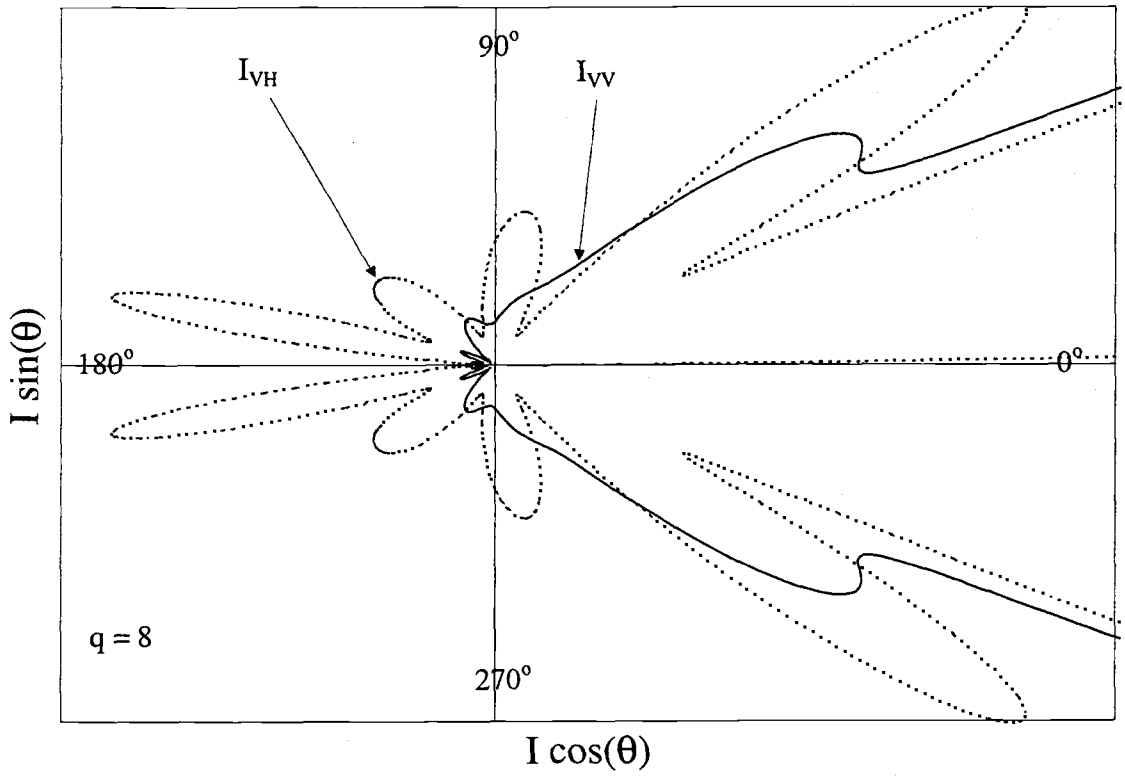

Figure 3-3 The angular variation of scattering intensity of a spherical particle as a function of angle for the case when q = 8.

While the concept of Mie scattering is simple, the mathematical expressions used to describe it and to generate Figures 3-2 and 3-3 are complex and do not have a closed form solution. The following expressions are the Mie formulae as expressed in *Principles of Optics* by Born and Wolf [1975]. Here the x axis is the angle θ and we see that as the particle diameter decreases, the Mie "undulations" die out and the I_{VV} angular variation of the scattering tends toward the Rayleigh limit of zero.

$$I_{VV} = I_{\parallel}^{(s)} = \frac{\lambda^{(I)2}}{4\pi^2 r^2}\left|\sum_{l=1}^{\infty}(-i)^l\left({}^{e}B_l P_l^{(1)'}(\cos\theta)\sin\theta - {}^{m}B_l\frac{P_l^{(1)}(\cos\theta)}{\sin\theta}\right)\right|^2 \qquad (3.1)$$

$$I_{VH} = I_{\perp}^{(s)} = \frac{\lambda^{(I)2}}{4\pi^2 r^2}\left|\sum_{l=1}^{\infty}(-i)^l\left(\frac{{}^{e}B_l P_l^{(1)'}(\cos\theta)}{\sin\theta} - {}^{m}B_l P_l^{(1)'}(\cos\theta)\sin\theta\right)\right|^2 \qquad (3.2)$$

Here $\lambda^{(I)}$ is the incident wavelength, r is the distance from the scatterer to the detector, ${}^{e}B_l$ and ${}^{m}B_l$ are complex coefficients of the electric and magnetic fields generated in the scatterer by the incident field, $P_l^{(1)}$ is a Legendre polynomial, and θ is the angle between the point of observation and the incident beam of radiation. The B coefficients are functions of the molecular polarizability and the incident light intensity. As in Chapter 2, $I_{VV} = I_{\parallel}$ and $I_{VH} = I_{\perp}$ refer to the intensity scattered with polarization parallel and perpendicular, respectively, to that of the incident light.

Numerical solutions to these formulae for selected conditions are given in tables by Chu, et al. [1957]. The tables allow one to calculate the scattered intensity as a function of angle and particle size but the process is quite tedious, as we discovered in using this approach in the early phases of these experiments. Several methods of

approximation exist for simplifying the calculation of Mie scattering intensities and a review of more convenient analytical solutions to Mie's formulae was recently published in the Journal of Aerosol Science [Kokhanovsky, 1997]. Next we consider two of these methods.

3.3.3 Rayleigh-Gans Approximation

In 1985, Drake and Gordon reported using a light scattering apparatus to record intensity as a function of angle for latex microspheres and used a model often referred to as the Raleigh-Gans (also termed Rayleigh-Debye) approximation to estimate the size of the spheres. The key assumption of the method is to subdivide the scatterer into small elements with dimensions much smaller than the wavelength of incident radiation such that each sub-particle is a Rayleigh scatterer. Furthermore, the method assumes that each sub-particle is unperturbed by the presence of the remaining sub-particles.

The Rayleigh-Gans expression used by Drake and Gordon is

$$I_{VV} = I_0 \left(\frac{3|J_1(x)|}{x + x^{-3/2}} \right)^2 \frac{(1+\cos^2\theta)}{2} \tag{3.3}$$

where θ is the viewing angle of the detector, I_0 is the Rayleigh scattering intensity which is proportional to a^6, J_1 is the first order Bessel function and x is given by

$$x = ka(1+m^2-2m\cos\theta)^{1/2} \tag{3.4}$$

where k is the wavevector, a is the radius of the scatterer and m is the index of refraction of the scatterer relative to the medium.

3.3.4 MieTab® Commercial Software

A more accurate calculation of Mie scattering intensities can be done using a FORTRAN algorithm written by Lentz [1976], which is recently available as a commercial program called MieTab®. In calculating $I^{(s)}$ in (3.1) and (3.2), Lentz simplified the sums by applying what he calls continued fractions to a method developed by Dave [1969] at IBM. The advantage was that the algorithm is fast and accurate. Using MieTab® one can calculate scattering curves in seconds for iterations in one parameter at a time. Also, the program offers several cluster size distribution models which are useful for fitting curves for polydisperse samples such as the clusters formed in jet expansions. A comparison of the angular variations of Mie scattering by the three methods is offered in Figure 3-4 for the case in which q = 8. Since the more convenient MieTab® program gave results in better agreement with the results from the tables of Chu [1957] than the Rayleigh-Gans approximation, it was used in all subsequent analyses of measured angular distributions.

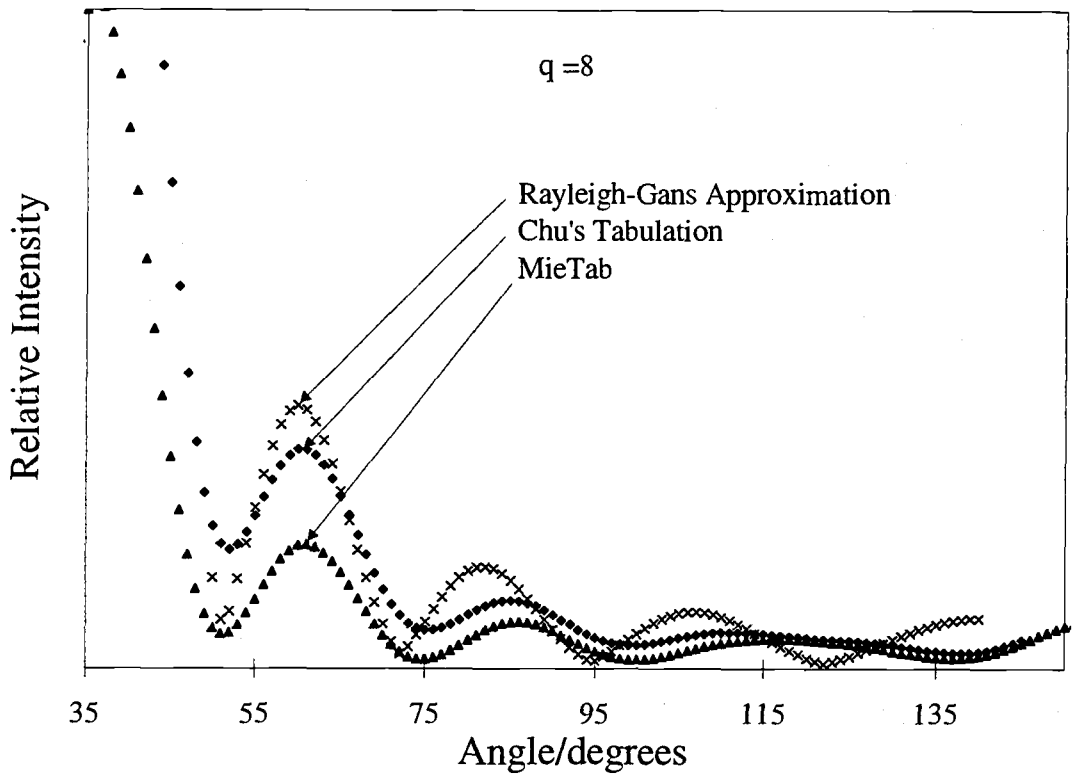

Figure 3-4 A comparison of the angular variations of Mie scattering by three methods for the case in which q = 8. Since the more convenient MieTab® program gave results in better agreement with results from the tables of Chu [1957] than the Rayleigh-Gans approximation, it was used in all subsequent analyses of measured angular distributions.

3.4 THE EXPERIMENT

3.4.1 Apparatus

3.4.1.1 Angular Scattering Apparatus

Figure 3-5 shows the angular scattering device for the jet expansion measurements. Scattered light was imaged through a 3.0 mm front aperture by a 35 mm focal length lens to a 1.5 mm back aperture and was detected with an RCA 1340 photomultiplier tube. All elements were mounted in a line on a delrin rod attached to a pivot point at the jet center. The pivot was driven by a Hurst stepper motor and EPC-015 controller. The detector and stepper motor were inside the vacuum chamber and the controller, photomultiplier signal out and MHV supply were attached with vacuum feedthroughs. The detector had only 20° angular resolution with the 3.0 mm aperture and lens—a compromise necessary for improved detection for the low scattering intensity expected for studies of medium to small clusters. For very large clusters, the intense scattering permitted elimination of the lens so that the 1.5 mm aperture determined the limiting resolution of 1°. We collected the signal using a Tektronix TDS 620A 500 MHz digital oscilloscope.

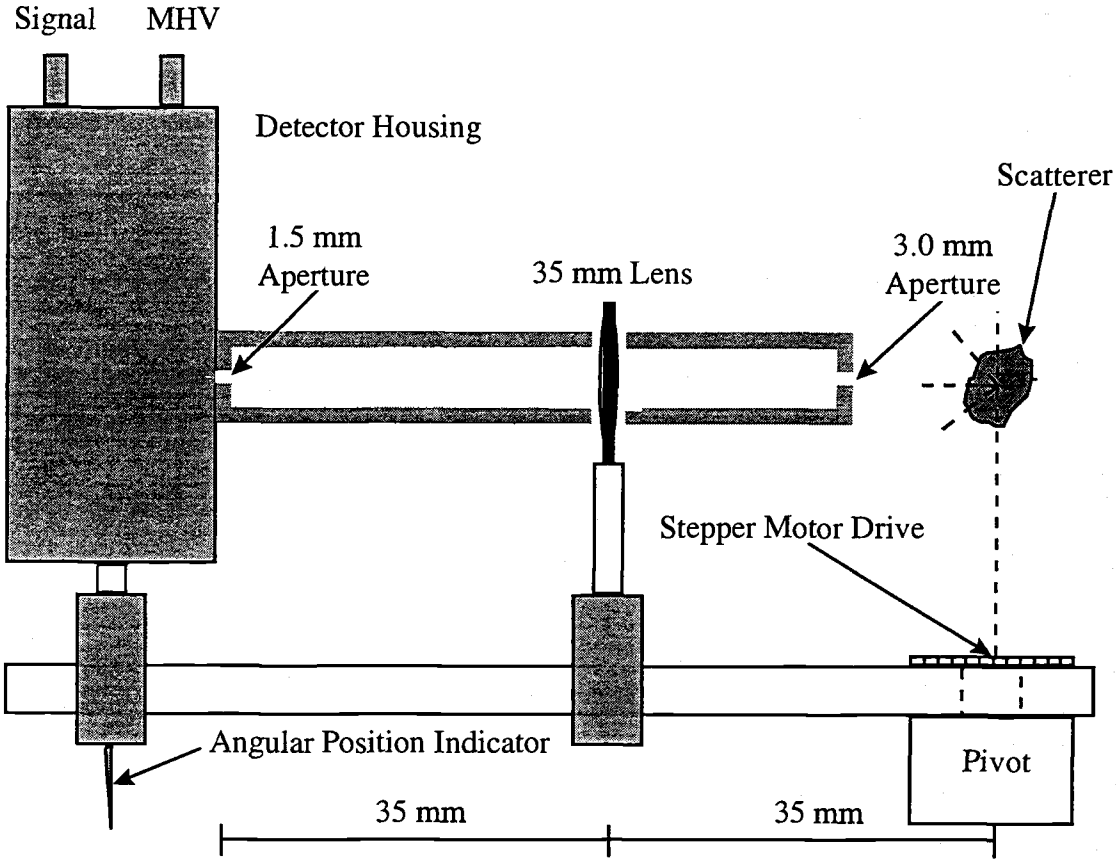

Figure 3-5 In-vacuum angular scattering apparatus.

3.4.1.2 Laser Systems

Figure 3-6 shows the experimental layout for the angular scattering-CARS experiment. The main component of the CARS system was a custom-built Continuum Nd:YAG laser. It produced a single mode, frequency doubled output beam of 532 nm with a 50 ns pulse width. Single mode operation was induced by injection seeding with a Lightwave Series 122, 50 mW narrow band, diode pumped Monolithic, Isolated, Single-frequency, End-pumped Ring (MISER) laser [Lightwave Electronics]. The MISER cavity was a Nd:YAG crystal, frequency stabilized with precise temperature control.

The Continuum Nd:YAG was used simultaneously as the ω_1 source and to pulse amplify the CW output of a tunable Coherent 699-29 ring dye laser, which provided the tunable Stokes beam. This ring dye laser was pumped with a 7 W Coherent I-90-6 Argon ion laser. The tunable CW output propagated through a Faraday isolator to a chopper wheel operating at 20 Hz. The pulse amplification stage was necessary to increase the output energy of the chopped Stokes pulse (of the order of 10^{-5} mJ over the 50 ns pulse duration of the Nd:YAG laser). The amplification stage consisted of three dye cells that produced a gain of about one million. Two cells were transversely pumped and one was longitudinally pumped to enhance the spatial quality of the beam. All beams were brought to a common focus at the jet center using a folded BOXCARS arrangement [Eckbreth, 1978]. The coherent anti-Stokes signal beam was spatially filtered prior to further

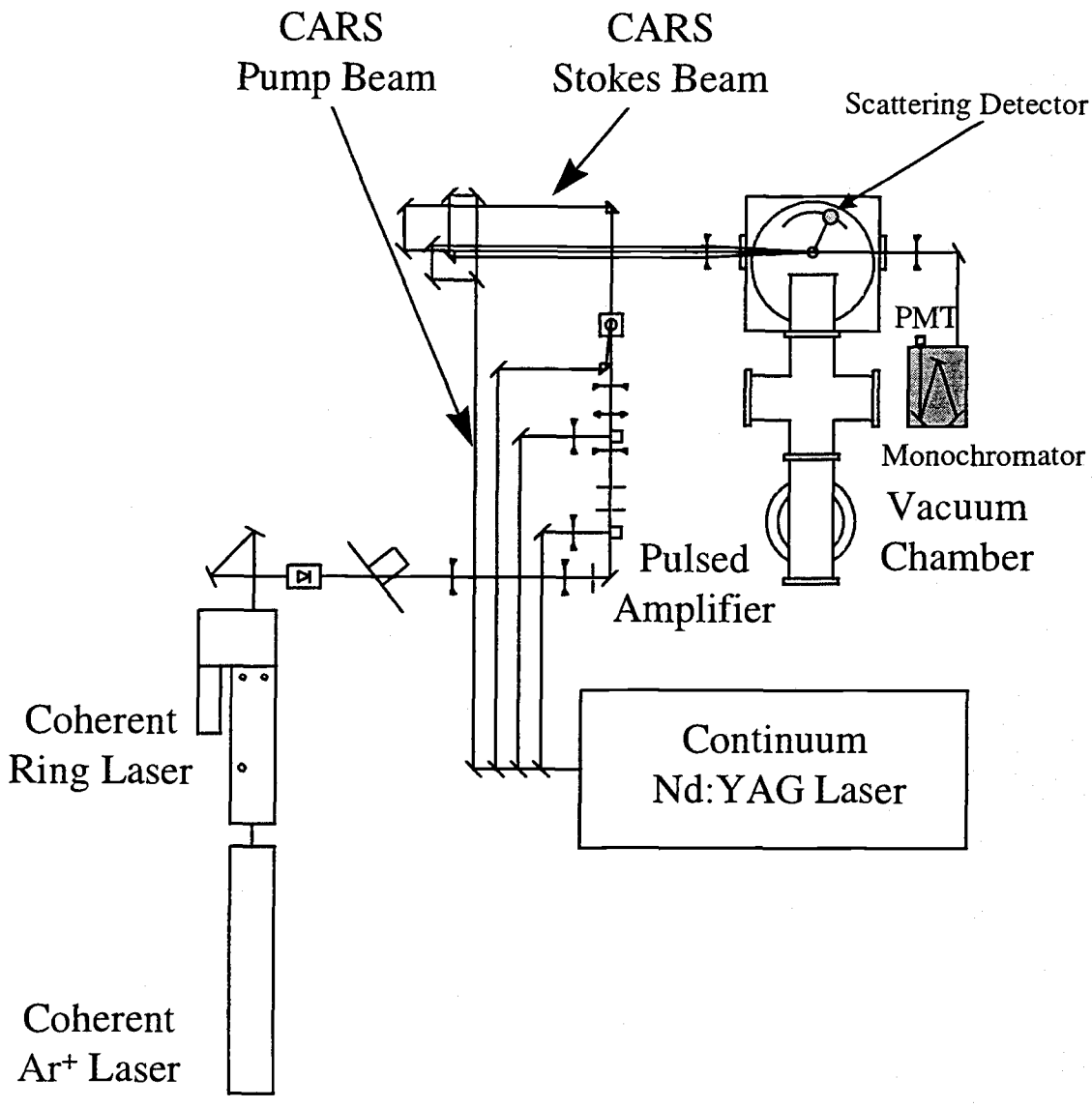

Figure 3-6 The Angular Scattering-CARS Apparatus.

discrimination by a 532 nm holographic filter and a McKee-Pedersen Instruments MP-1018 0.25 m dispersive monochromator. The CARS signal was detected with an RCA 1340 photomultiplier tube, gated with an SRS Model SR250 gated integrator and the last sample out of the SR250 was collected and displayed using a computer.

3.4.1.3 Pulsed Supersonic Jet

Clusters were formed in the supersonic jet apparatus shown in Figure 2-4 and described elsewhere [Pubanz, 1986]. The nozzle used for this experiment had a 0.3 mm orifice and a 0.3 mm thickness. It was mounted inside the vacuum chamber, cooled and pulsed at 20 Hz with a pulse width of about 150 μs which, on the time scale of the laser pulse, approximates a continuous flow. The background pressure did not exceed 250 mTorr—a pressure adequate to maintain a collision free region to 160 X/D.

3.4.2 Calibration Tests

3.4.2.1 Latex Microspheres

As a test of the apparatus and of Mie scattering theory, light scattering intensities were measured for latex microspheres of known diameter. We used four sizes of microspheres all purchased from Polysciences, Inc., Warrington, PA. The microspheres were monodisperse and in the form of solutions (2.6% by weight) in 15 mL of surfactant free, deionized water. The latex density was 1.05 g/mL with a refractive index of 1.6000. The sizes given by the manufacturer were 64 ± 9.6 nm diameter, 84.5 ± 21 nm diameter,

548 ± 16 nm, and 1072 ± 19 nm diameter, as determined using disc centrifugation. The microspheres were guaranteed stable (i.e., no aggregation) at 4°C for one year from the date of shipment. All experiments using the latex microspheres were done within this time frame.

3.4.2.2 Photometer Measurements

We conducted initial experiments using the microspheres and a Brice-Phoenix universal light scattering photometer. The scattering source was the 514.5 nm line of a Spectra Physics 164 Argon ion laser. We first measured light scattering at 90° for each microsphere sample as a function of concentration, to ensure that no aggregation occurred for samples subject to angular studies. For analysis, each solution was placed in a cylindrical cuvette positioned at the pivot point for the arm holding the photomultiplier tube in the light scattering photometer. For selected concentrations, the instrument was then used for measurement of the scattering signal from 45° in the forward direction to 135° in the backward direction in increments of 1°. The angular resolution was 1°.

3.4.2.3 Jet Apparatus Measurements

The same latex microsphere samples were next used to check the angular scattering apparatus employed in the jet expansion experiments described in section 3.4.1.3. We followed the same procedure as in the light scattering photometer experiment except that we stepped the detector in angular increments of 5°. For measurement convenience, we performed a CW experiment using a Coherent I-90-6

Krypton ion laser source at 650 nm. This was followed by an experiment at 532 nm using the pulsed Continuum Nd:YAG laser described in section 3.4.1.2, since this corresponded to the same arrangement needed for concurrent CARS measurements.

We did a few experiments using expansion conditions chosen to produce very large clusters. These experiments did not require high light collection efficiency because of the intense scattering so that it was possible to improve the angular resolution. We reconfigured the Angular Scattering Apparatus by removing the 35 mm lens, increasing the back aperture to 5 mm, and reducing the front aperture to 1.5 mm. These modifications resulted in an angular resolution of 1°.

3.4.2.4 Characterization of the Supersonic Jet

The data interpretation is done assuming that the maximum elastic scattering signal arises from the high density centerline of the jet. Therefore, a crucial alignment is to center the jet axis on the Rayleigh detector field of view. Figure 3-7 shows the scattered intensity at 90° as the laser crossing axis was moved vertically across the detector field of view. This information allowed us to identify the laser beam position for maximum signal. Although, not the main purpose of this work, these measurements also yield information about the off-axis characteristics of the jet expansion. For example, Figure 3-8 is the jet profile on an axis Z orthogonal to X that reveals the radial density distribution of the jet as a function of distance from the nozzle. This distribution is similar to that measured with the other jet expansion apparatus used in the Rayleigh-

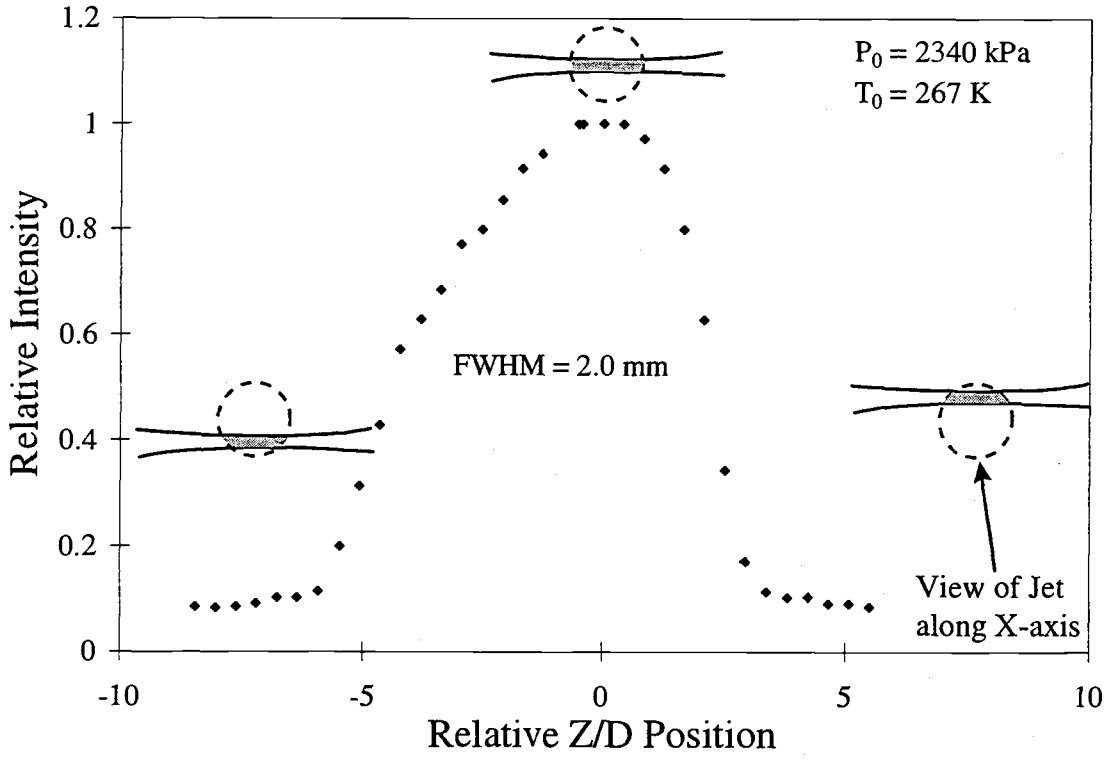

Figure 3-7 Scattered light intensity at 90° at X/D < 1 as the laser crossing axis was moved vertically across the detector aperture. This information allowed us to center the jet on the detector aperture to obtain maximum signal.

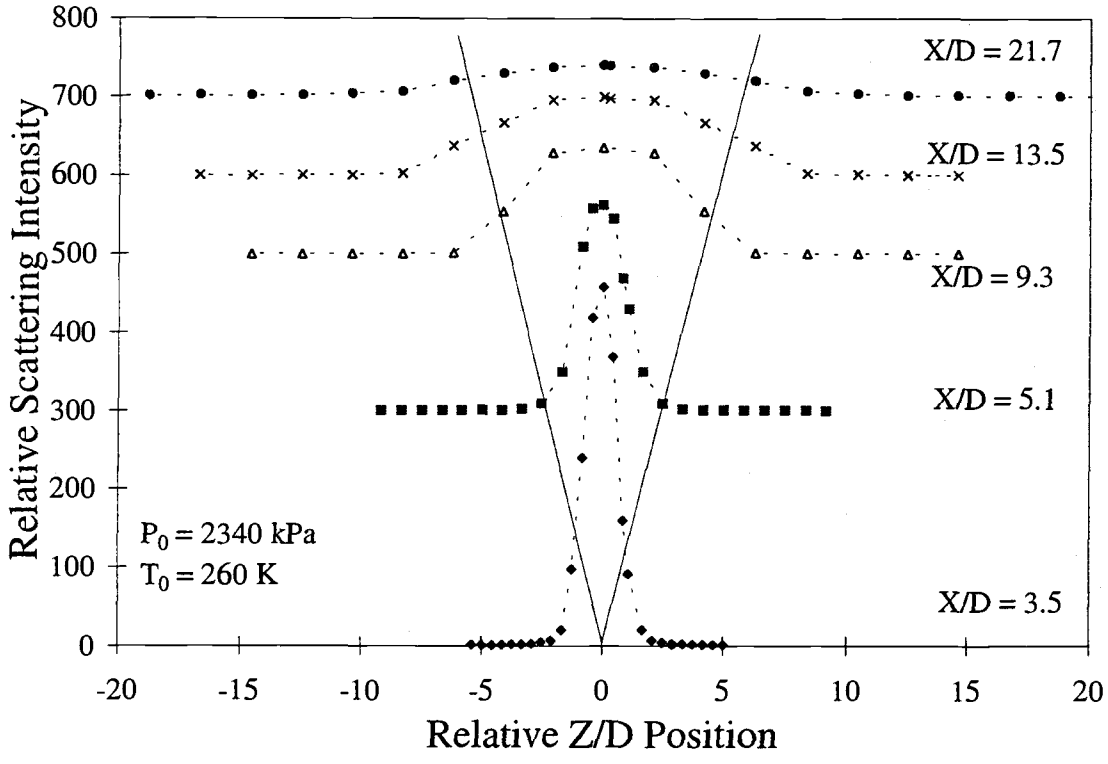

Figure 3-8 Radial density distribution in a supersonic jet expansion of neat CO_2 with initial conditions P_0 = 2340 kPa, T_0 = 260 K, and nozzle diameter = 0.3 mm. The limiting full cone angle for the expansion is 44°. The vertical X/D position is not to scale.

CARS work described in Chapter 2, section 2.8.1. In both cases, the scattering signal for the clusters is localized more on the centerline of the expansion than is predicted for a non-clustering jet. From the full-widths at half maximum of the distributions, the full angle of the expansion cone for the clusters is 44°, which is the same as the value shown in Figure 2-5. This is small compared to a cone angle of 88° calculated from (2.64) and (2.65) for a non-clustering jet of CO_2.

3.4.3 Scattering as a Function of Angle for CO_2 Clusters

3.4.3.1 Neat CO_2 Expansion

Combined angular scattering-CARS data were taken as a function of distance X from the nozzle, as measured in units of X/D where D is the nozzle diameter. Many experiments were done but the results presented here are for data taken at four X/D values for a neat CO_2 expansion. The nozzle driving pressure and temperature were held constant for all measurements and the values P_0 = 1400 kPa and T_0 = 260 K were chosen to duplicate, as much as possible, the expansion conditions used for the 90° Rayleigh-CARS measurements presented in Chapter 2. The purpose was to confirm from the absence of angular variations, that the clusters were indeed small enough that the assumption of Rayleigh scattering was valid.

3.4.3.2 Very Large CO_2 Clusters

In an effort to make clusters where the mean diameter would hopefully be of the order of the wavelength of incident light, a few experiments were done under very extreme clustering conditions. The purpose was to establish the upper limit of sizes which might be produced in such expansions and to determine to what extent the angular distributions fit the Mie predictions. We found that only when the initial pressure and temperature were such that liquid actually formed behind the nozzle (i.e., the initial point A is to the left of the liquid-gas coexistence curve in Figure 2-6), did the expansion produce very large clusters. These showed dramatic visual scintillations and, in the case of CARS, wildly varying (useless) intensities. Although the elastic scattering signal was also "noisy", the intensities averaged to reproducible values so that angular measurements were feasible. The conditions thus represent an upper bound to the size of CO_2 clusters that one might expect to form in jet expansions.

3.5 RESULTS AND DISCUSSION

3.5.1 Tests with Latex Microspheres

3.5.1.1 Rayleigh Scattering Model

When the particle diameter is much less than the wavelength of incident radiation, the I_{VV} Rayleigh scattered intensity at 90° should exhibit an r^6 dependence. This result is consistent with the observations for the 64 nm and 84.5 nm diameter latex microspheres

when scattering at 90° was measured for 514 nm incident radiation. Figure 3-9 shows the relative scattering intensities along with the theoretical line of slope d log I/d log r = 6. The vertical position of the line is adjusted to match the 64 nm measurement so the close correspondence of the origin is considered remarkable, as is the close accord of the 84.5 nm value with the predictions. The 548 nm and 1072 nm diameter latex microspheres also exhibited a high scattering intensity at 90°, but not as high as the Rayleigh prediction, which would correspond to sizes of about 225 nm and 725 nm, respectively. These samples showed an enhanced scattered intensity in the forward direction, which is consistent with the Mie scattering model, as examined in the next section.

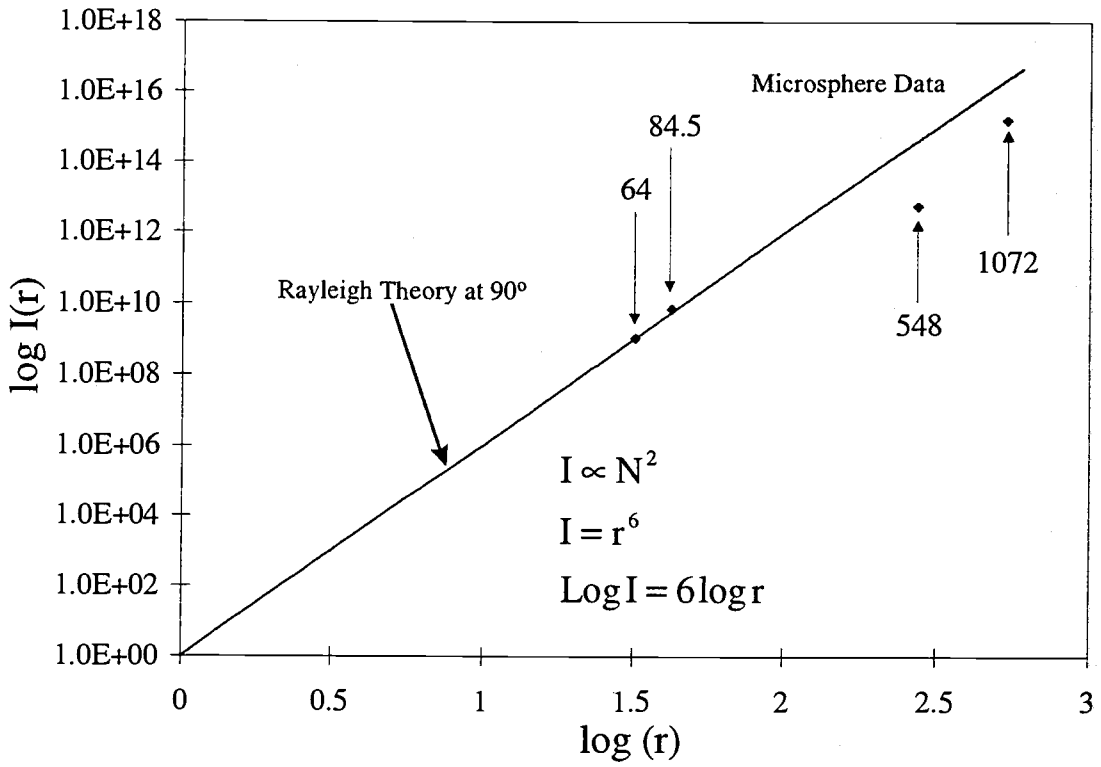

Figure 3-9 Comparison of the predicted r^6 dependence of the 514.5 nm Rayleigh intensity with measured values for particles of 64 nm, 84.5 nm, 548 nm, and 1072 nm diameters. The line is adjusted to match the intensity at 64 nm and the slope of the line is 6 for this log-log plot.

3.5.1.2 Mie Scattering Model: Large Microspheres

As a particle size increases to values comparable to the wavelength of the incident light, the pronounced angular variations of the Mie scattering intensity become apparent. For example, Figure 3-10 shows theoretical I_{VV} curves predicted using MieTab® as the diameter increases from 100 nm to 400 nm. The wavelength of the incident light is 532 nm. For 100 nm particles, the angular distribution of the I_{VV} intensity is nearly constant, as expected for Rayleigh scattering. However, as the size increases, the forward scattering is greatly enhanced and, for 400 nm particles, we see distinct undulations. Such angular variations, predicted by Mie theory, are very obvious in the measurements made for the larger microspheres, as seen in Figures 3-11 and 3-12 for the 548 nm and 1072 nm latex samples, respectively. In each case the solid line represents the theoretical I_{VV} curve calculated for 514.5 nm excitation using MieTab®. The undulations match well with the measurements and the dashed and dotted traces demonstrate that a relatively small change in the particle diameter (~ 10%) results in a large shift in the maxima and minima. The steep rise in the experimental scattered intensity in the forward direction is in poorer agreement, tending to favor a smaller diameter. Even here, the size is within 10% of the manufacturers specification, thus, one can be optimistic that the angular measurements give realistic sizes of clusters if the size is of the order of the wavelength of incident light.

3.5.1.3 Detector Resolution

The data shown in Figures 3-11 and 3-12 were obtained using the commercial light scattering photometer which had an angular resolution of about 1°. Test measurements were also made with the angular apparatus in the jet expansion cube. In one configuration of this, the angular resolution (~1°) was comparable to that of the photometer instrument and, as seen in Figure 3-13, the 1072 nm sphere scattering data for the photometer and cube are in good accord in the case of cube measurements for small clusters, some sacrifice of angular resolution was made by adding a lens (see section 3.4.1.1) to collect more scattered light. From a ray tracing diagram, we determined that the detector resolution was about 20°. To see the effect of this, we convolved the cube scattering data to 20° and the result is shown in Figure 3-13. It is apparent that the undulations are blurred by this process. This blurring will be even more the case for "real" cluster samples which are polydisperse. Some sense of this effect can be seen in Figures 3-11 and 3-12, where the theoretical maxima move significantly for a ± 10% variation in cluster size. Thus, integration over any realistic size distribution function is likely to wash out the scattering undulations.

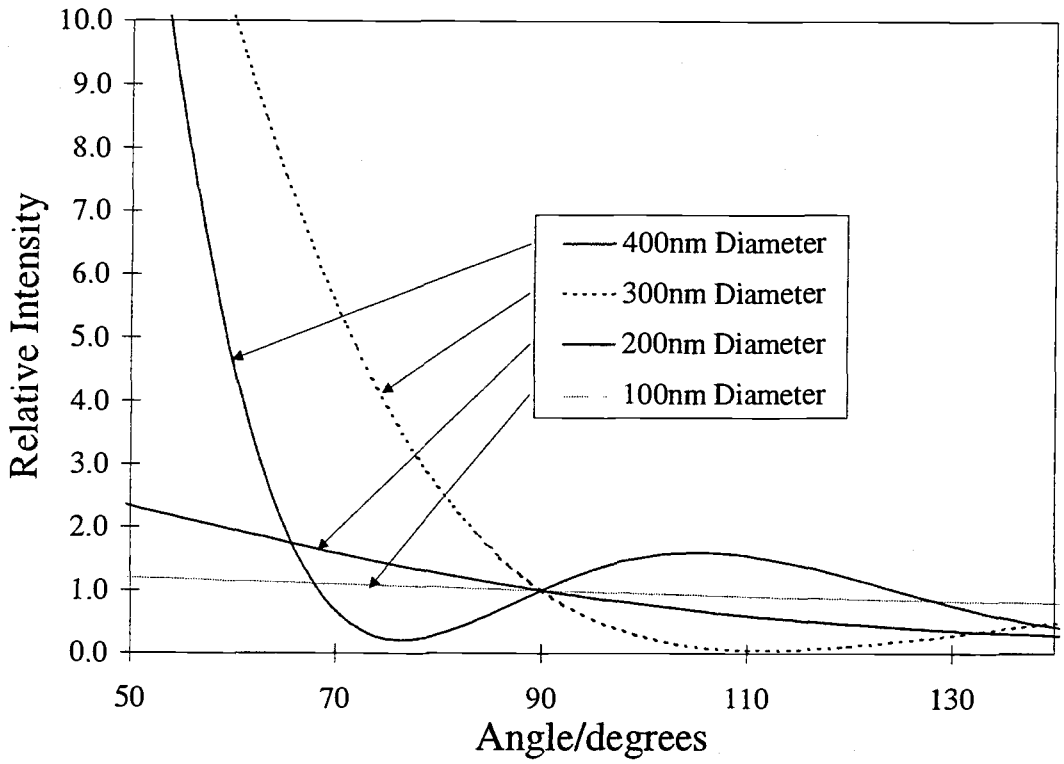

Figure 3-10 Theoretical intensity curves predicted using MieTab® as a particle diameter increases from 100 nm to 400 nm. A wavelength of 532 nm is assumed for the incident beam.

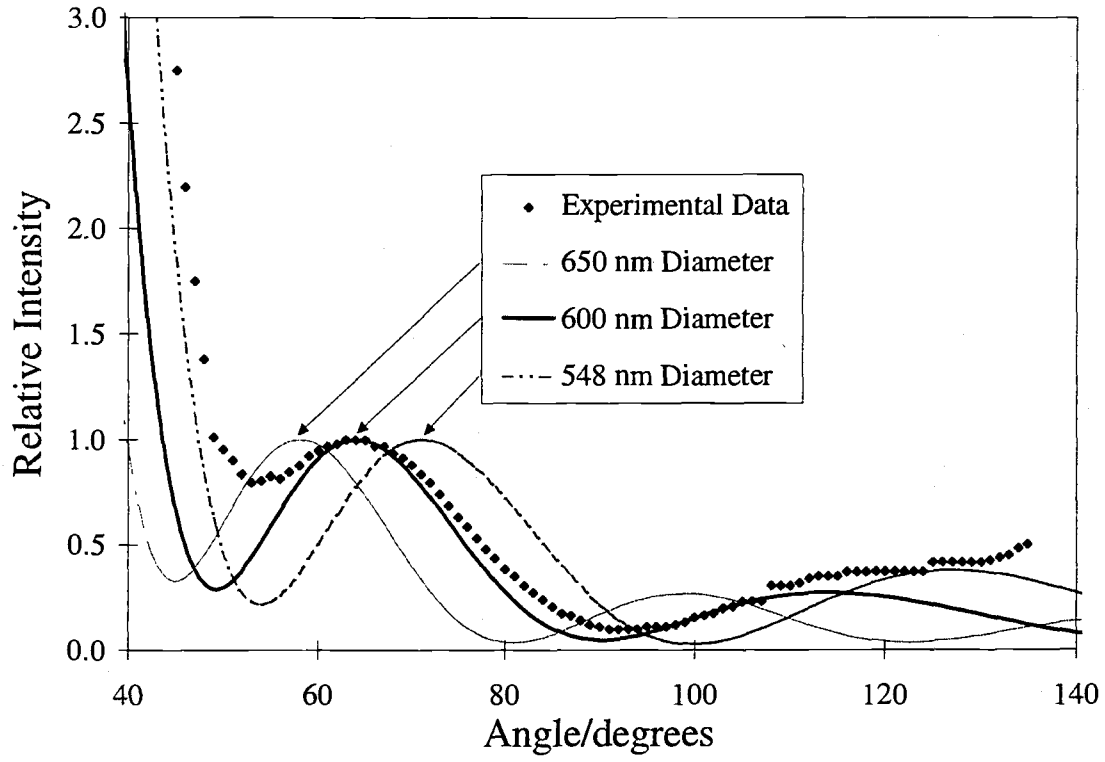

Figure 3-11 The angular dependence of 514.5 nm scattering for latex microspheres of 548 nm diameter. The solid line is the best fit using MieTab®. The dashed lines show the effect of varying the best fit size by ± 8%.

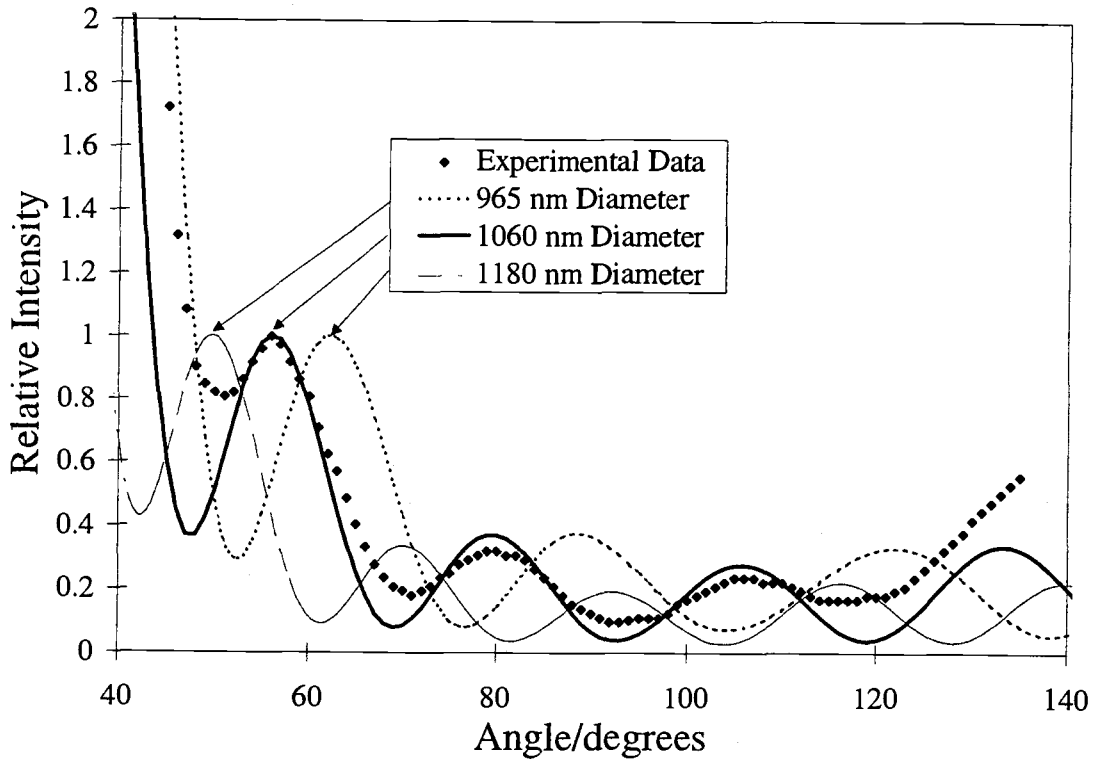

Figure 3-12 The angular dependence of 514.5 nm scattering for latex microspheres of 1072 nm diameter. The solid line is the best fit using MieTab®. The dashed lines show the effect of varying the best fit size by ± 10%.

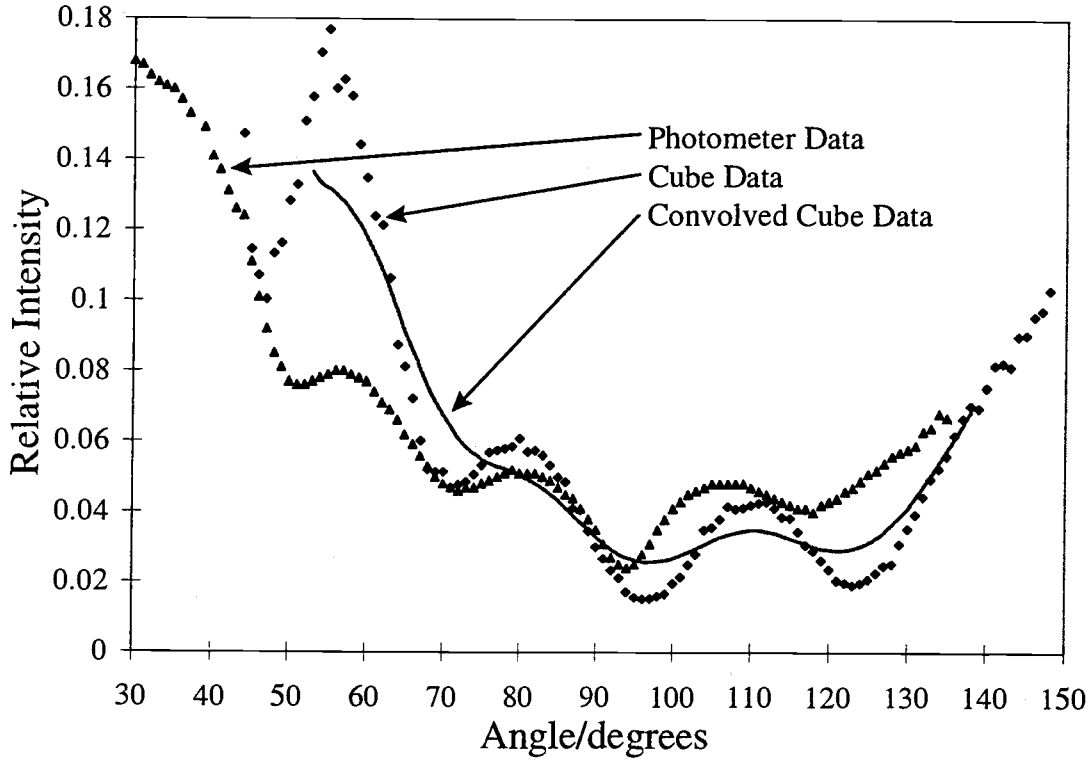

Figure 3-13 Comparison of 514.5 nm scattering results for the 1072 nm latex microspheres displayed for photometer and cube apparatuses. The solid line shows the effect of convolving the cube data to simulate the lower 20° angular resolution used in some of the cluster measurements.

3.5.1.4 Mie Scattering Model: Small Microspheres

Angular scattering of the smaller 64 and 85 nm spheres was also measured and is shown in Figures 3-14 and 3-15. No undulations are seen in this case and the variation of scattering intensity was modest. For example, the I_{VV} (45°)/I_{VH} (90°) intensity ratio was only ~1.4 for both samples, one to two orders less than observed for 548 and 1072 nm spheres. The lines shown in the figures represent an attempt to fit the slope of the scattering data in the range 45° to 90° (the backward scattering data from 90° to 140° is not used because the increase here is attributed to an artifact caused by reflection of forward scattered light from the glass cuvette). It is clear that only a crude estimate of size (a factor of ~2) is possible from these angular measurements but even this may be of some use in cluster studies.

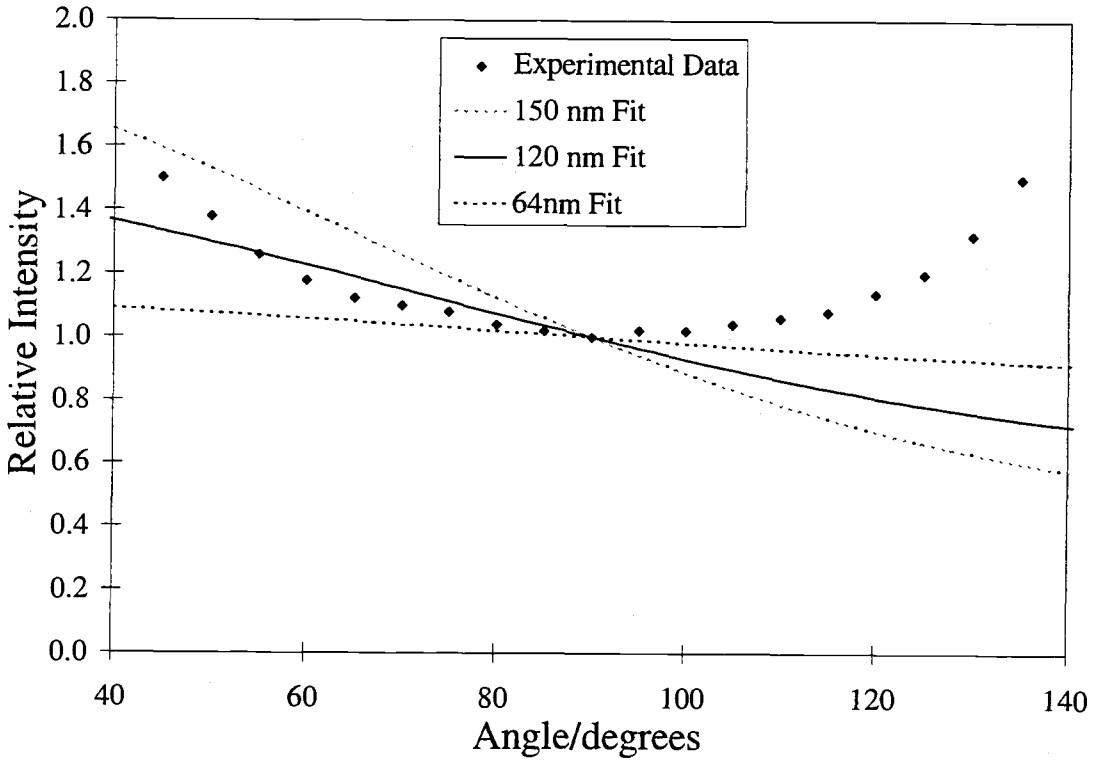

Figure 3-14 The attempt to fit scattering intensity as a function of angle for 64 nm latex microspheres using MieTab®.

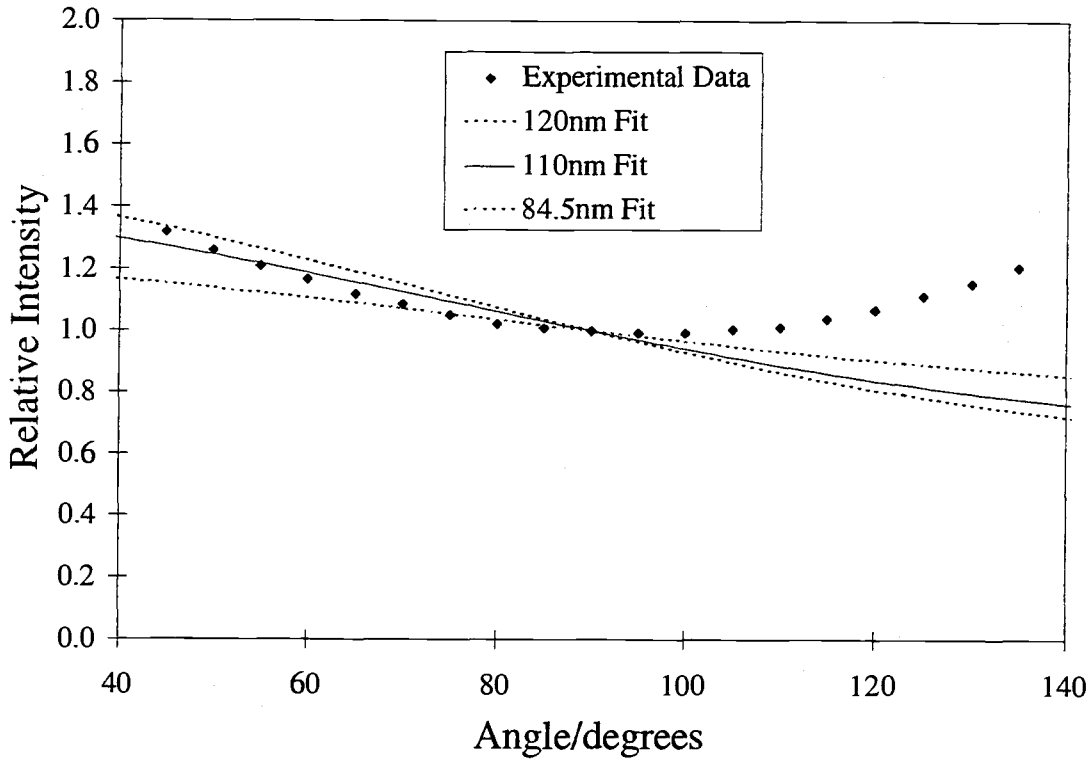

Figure 3-15 The attempt to fit scattering intensity as a function of angle for 84.5 nm latex microspheres using MieTab®.

3.5.2 Estimating Size of Clusters Produced in a Supersonic Jet

3.5.2.1 Scattering for Small Clusters

To establish a baseline for reference, several measurements were made for an expansion with the nozzle temperature at 298 K and for a pressure where the clusters are expected to be very small. Figure 3-16 shows light scattering in such a non-clustering jet as a function of angle at three different X/D positions. Note that the scattering is weak relative to the background and shows very little variation with angle, thus, revealing that the mean diameter of the scatterers is much less than the wavelength of light.

If one cools the nozzle, the extent of clustering increases dramatically and is a sensitive function of pressure. For example, Figure 3-17 shows scattering as a function of angle and pressure at X/D = 16. We see that data for the two lower pressures exhibit no angular dependence of the scattering. However, that for the highest pressure shows a definite increase in the forward scattering direction as observed previously for 64 nm and 84.5 nm microspheres. This perhaps indicates that the cluster size is increasing to something of comparable magnitude.

3.5.2.2 Simultaneous Rayleigh-CARS and Angular Scattering Measurements

One series of experiments was done in which both Rayleigh-CARS and angular scattering data were taken for a neat CO_2 expansion. The expansion conditions were chosen to be as close as possible to those used in Chapter 2 where a mean diameter of

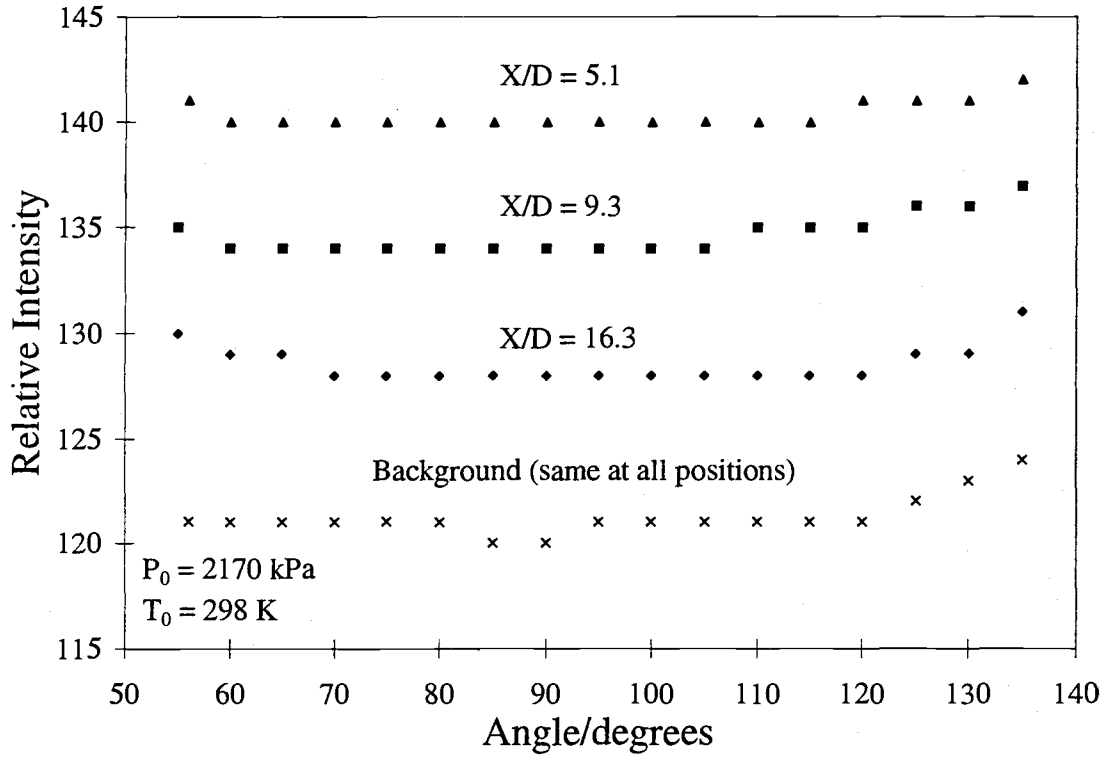

Figure 3-16 Light scattering in a non-clustering jet as a function of angle at three different X/D positions.

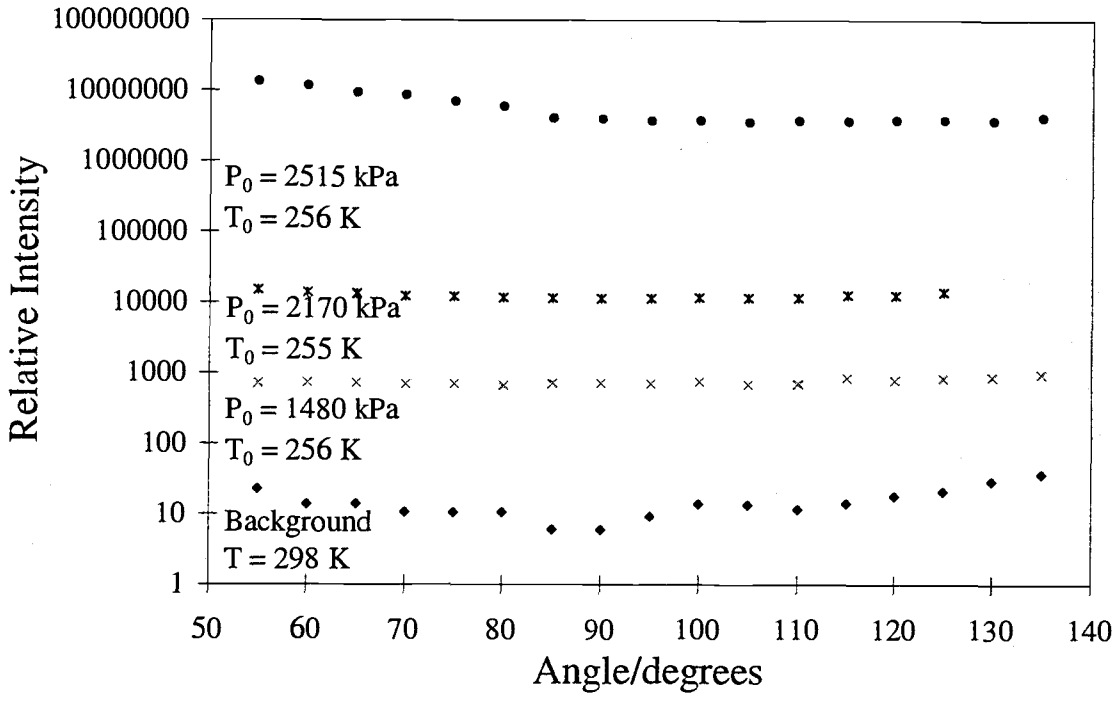

Figure 3-17 Scattering as a function of angle and pressure at constant position (X/D = 16) in the jet.

13 nm was deduced. Figure 3.18 shows CARS spectra of the monomer Q branch at 1285.4 cm^{-1} and the cluster peak at about 1276 cm^{-1} as a function of X/D. The spectra were all referenced to the O(6) line of the monomer at 1276.85 cm^{-1} and smoothed using a Fourier smoothing routine at 50% rejection. Figure 3-19 shows the 532 nm elastic scattering as a function of angle taken simultaneously with the CARS measurements. The result clearly shows no angular dependence for the scattering, thus, we conclude that the clusters formed in this experiment are indeed within the Rayleigh limit (i.e., particle diameter $<< \lambda$). We then applied the Rayleigh-CARS size analysis to quantitatively determine the mean cluster size in this range as described in Chapter 2. A mean size of 14.4 ± 2.0 nm results for this set of data in excellent agreement with the value of 12.4 nm reported in Chapter 2 for similar measurements with the other experimental apparatus.

3.5.2.3 Size Estimate Using Mie Scattering for Large Clusters

The question finally addressed was: can expansion conditions be found which produce such large clusters that an appreciable angular variation in the scattering intensity is seen? It seems remarkable that, when the initial pressure and temperature are such that liquid actually forms behind the nozzle, the expansion will produce a spray of very large clusters. The mean diameter of these clusters might well be of the order of the wavelength of incident light and one could hope to fit the scattering intensity as a function of angle using Mie's formulae. Figure 3.20 shows that, indeed, if one cools the nozzle to very low temperatures, the resultant clusters are large enough to show a definite

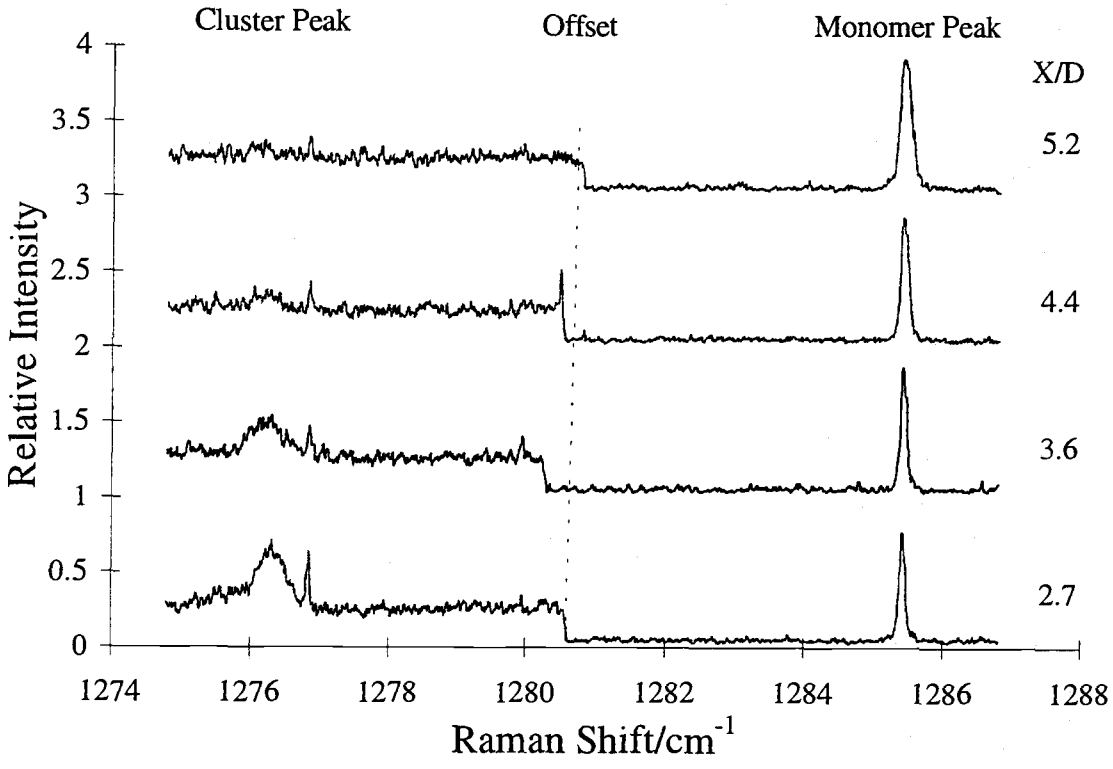

Figure 3-18 CARS spectra of one branch of the $\nu_1/2\nu_2$ Fermi diad of CO_2 from the monomer Q branch at 1285.4 cm^{-1} to the cluster peak at about 1276 cm^{-1} as a function of X/D. The spectra were all referenced to the O(6) line of the monomer at 1276.85 cm^{-1} and smoothed using a Fourier smoothing routine at 50% rejection. The expansion conditions were P_0 = 1400 kPa and T_0 = 265 K.

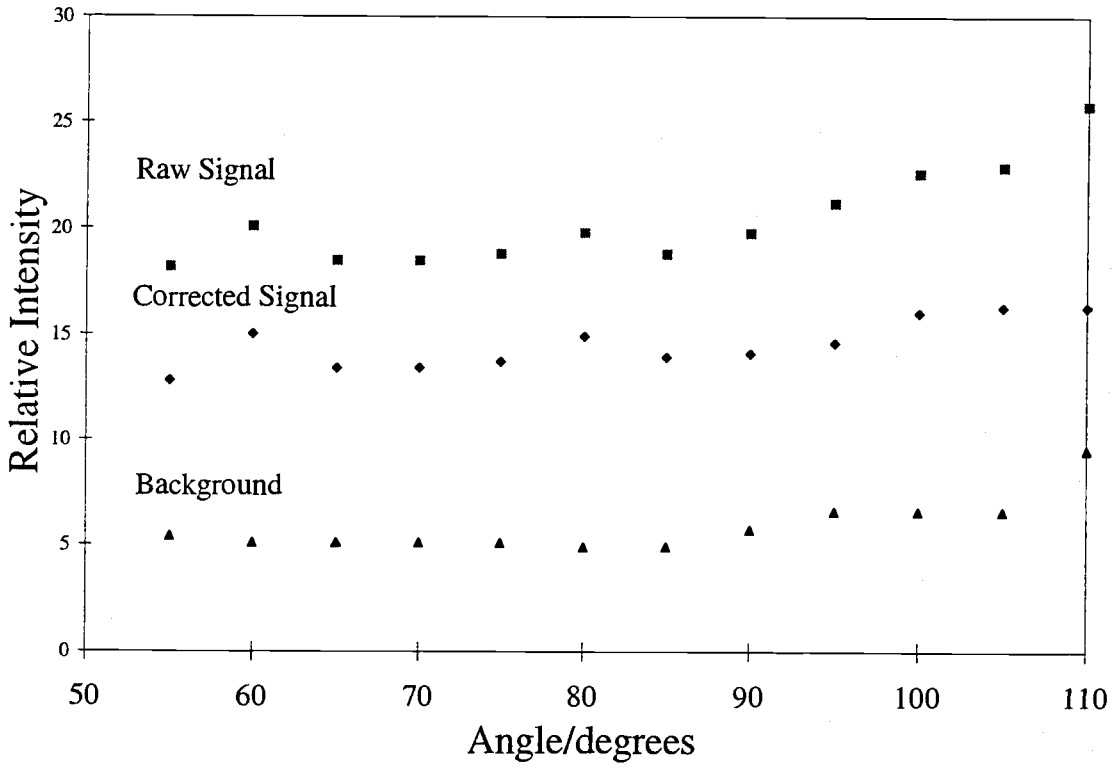

Figure 3-19 The I_{VV} elastic scattering as a function of angle taken simultaneously with the CARS data at X/D = 2.7 shown in Figure 3-18.

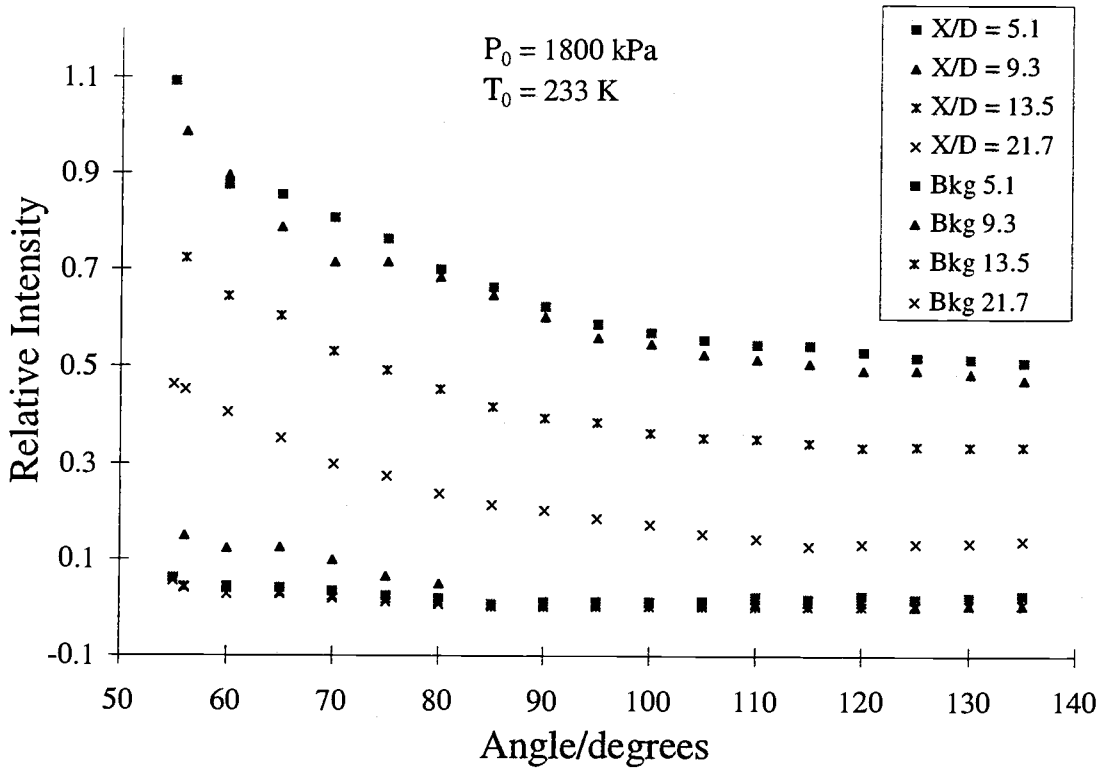

Figure 3-20 The I_{VV} scattering profiles when the expansion conditions are such that very large clusters are formed in an expansion of neat CO_2.

enhancement of scattering in the forward direction. This effect was even more pronounced for the expansion shown in Figure 3.21, where the background was very small and has been subtracted. Figure 3.21 also shows curves calculated for the I_{VV} scattering intensity as a function of angle for the very large clusters. For this procedure, different mean cluster diameters were assumed, along with the log-normal distribution described in Chapter 2. For these traces, a σ value of 1.2 was used since it gave a reasonable measure of the distributions obtained for small clusters by mass spectrometry [Falter, 1970]. Although none of the fits are ideal, the curves do indicate that the mean cluster diameter is in the range of 400 nm to 500 nm. This result is interesting since, to our knowledge, this is the first experimental indication that such large aggregates could be formed in a free jet expansion.

3.6 CONCLUSIONS

The differential cross section for scattering of a plane monochromatic wave from a small particle contains an angular dependence, which is a strong indicator of the size of the scatterer. Microspheres of known size were used for "calibration" which aided in the fitting of angular scattering profiles of clusters formed in a neat CO_2 supersonic jet expansion. Under very extreme expansion conditions, clusters with a mean diameter of 400 nm to 500 nm were produced, as deduced from fits of the angular scattering curves using Mie's formulae. Measurements and calculations were also made for the milder neat CO_2 expansion conditions for which the absence of angular intensity variations and the Mie calculations confirm that these clusters were indeed much smaller than 500 nm. This

observation validates using a simple quadratic size dependence of the Rayleigh scattering intensity in the combined Rayleigh-CARS analysis which gave a mean diameters of 14.4 ± 2.0 nm. We conclude that the Rayleigh-CARS scattering model is a good choice to measure cluster sizes in the 1 - 100 nm range ($N_c = 10^2$ to 10^8) and that Mie theory can be used to model angular scattering results to obtain mean cluster sizes for diameters > 100 nm.

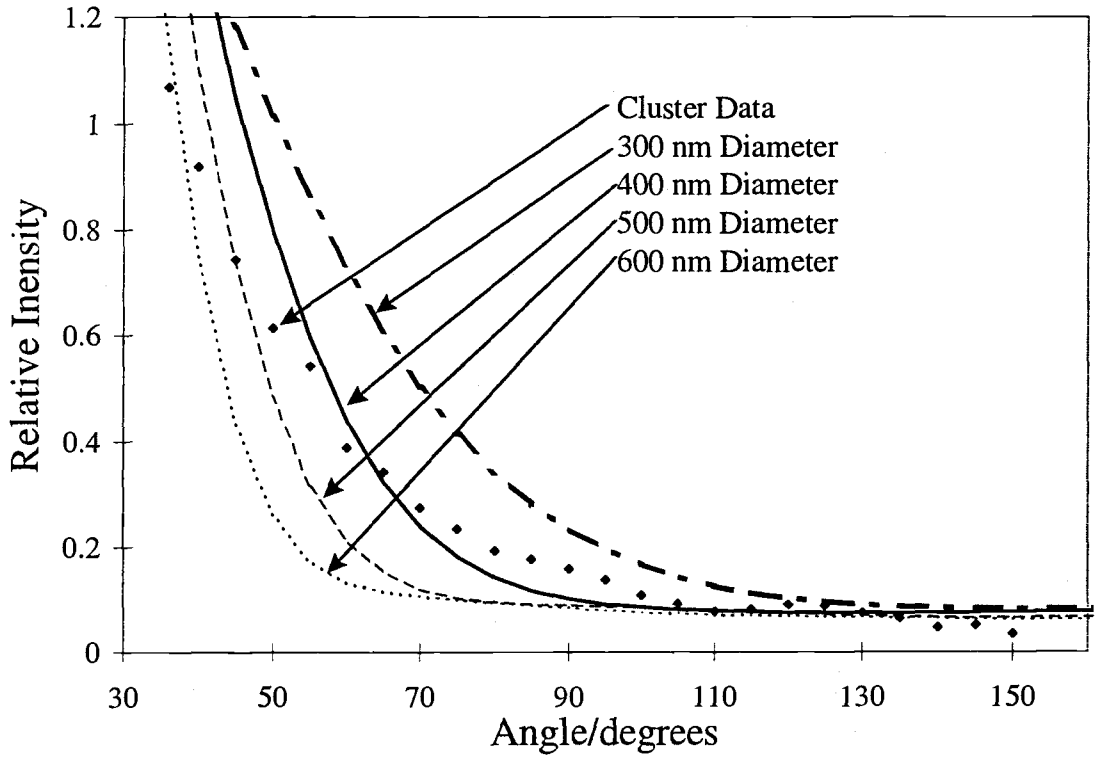

Figure 3-21 The I_{VV} scattering intensity as a function of angle for very large clusters with the corresponding best fit. The expansion conditions were T_0 = 238 K and 1800 kPa.

4. CONCLUSIONS

The coherent anti-Stokes Raman scattering (CARS) intensity of a vibrational transition is approximately independent of the extent of molecular aggregation, whereas Rayleigh scattering intensity increases quadratically with the number of monomer units contained in a cluster. Therefore, Rayleigh scattering is a good qualitative method for determining sample densities and cluster growth in molecular jets. Combined with CARS results, Rayleigh scattering data yield quantitative mean cluster sizes in agreement with those predicted by empirical scaling "laws" and cluster cooling curves. Also, when the extent of clustering is sufficiently high, and the clusters are very cold, the CARS spectra exhibit a peak red-shifted from the monomer that we propose is due to molecules on the surface of the cluster. The size deduced from a comparison of the surface peak to the core peak gives sizes in excellent agreement with the Rayleigh-CARS method. This may lead to deducing a reasonable width of either a Gaussian or log-normal cluster size distribution. Finally, for very cold, dilute, 5% CO_2 in the expansions, two new features are seen at 1280 cm^{-1} and 1281 cm^{-1}, and these are attributed to metastable pentagonal bipyramidal and icosahedral structures predicted from theoretical calculations by van de Waal [1983].

The differential cross section for scattering of a plane monochromatic wave from a small particle also contains an angular dependence, which is a strong indicator of the size of the scatterer. Microspheres of known size were used for "calibration" which aided in the fitting of angular scattering profiles of clusters formed in a neat CO_2 supersonic jet expansion. Under very extreme expansion conditions, cluster diameters about a mean of

400 nm to 500 nm were produced, as deduced from fits of the angular scattering curves using Mie's formulae. Measurements and calculations were also made for the milder neat CO_2 expansion conditions which gave 14.4 ± 2.0 nm mean diameters from the Rayleigh-CARS method.

The absence of angular intensity variations and the Mie calculations confirm that the clusters formed in all but the most extreme expansion conditions were indeed much smaller than 500 nm—the condition necessary to justify using a simple quadratic size dependence of the Rayleigh scattering intensity. Therefore, the Rayleigh scattering model is sufficient to study clusters in the $N_c = 2$ to $N_c = 10^8$ size range. For larger clusters, we demonstrated that Mie theory can be used to model scattering results and obtain a mean cluster size.

BIBLIOGRAPHY

Abraham, Kim, Stein; J. Chem. Phys. **75**(1), 403-410 (1981).

Bartell, L. S., Laszlo, H. and Valente, E. J.; J. Phys. Chem. **93**, 6201-6205 (1989).

Barth, H. D. and Huisken, F.; Chem. Phys. Lett. **169**(3), 198-203 (1990).

Beck, R. D., Hineman, M. F. and Nibler, J. W.; J. Chem. Phys. **92**(12), 7068-7078 (1990).

Bell, A. J., Mestdagh, J. M., Berlande, J., Biquard, X., Cuvellier, J., Lallement, A., Meynadier, P., Sublemontier, O. and Visticot, J-P; J. Phys. D: Appl. Phys. **26**, 994-996 (1993).

Bloembergen, N., ed.; *Nonlinear Spectroscopy*, Proceedings of the International School of Physics, North-Holland Publishing Co., Amsterdam-New York-Oxford (1977).

Born, M. and Wolf, E.; *Principles of Optics*, 5th ed., Pergamon Press, Oxford (1975).

Brown, K.; Ph.D. dissertation, Oregon State University, Corvallis, OR (1991).

Chu, C. M., Clark, G. C. and Churchill, S. W.; *Tables of Angular Distribution Coefficients for Light Scattering by Spheres*, Eng. Res. Inst., Univ. of Michigan, Ann Arbor, MI (1957).

Crew, M. D.; Ph.D. dissertation, Oregon State University, Corvallis, OR (1997).

Dave, J. V.; IBM J. Res. Develop. **13**, 302-313 (1969).

Drake, R. M. and Gordon, J. E.; Am. J. Phys. **53**, (10), 955-962 (1985).

Eckbreth, A. C.; Appl. Phys. Lett. **32**(7), 421-423 (1978).

Evans, G. T.; personal communication (1996).

Falter, H., Hagena, O., Henkes, W. and Wedel, H. V.; Int. J. Mass Spectrom. Ion Phys. **4**, 145-163 (1970).

Farges, J.; Journal of Crystal Growth **31**, 79-86 (1975).

Goyal, S., Schutt, D. L. and Scoles, G.; J. Phys. Chem. **97**, 2236-2245 (1993).

Goyot-Sionnest, P. and Shen, Y. R.; Phys. Rev. B **38**(12), 7985 (1988).

Gspann, J. and Körting, K.; J. Chem. Phys. **59**(9), 4726-4734 (1973).

Hagena, O. F. and Obert, W.; J. Chem. Phys. **56**(5), 1793-1802 (1972).

Hagena, O. F.; Surface Science **106**, 101-116 (1981).

Harvey, A. B., ed.; *Chemical Applications of Nonlinear Raman Spectroscopy* Academic Press, New York (1981).

Hieftje, G. M., ed.; *New Applications of Lasers to Chemistry*, ACS symposium series, (1978).

Hobbie, E. K. and Sung, L.; American Journal of Physics **64**(10), 1298-1303 (1996).

Jackson, J. D.; *Classical Electrodynamics*, John Wiley and Sons, New York (1975).

Kaelberer, J. B., Etters, R. D. and Raich, J. C.; Chemical Physics Letters **41**(3), 580-582 (1976).

Kerker, M.; *The Scattering of Light and Other Electromagnetic Radiation*, Academic Press, New York, pp. 54-59 (1969).

Kokhanovsky, A. A. and Zege, E. P.; J. Aerosol Sci. **28**(1), 1-21 (1997).

Lee, K. H., Triggs, N. E. and Nibler, J. W.; J. Phys. Chem. **98**, 4382-4388 (1994).

Lentz, W. J.; Applied Optics **15**(3), 668-671 (1976).

Levenson, M. D. and Kano, S. S.; *Introduction to Nonlinear Laser Spectroscopy*, Academic Press, New York, (1988).

Lightwave Electronics: *Diode-Pumped Solid-State Non-Planar Ring Laser Users Manual*, Mountain View, CA.

Maker, P. D. and Terhune, R. W.; Phys. Rev. A **137**(3), 801-818 (1965).

Mie, G., Ann. Phys. **25**, 377-445 (1908).

Miller, D. R.; in: *Atomic and Molecular Beam Methods*, Vol. 1, G. Scoles, ed., Oxford University Press, New York, (1988).

Montero, S., Personal communication with J. W. Nibler, (1992).

Nibler, J. W. and Knighten, G. V.; in: *Raman Spectroscopy of Gases and Liquids*, Topics in Current Physics, Vol. 11, Weber, A., ed., Springer-Verlag, Berlin (1979).

Nibler, J. W. and Pubanz, G. A.; in: *Advances in Nonlinear Spectroscopy*, Vol. 15, Clark, R. J. H and Hester, R. E., eds., Wiley, New York, (1988).

Pubanz, G. A.; Ph.D. dissertation, Oregon State University, Corvallis, OR (1986).

Raman, C. V.; Indian Journal of Physics **2**, 387-398 (1928).

Richardson, A.; M. S. Thesis, Oregon State University, Corvallis, OR (1993).

Richter, J-P.; *The Literary Works of Leonardo DaVinci*, 3rd ed., Phaidon, London, pp. 237-239 (1970).

Sharpe, S. W., Zeng, Y. P., Wittig, C. and Beaudet, R. A.; J. Chem. Phys. **92**(2), 943-958 (1990).

Shen, Y. R., ed.; *The Principles of Nonlinear Optics*, Wiley Interscience, New York (1984).

Stein, G. D. and Armstrong, J. A.; J. Chem. Phys. **58**, 1999 (1973).

Stein, G. D. and Moses, C. A.; Journal of Colloid and Interface Science **30**(3), 504-512 (1972).

Strutt, J. W.; Phil. Mag. **xli**, 447-454 (1871).

Tolles, W. M., Nibler, J. W., McDonald, J. R. and Harvey, A. B.; Applied Spectroscopy **31**(4), 253-271 (1977).

Tolles, W. M. and Harvey, A. B.; Introduction to Nonlinear Phenomena in: *Chemical Applications of Nonlinear Raman Spectroscopy*, Academic Press, New York (1981).

Torchet, G., Bouchier, H., Farges, J., de Feraudy, M. F. and Raoult, B.; J. Chem. Phys. **81**, 2137-2143 (1984).

Torchet, G., de Feraudy, M-F., Boutin, A. and Fuchs, A. H.; J. Chem. Phys. **105**(9), 3671-3678 (1996).

van de Waal, B. W.; J. Chem. Phys. **79**(8), 3948-3961 (1983).

Wilson, E. B., Decius, J. C. and Cross, P. C.; *Molecular Vibrations*, Dover, New York (1955).

Yang, M.; Ph.D. dissertation, Oregon State University, Corvallis, OR (1990).